REDUCTION OF THE EMISSIONS FOR TRAILING SUCTION HOPPER DREDGES DURING OPERATION

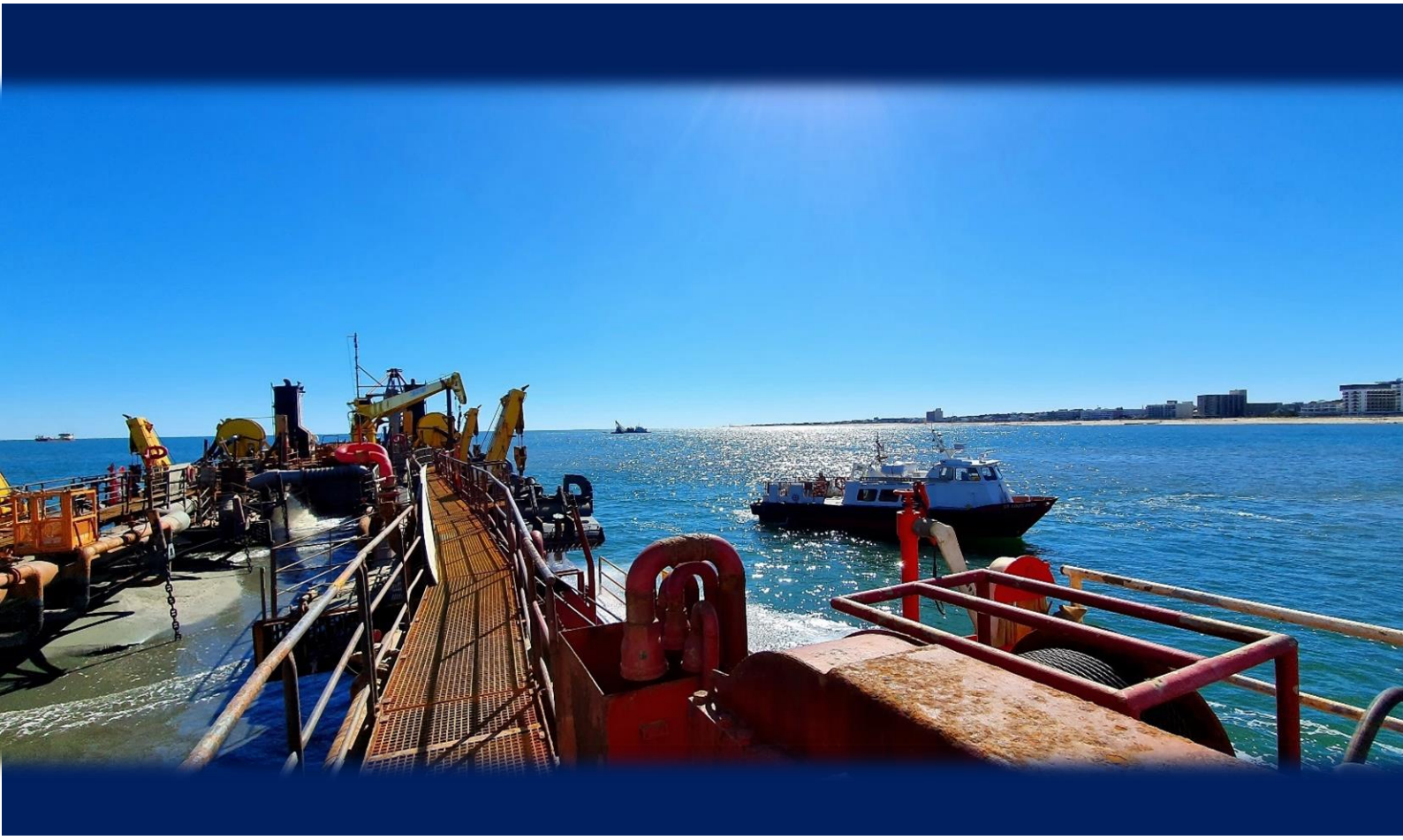

C.M.D. de Roode

SDPO.20.012.m.

TU Delft

GREAT LAKES DREDGE & DOCK IMPROVEMENTS

- page intentionally left blank -

REDUCTION OF THE EMISSIONS FOR TRAILING SUCTION HOPPER DREDGES DURING OPERATION

C.M.D. de Roode
4150090

In partial fulfilment of the requirements for the degree of
Master of Science in Marine Technology

Thesis committee

Chair:	Dr. ir. S.A. Miedema	Delft University of Technology
Daily supervisor:	Dr. ir. P. de Vos	Delft University of Technology
Industry supervisor:	R.C. Ramsdell	Great Lakes Dredge and Dock
3rd committee member:	Dr. ing. S. Schreier	Delft University of Technology

12 May 2020

Preface

In front of you lies my master thesis, which for the majority of the time I wrote at Great Lakes Dredge and Dock in America. During this journey I gained more knowledge and experience than I thought. Not only did I learn about the dredging industry and dredges, but also about the American culture and business. To see dredges operating myself was quite a clarifying experience. In the office I got to know the interaction between co-workers and see what must be done to make the actual dredging possible. In my free time I got to see Chicago and the suburbs and got a taste of the atmosphere in those areas. I was once surprised when I woke up in the morning by some brightness. I thought I forgot to close the curtains, but I didn't. I opened them and the fact that I just woke up amplified the joyful feeling when I saw the in snow covered apartments outside. Unfortunately, it only happened three times during my stay in the winter. Maybe it was because I was always wearing my leather jacket outside even though a few colleagues were warning me of the cold weather that definitely would come. Talking about my colleagues, every single one of them was a great help. They were always kind enough to make time to guide me through the process of completing my research.

I spent most time with Michael Beton, and I am very thankful for that. And yes, he is aware that in Dutch his surname means concrete. And no, I couldn't even make a joke about it as it was one of the first facts he mentioned when we met. He mostly guided me through the process of creating the model so it can be used in practise. We also discussed different paths that the model could take during its development. Raylene was situated in the cubical next to the one of Michael. I want to thank her, especially for the last two months when I sat down with Michael more than usual, for her time and the information she provided. Robert Ramsdell, he guided me through the graduation process in accordance with the company. First of all, I am thankful he granted me the opportunity to do research at GLDD. Second, I respect him for making time for me within his schedule and also taking the time to help.

My supervisor from the university, Sape Miedema, I would like to thank him for his time and effort he put into my graduation. And most of all for making graduating at GLDD available for students. I believe there are many advantages of graduating abroad, one of them is self-improvement. Lastly, Peter de Vos, who supported me throughout the graduation and provided constructive feedback. I want to thank him for all the help he gave me and his flexibility for having meetings.

Summary

The International Maritime Organisation (IMO) is a specialized agency responsible for the safety and security of shipping and the prevention of marine and atmospheric pollution by ships. Air pollution is one of the contributors, CO_2 emission is recognised as the biggest contributor to the increasing temperature of the Earth. Global warming is a controversial topic and actions are taken to reduce further rising of the temperature on Earth. The IMO has set limits for vessels on the emission of NOx and SOx. Currently, the IMO is negotiating on how to limit the emissions of CO_2 to reach a reduction of 50% in comparison to 2008.

The largest dredging company in the United States is Great Lakes Dredge and Dock (GLDD). GLDD operates multiple large dredges, including six trailing suction hopper dredges (TSHD). These dredges trail two dragheads across the ocean floor, excavate the soil and pump it into the hopper, a large hold within the dredge. When the limit of the capacity of the hopper is reached, the dredge sails to the dumping area where it discharges the soil to its destination.

The purpose of this research is to provide an emission model for TSHDs showing an emission profile (CO_2, SOx and NOx) per cycle of operations, and present emission reduction methods. Within the emission model there are eight main parts that are connected and create the results. The results are shown per cycle of operation and are calculated per phase. The six main phases of a cycle of operation are: Loading, transit loaded, connecting, discharge, disconnecting and transit empty. The first part of the emission model determines the hull resistance. The second part consist of the trailing resistance. This part is split up into three more detailed segments: the calculations for the cutting force, cutting depth and trailing force. The trailing and hull resistance together form the total resistance within the loading phase. For the transit phases, only the hull resistance is used for the total resistance. With the total resistance known, the propeller is matched to the main engine in the third part. The fuel consumption and emitted emissions are calculated in the fourth and fifth part. The power requirement for the other engines, pumps and auxiliary equipment are calculated in part 6^{th} through 8^{th}. For each job, specific input is required for the calculations. Combining this input and the calculation parts, the emissions, fuel consumption and fuel cost are given per dredged m^3.

Five methods to reduce the emissions for TSHDs are researched. First, the type of power arrangement is researched. A mechanical power arrangement with a combined drive and a direct drive, an electrical power arrangement and a hybrid power arrangement are investigated. The variations of power arrangements are implemented on the Dodge Island. Second, the difference between a fixed (FPP) and controllable pitch propeller (CPP) is researched. Most modern day TSHDs use a CPP, as the efficiency during the wide variation of operating conditions is greater than a FPP. The third method to reduce the emissions is to find the optimal loading speed. The optimal speed is researched for a floating visor and a fixed visor. The most common solutions to comply to the limit of the SOx emission is using ultra low sulfur diesel or installing a scrubber. The fourth reduction method is focussed on the use of scrubbers. The most used types of scrubber are the dry, open loop, closed loop and hybrid scrubber. The last method to reduce the emissions is shutting off the engines when not in use. The trade-off is the wear of the engine. To verify the results of the emission model, the fuel consumption of multiple completed jobs is compared with the predictions of the emission model.

The results show that for the Dodge Island a mechanical power arrangement with a combined drive emits the least CO_2. With a CPP, the fuel consumption and thus the emissions are reduced. It is found that the optimal loading speed depends on the manually set limit for the penetration depth of the jets. Within the model the optimal speed is 0.70 m/s. The most promising scrubber for TSHDs is a closed loop scrubber which reduces the SOx emission with 96% and reduces the particular matter with 60%. Reviewing one operation of the Dodge Island shows a reduction of 0,5% in fuel with shutting off the main engines when not in use.

Abbreviations

APPS	the Act to Prevent Pollution from Ships
BT	Bowthruster
CD	Combined drive
CH_4	Methane
CO_2	Carbon dioxide
CPP	Controllable pitch propeller
CSD	Cutter suction dredge
DD	Direct drive
DE	Dredge engine
DP	Dredge pump
EEDI	Energy Efficiency Design Index
EIAPP	Engine International Air Pollution Prevention
EPA	Environmental Protection Agency
F-gasses	Fluorinated gasses
FPP	Fixed pitch propeller
Gen	Generator
GHG	Greenhouse gasses
GLDD	Great Lakes Dredge and Dock
IAPP	International Air Pollution Prevention
IMO	International Maritime Organisation
JP	Jet pump
LAA	Lower arm angle
MARPOL	International Convention for the Prevention of Pollution from Ships
MD	Mechanical dredge
ME	Main engine
MEPC	Marine Environment Protection Committee
N_2O	Nitrous oxide
NO	Nitric oxide
NO_2	Nitrogen dioxide
NOx	Nitrogen oxides
O_3	Ozone
PM	Particular matter
PSD	Prevention of Significant Deterioration
PTO	Power take-off
rpm	Revolutions per minute
rps	Revolutions per second
SEEMP	Ship Energy Efficiency Plan
SO_2	Sulfur dioxide
SOx	Sulfur oxides
SPT	Standard penetration test
TSHD	Trailing suction hopper dredge
U.S.	United States
ULSD	Ultra low sulfur diesel
USCG	United States Coast Guard

Contents

1

INTRODUCTION

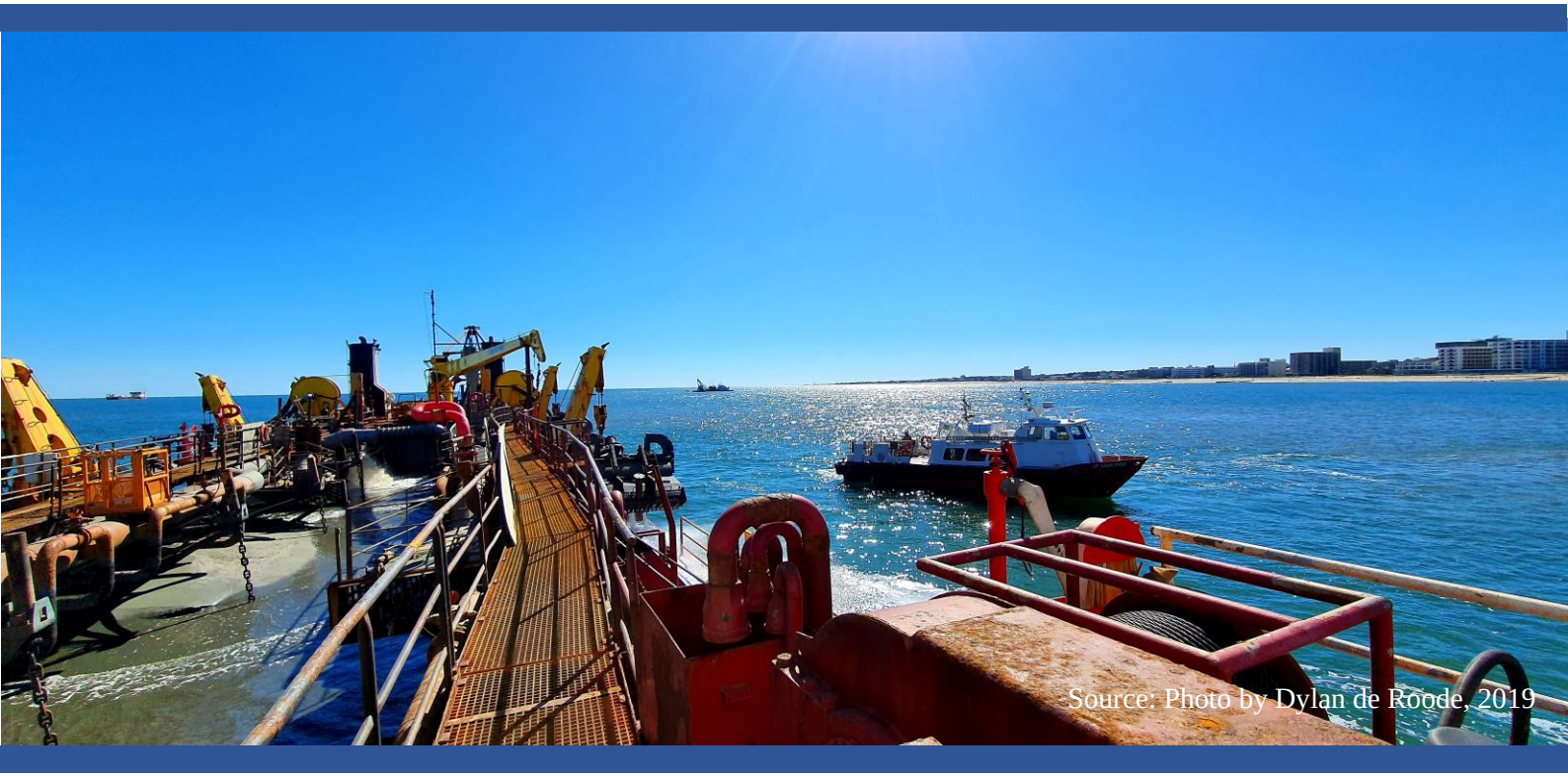

Source: Photo by Dylan de Roode, 2019

1. Introduction

For many years, global warming has been a controversial topic. More and more research is conducted and action are taken to recover the imbalance caused by the contribution of greenhouse gasses (GHG) by the human population. An example of reducing the GHG is found in Norway. Oslo, the capital of Norway is determined to make a zero-emission taxi system by 2023 [1]. More focussed on the shipping industry and air pollution, counter measurements are taken by the International Maritime Organization (IMO). They strive to reduce the carbon emissions with 50% by 2050 [2]. These measurements, in terms of emission restrictions, are also affecting the dredging industry. Dredges are used to keep harbours and waterways clear of sludge, mud and other obstacles the river carries. The sediment that is contained from the bottom floor is used to facilitate land or create new one. As ships increase in size, dredging is important to maintain harbour accessibility. The operation of dredging consumes energy and it produces emissions. To pass the future restrictions of emissions, the pollution of ships including dredges have to be reduced.

The purpose of this research is to provide an emission model and present methods to reduce the emissions of trailing suction hopper dredges during operation. The methods are viable with Great Lakes Dredge and Dock Company (further mentioned as “GLDD” or “the company”) and the future outlook of the regulation agencies in the United States of America (U.S.). An emission model to predict the energy consumption and emitted emissions (CO_2, SOx and NOx) of hopper dredges during operations is made and different methods to reduce the emissions by dredges is researched.

The introduction is split up into five sub chapters. The first chapter presents a description of the problems that lead to this research. This is followed up by the research question where the main and sub questions are described. How the research is conducted is described in the third sub chapter, the research strategy. In the fourth sub chapter, the scope of the research is given. Boundaries are set to validate the research. The report structure is presented in the last sub chapter.

1.1 Problem Description

The main problem is the international restrictions on emissions. These legislations force the dredging industry to become environmentally less pollutant. Measurements are to be taken to comply with the current and future restrictions.

The restrictions on emitted emissions imply a second problem, the quantity of the emitted emissions is not present. This is presented in an emission model where the emissions CO_2, SOx and NOx are shown. Knowing the quantity of the emissions emitted for TSHDs during an operation forms the basis for the reduction methods. As largest dredging company of the U.S., GLDD plays a big role within the dredging industry. The Environmental Protection Agency (EPA) provides emission legislations within the U.S. and the company has to comply with those legislations. More stringent rules can also vary from State to State and Local authorities. Fines are received if regulations are neglected and job offers could be declined if dredges do not comply with the emission standards.

The last problem is in addition to the second one. For future and current dredges, it is legally mandatory to comply with the regulations. To date, multiple methods to reduce the emissions are available worldwide. Focussing on TSHDs that are operational in the U.S., the methods to reduce the emissions are not clear. The results of this research provide solutions to the problems described above.

1.2 Research Question

To substantiate the solution the following research question is defined:

What is the total emission profile for trailing suction hopper dredges during operation and what are viable methods to reduce their emissions?

In order to answer the research question, sub questions are defined:

1. What is the total energy requirement for a THSD per dredged m^3?
2. What is the emission profile for a THSD per dredged m^3?
3. What is design philosophy of Great Lakes Dredge and Dock Company?
4. What methods are available and viable to reduce the emissions of TSHDs in operation?

The first goal of this research is to create a model that shows the emission profile of a TSHD per cycle of operation. The second goal is to find methods to reduce the emissions for TSHDs during operation that are useful for GLDD. A model is made to show the emissions emitted per operation. The input of the model are variables that are known or are assumed before starting a dredge job, either given by the contractor or measured by the company itself. The aim is to create a model as accurate as possible in terms of fuel consumption. The total fuel consumption of dredges of multiple finished operations are compared to confirm the accuracy. To be able to find methods to reduce the emissions, multiple steps are taken. First of all, the amount of consumed energy is necessary. The energy consumption is calculated per phase of the operation. The first sub question covers the total energy consumption that is determined by combining the energy requirement for all the phases. The power arrangement and type of engines are a crucial part for the emission profile. Those two components are used to convert the energy requirement into emitted emissions. The second sub question covers these calculations. To determine viable methods for the reduction of the emissions, the future outlook of the regulations and the design philosophy of the company are researched in the third sub question. In addition, viable methods to reduce the emission profile are determined and presented in the last sub question. The viability of the methods depends on the design philosophy of GLDD and the expectations of the emission reductions by regulatory agencies.

1.3 Research Strategy

Information about the subjects that are researched is needed to create an understanding of the work. To get a better understanding, literature is studied. A study of relevant literature is split up into three categories. The first one focuses on dredging, the process of dredging is studied as well as the working principle of TSHDs. The next subject is the greenhouse gasses. One of the questions that is answered is what caused the environment to change so dramatically and why should we care? Also, the content of emissions and how they are created is researched. Lastly, the regulations that react to the environmental changes are discussed. The parties involved and their contribution to the environment is described. In order to retrieve information about the work provided by GLDD, communication with the company is important. Many employees have valuable information that can contribute to the research. In addition to the literature study as described above, information from the field is also gathered. A site visit is arranged to see the a TSHD in operation. Experiencing a TSHD in action during the visit is valuable for a better understanding of the working principle. Measurements are taken while the dredges are in operation and the results of the model is verified with those particular measurements. In terms of improvement, the crew and captain on board of the dredges can have valuable information for efficiencies in the working environment. Night and day, the crew is operational and are completely familiar with the dredges. Another source of information that is used is forums. Especially in the final stages of the research, methods to reduce the emissions are offered. Forums contain valuable information about the trends and the current innovations to reduce the emissions as it is a widely discussed topic within the shipping industry. To determine the emissions emitted by THSDs, a model is made. First, the model is made using one dredge to achieve a working model. Calculations are made per phase of

operation to make the model more clear. For the sailing phases, the resistance is determined first. With the resistance, the amount of power that is required to propel the dredge is calculated. Among other specifications, the propeller and engine characteristics as well as the hull shape are taken into account. Multiple calculation parts are included in the model to create an independent model able to determine emissions without using other programs or models. The determination of the trailing forces, hull resistance, pumping power requirements, electrical load balance and engine power requirements are included. Any specifications such as power arrangement, type of engines and type of propeller are taken as a variable to create a model that is capable of calculating the emissions for a variety of dredges. The model is verified with operations executed in the past.
At this stage, information about the present is known. It is time to look at what the future holds in order to make the best decisions for the methods to reduce the emissions. At first, the future outlook for the regulations are studied. Main agencies like the U.S. Corps of Engineers, the EPA and the IMO are used to gather information about the future of the regulations. The vision of GLDD plays a big part in the viability of methods to reduce the emissions. Combining the design philosophy and vision of GLDD and the future outlook of the regulations, the viability of the reduction of the emissions are determined. Methods to reduce the emissions are studied after the future outlook of both the company and the regulatory agencies are known. Information from the forum(s) and the crew of dredges are taken into account. Furthermore, solutions to reduce the emission found in literature are used as well. The solutions should be in addition to the vision of GLDD and the future outlook of the regulations. The outcomes of the methods are presented and elaborated with recommendations.

1.4 Scope of the Research

Boundaries are set to be able to accurately answer the research question within the given time limit. The boundaries that are taken into account are listed below:

Emission Model:

- The research is focussed on one type of dredge, the TSHDs.
- All active main energy users active on board a TSHD are taken into account.
- Saturated sand is used to calculate the draghead production and resistance.
- The model is capable of calculating the cutting forces of grain sizes d_{10} between 0.1 mm and 3.0 mm.
- The following emission according to the power consumption are determined: CO_2, NOx and SOx.
- Calculations are based on calm weather and sea conditions.
- Full load conditions are used for the entire period of loading.

Reduction Methods:

- The reduction methods are focussed on the United States.
- The methods to reduce the emissions are focussed on the following emissions: CO_2, NOx and SOx.
- The viability of the methods is based on the design philosophy of GLDD and the expected upcoming restrictions of emissions.
- The reduction of the emissions is based on one cycle of operation which contains six main phases; loading, transit loaded, connecting, discharge, disconnecting and transit empty.
- The emissions profile is limited by one cycle of operation, all other processes that require energy and are not directly related to the operation are neglected. This includes the process of designing, building and demolition of the vessel.
- Equipment on board of the first analysed dredge (the Dodge Island) are used
- The methods are based on existing products or services
- The focus of the methods is on beach nourishments
- No alternative fuels to reduce the emissions are researched

1.5 Report Structure

The structure of the thesis is divided into four chapters. Chapter 2 covers the literature review for the research. This chapter provides information about TSHDs, greenhouse gasses, regulations for air pollution and GLDD.

In the third chapter, the model to determine the emission profile for an operation of a TSHD is presented. The operation is split up into six main phases and each of those phases requires a certain amount of power. The power demand is explained per phase. In the flowchart of Figure 1, the relations between the movers and the phases are shown. The power demand is split up into three main actions that require power. The required power for those actions is provided by (prime) movers. The number of movers depends on the power arrangement of the dredge. The links between the movers and the actions are also dependent on the power arrangement. Manoeuvring, providing pumping power and providing auxiliary power are the three main actions (or processes) that require power. These three processes are calculated in the model for each phase.

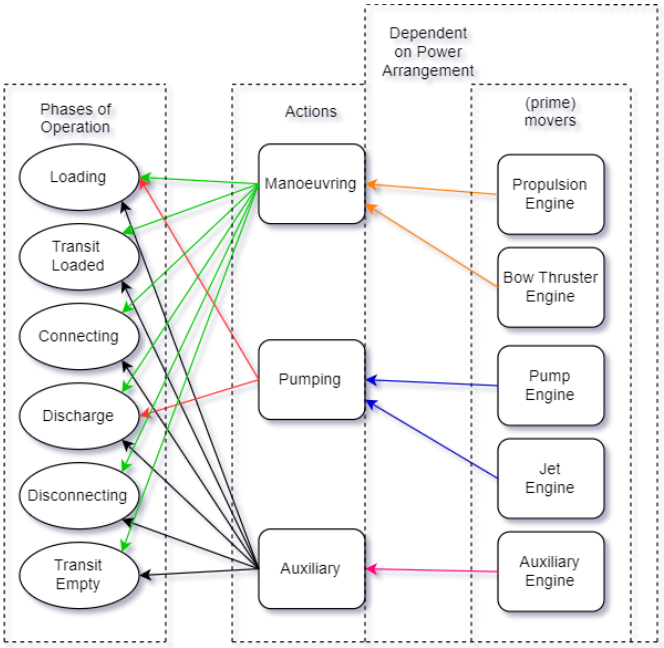

Figure 1: Flowchart of Relation between Phases and Movers

The goal of the model is to show the emissions per operation. Chapter 3.1, Specifications of describes the dredge that is used to verify the model. The main specifications such as the power arrangement and dimensions of the dredge are described. The next sub chapter, chapter 3.2 describes the complete model per calculation part. The power demand of the movers is determined and combined with the actions that are to be executed per phase. The flowchart in Figure 2 shows how the emissions are determined for the manoeuvring part for a given speed.

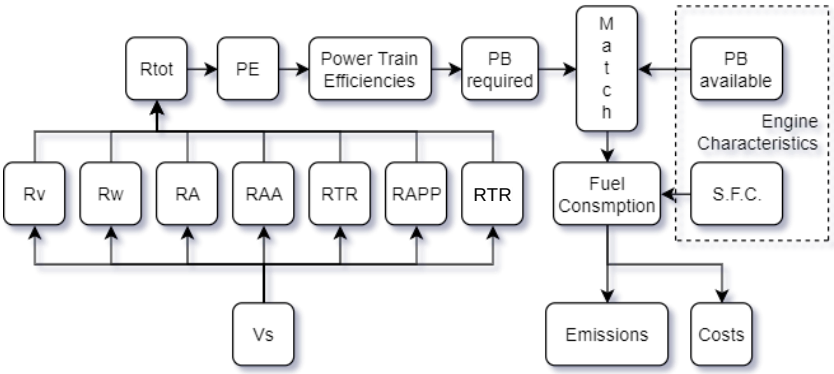

Figure 2: Flowchart of the Action Manoeuvring

The calculations to determine the resistance of the dredge in loading conditions are complex and require a more enhanced description. The resistance of the draghead and the suction pipes (also known as trailing forces, expressed in R_{TR}) are calculated in detail according to the flowchart in Figure 3. The actions Pumping and Auxiliary are less complicated and the process is also explained in chapter 3.2. In chapter 3.3, the verification of the model is done according to operations already completed by GLDD. All the inputs for the model are taken from the specific operation. The amount of fuel that is used according to the recorded data by GLDD is compared with the predicted amount of used fuel according to the model.

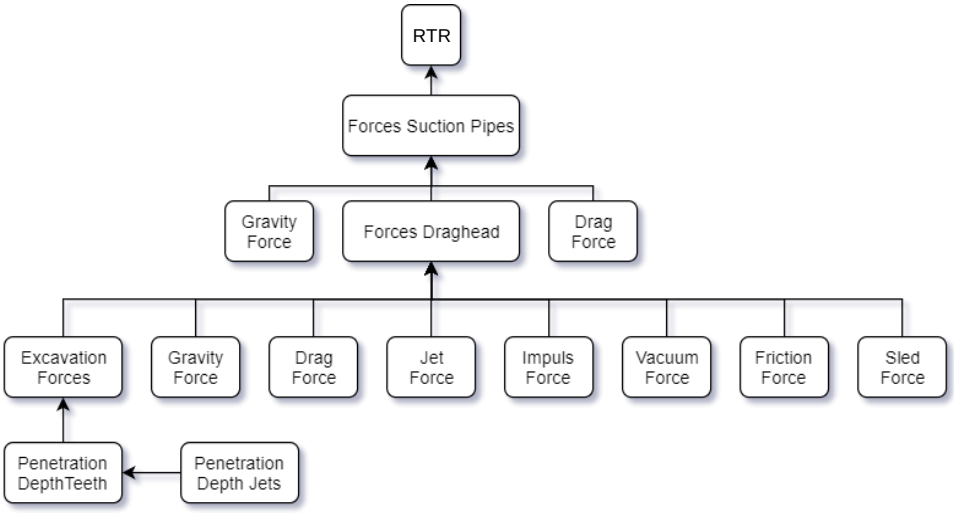

Figure 3: Flowchart of Action: Manoeuvring with in Detail the Total Trailing Resistance (RTR)

Within the chapter 4, methods to reduce the emissions and the viability of the methods are described. The conditions to determine the validation of the methods is described within the first sub chapter. This is followed up by a description of the methods to reduce the emissions and the magnitude of the effect. A conclusion and recommendations about the emission model and the reduction methods are given in the last chapter.

2

LITERATURE REVIEW

Source: Photo by Dylan de Roode, 2019

2. Literature Review

Basic information about the essential topics of the research is given in this chapter. The hopper dredge is introduced in the first sub chapter. Followed up by a description of the greenhouse gasses in the second sub chapter. Within the third and last sub chapter, the environmental regulations that affect the hopper dredges is presented.

2.1 Dredging: Trailing Suction Hopper Dredges

Within the first sub chapter, different types of dredges are introduced. This is followed up by the second sub chapter, which describes the history of hopper dredges. The establishment of GLDD is stated in the third sub chapter. How hopper dredges operate is explained in the fourth sub chapter.

2.1.1 Types of Dredges

As technological developments continue and dredges get more advanced, multiple solutions of clearing the bottom of waterways, lakes and seas are implemented. Designed for the same purpose, different methods of dredging are being developed. The main types of dredges are described below [3]:

1. Mechanical dredges
2. Hydraulic dredges
3. Hydrodynamic dredges

There are three types of mechanical dredges, the grab dredge, bucket dredge and the backhoe dredge [4]. The grab dredge, also known as the clamshell dredge, uses its mechanical clamp to grab the soil and dump it in the barge. To maintain stability and position, the dredge is moored with anchors or spuds. A bucket dredge is one of the oldest dredges. It uses its chain of buckets to scoop up the soil that needs to be excavated. The soil then is dropped into barges so it is transported to a disposal area. Bucket dredges are used for any material where liquifying the material (blasting) is not required. A backhoe dredge is based on the same principle as the grab dredge, except it uses a half-open shell to dig up the soil. The soil is then dumped into a barge. The backhoe dredge also gains stability by being moored with anchors or spuds.
Trailing suction hopper dredges and cutter suction dredges are listed as hydraulic dredges. The TSHD is explained in detail in chapter 2.1.3.. Cutter dredges are equipped with a rotating cutter. Spuds of the dredge make their way into the ground to secure the barge. The cutting arm is lowered to the seabed and by rotating the cutter and swinging the arm with anchors, soil is excavated. The loosened soil is then sucked up into a pipe which transports the material to its destination. Depending on soil characteristics and the distance to be moved, boosters are used to maintain the flow of the material. Once a full swing is made, the dredge moves forward by lifting the primary spud and using a second secured spud to propel the barge forward. Once in position to make another swing the primary spud secures itself in the ground.
A hydrodynamic dredge is a water injection dredge [5]. The water injection dredge works differently as it does not collect the dredge material. Multiple water jet nozzles are attached to a horizontal water jet bar. Once the bar is lowered into the water, jet pumps create a high flow of water through the nozzles. This causes the soil to fluidize and rise from the bottom. Ocean currents carry the fluidised soil away from the dredging area.

2.1.2 The History of TSHDs in the United States

Records of dredging with vessels began as early as 4000 B.C. in the time where the Egyptians were thriving and humongous structures on land were being built [6]. The first known ocean-going hopper dredge built in the United States was the General Moultrie [7]. It was operational in 1857, constructed of wood, and propelled by a single non-condensing engine. It was capable of dredging 250 m^3 per working day. The General Moultrie was a casualty of the Civil War between 1861 and 1865. While improving the mouth of the St. Johns River in 1871, Q.A. Gillmore was authorized to convert a steamer

into a hopper dredge. The Woodbury, was converted to deepen the Cape Fear River in Wilmington, North Carolina. This was the second steamer converted into a hopper dredge. In 1884, the government started putting out contracts for widening and deepening canals and harbors. These government contracts laid the foundation for private companies to be stablished and flourish. Joseph Edwards Dredging Co., Metropolitan Dredging Co. and Great Lakes Dredge and Dock (named Lydon & Drews dredging company in that time) was founded in the period of 1890 – 1900. The number of hopper dredges being built started to increase. Instead of wooden hulls the dredges were made of steel hulls. The hopper capacity increased, as well as the horsepower on board and the amount of dredged material per working day. Following World War I laws and legislation were created by the federal government to stimulate and protect the American economy. Around the 1940s, two main causes affected the number of dredges being built. World War II began in 1939 and technological advances were being made. Old dredges had to be replaced with new ones. The new dredges would be more efficient and had even larger hopper capacity, greater manoeuvrability and higher speeds. The old dredges were demolished or refitted with new engines and dredging equipment. Dredges and technology continue to advance. Companies began to globalize as the need for international jobs to be completed became more prevalent. Multiple types of dredges were developed and focussed on more specific types of operations. As commercial vessels were getting larger, more canal deepening was needed. This also meant that larger dredges were needed to fulfil the need for deeper canals and port entries.

2.1.3 Working Principle of a TSHD

One of the vessel types used to recreate landscapes and deepen waterways is the TSHD. It is an ocean-going vessel that is used for a variety of operations [8]. In Figure 4: Representation of a TSHD, a view of a TSHD is presented. The biggest part of a TSHD is a large empty space meant to hold the excavated material, this is called the hopper. To loosen the soil of the dredged area, dragheads are trailed over the bottom. They excavate and suck up the soil. A vacuum is created in the draghead by centrifugal dredge pumps. With the movement of the vessel, water jets and the created vacuum, the soil of the sea bed is transported to the hopper. The soil enters the hopper through the suction pipes. While in transit, two (or less common one) dragarms are equipped on each side and rested on the deck of the vessel. When the dredge is loading, the dragarm(s) are lowered into the water until the draghead touches the bottom. Winches are used to substantiate the draghead and dragarm on both sides. The wheelhouse is in the front (in this case) of the vessel. TSHDs have got some advantages over the other types of dredges [8]. They are more manoeuvrable, which enables them to work within a larger variety of areas. As most TSHDs are ocean-going, they can sail across the ocean or sea to access the dump or dredge area. However, TSHDs are not without limitations. These limitations are mostly due to weather and sea conditions while dredging. The swell compensators absorb the variation of the height of the waves to a certain limit. Above that limit, the draghead loses connection with the sea floor and smash back on it due to the motions of the vessel caused by the waves. Accuracy of the area that has to be dredged is another downside of the TSHD. In general, the precision of the position of the draghead is not very accurate. Some causes of the inaccuracy are the current, the motion of the vessel and the structure of the sea floor. The main components of dredging that are explained in more detail in the following sub chapters are the dragarm hoisting, dragarms and dragheads.

Figure 4: Representation of a TSHD

Source: GLDD

2.1.3.1 Dragarm Hoisting

The dragarms are kept in place by three different types of hoisting. In Figure 5, the swell compensator and davits are visualised and numbered.

Figure 5: View from the Bridge of the Dodge Island

Source: Photo by Dylan de Roode, 2019

The davit closest to the connection of the dragarm (also referred to as suction pipe) and the hopper is called the trunnion davit (1). The davit in the middle which holds the gimbal of the suction pipe, is called the gimbal davit (2). For both davits, no swell compensator is installed. The final davit is the draghead davit, which supports the draghead (3). In between the draghead davit and its winch is a swell compensator (4). The swell compensator is hydraulically driven. To keep the compensator in a centred position, a certain amount of force is required. An increase of force in a positive vertical motion results in the retraction or expansion to increase or decrease the distance between the draghead and the dredge. The swell compensator makes sure that the draghead maintains its position on the sea floor. A schematic visualisation is presented in Figure 6: Swell Compensator Schematically . To maintain the suction force of the draghead, a continuous connection between the bottom of the sea and the draghead is necessary. The continuous movement of the water surface creates motion of the dredge. The swell compensator compensates the heave, roll and pitch motions of the dredge with a result of no vertical motion of the draghead. The dragarms are attached to the side of the dredge, therefore, a vertical motion is one of the resulting forces of rolling and pitching. All other motions of the dredge are eliminated to a certain extend by the free movement of the attachment of the suction pipe to the hopper or the gimbal in the centre of the suction pipe. A pure surge motion only accelerates or decelerates the vessel and has no effect to the connection of the draghead with the bottom surface.

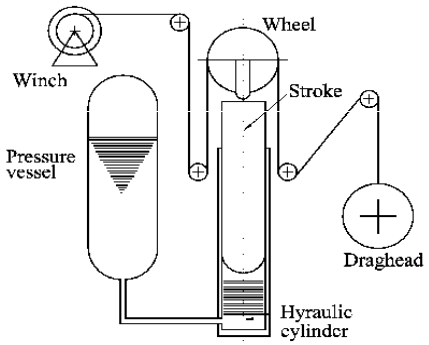

Figure 6: Swell Compensator Schematically [9]

The largest load on the generator(s) is the lowering of the suction pipe with the winches and davits, to be more precise, right before the suction pipe and draghead hit the water surface.

2.1.3.2 Dragarm

Part of the dragarm is the suction pipes, they connect the hopper to the draghead. The dredges that are used for this research all have suction pipes consisting of two parts, a lower and an upper part. The dragarm including the draghead is shown in Figure 7: Dragarm of a TSHD. The trunnion is connected to the upper part of the suction pipe (1) through a sturdy rubber hose (2) and an arm piece assembly (3). The connection between the upper and the lower suction pipe (4) is through another rubber hose and a turning gland assembly (5). This assembly allows three degrees of rotational freedom. The draghead is mounted to the lower suction pipe directly which does not allow any freedom of movement. The rotational movement of the draghead (6) is made possible because of the turning gland assembly. The last main component of the suction pipe is the jet hose (7). This hose transports the water through pressure to the nozzles.

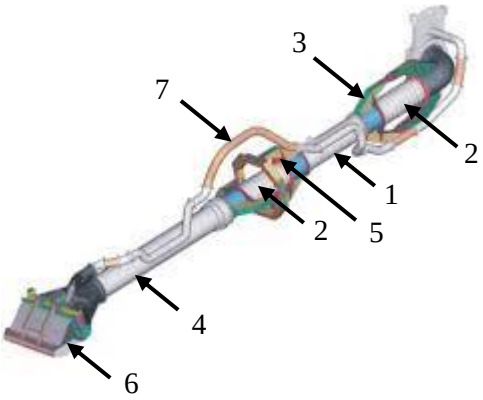

Figure 7: Dragarm of a TSHD

Source: https://www.royalihc.com/-/media/royalihc/products/dredging/hopper-dredging/trailing-suction-pipe-systems/d2-ps-suction-pipes-2015.pdf

2.1.3.3 Draghead

The draghead is connected to the end of the suction pipes. The main function is to excavate and fluidise soil so it can be transported to the hopper. A section view of a Tame Dragon Draghead is shown in Figure 8. The cutting teeth (1) are attached to the end of the visor (2). The visor is able to rotate and on the top of the visor a pin system (3) is mounted. This system enables the visor to be fixed at certain angles. The holes of the pin system determine the minimum and maximum angle of the visor during excavation. A floating visor is not fixed and rotates freely. Only the weight of the visor pushes the teeth into the soil. A fixed visor is forced to push the teeth into the soil to excavate a minimum layer depth.
Excavating soil consumes a lot of energy, to lower the energy requirement, jets are installed (4). Under high pressure, depending on the power of the jet engine, water is pushed through nozzles. The force of the water ejected by the nozzles fluidises the soil. This reduces the energy required to cut the soil dramatically. The mixture enters the suction pipes through the vacuum of the draghead created by the pumps.

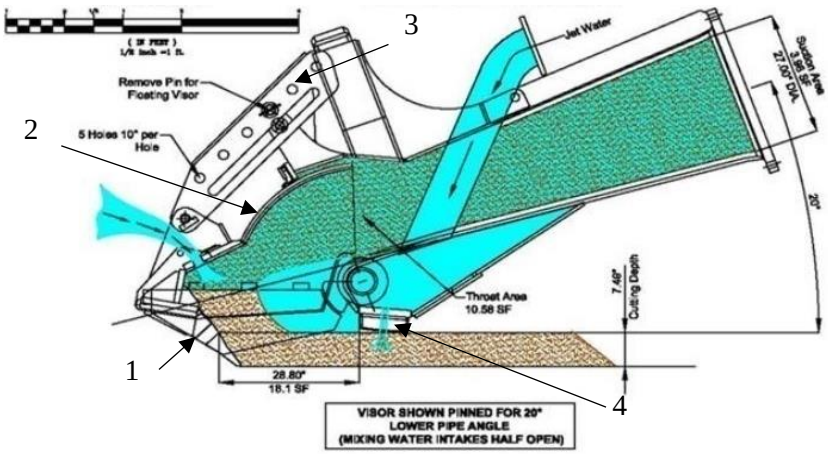

Figure 8: Section View of a Tame Dragon Draghead

Source: Great Lakes Dredge & Dock Excavation Presentation

The total cutting depth is determined by the following parameters:

- Speed of the dredge
- Length of the visor
- Weights of the visor
- Angle of the visor
- Width of the visor
- Length of the cutting teeth
- Angle of the cutting teeth
- Number of cutting teeth
- Penetration depth of the jets
- Weight of the draghead (with fixed visor)
- Lower arm angle (with fixed visor)

The draghead is directly attached to the distant end of the lower part of the suction pipe. This means that the angle of the lower suction pipe determines the angle that the bottom of the draghead makes with the ground. This angle is called the lower arm angle (LAA). In Figure 8 the LAA is 20 degrees, and the nozzle is not parallel with the ground as shown. The Tame Dragon Draghead is designed to have a lower arm angle of 25 degrees for the draghead to be parallel with the ground. The swell compensator makes sure the LAA varies as little as possible. With a fixed visor, the LAA directly influences the cutting depth and thus the total trailing resistance.

2.1.3.4 The Operation Cycle

Below, the components of a TSHD operation cycle are described. The cycle is divided into four or six phases. When discharging by the pipeline, the cycle contains six phases. When discharging by bottom dumping, the connecting and disconnecting phases don’t occur which leaves the cycle with four phases.

1. Loading
2. Transit Loaded
3. Connecting
4. Discharge
5. Disconnecting
6. Transit Empty

For a complete overview of the phases, a time diagram per operation is included in Figure 9: Timeline Volume Hopper TSHD . The vertical axis represents the tonnage of the dredge and the horizontal axis represents the time. In Figure 9 bottom dumping is used for the discharge method. When discharging by pipeline is used, the time to discharge is significantly longer.

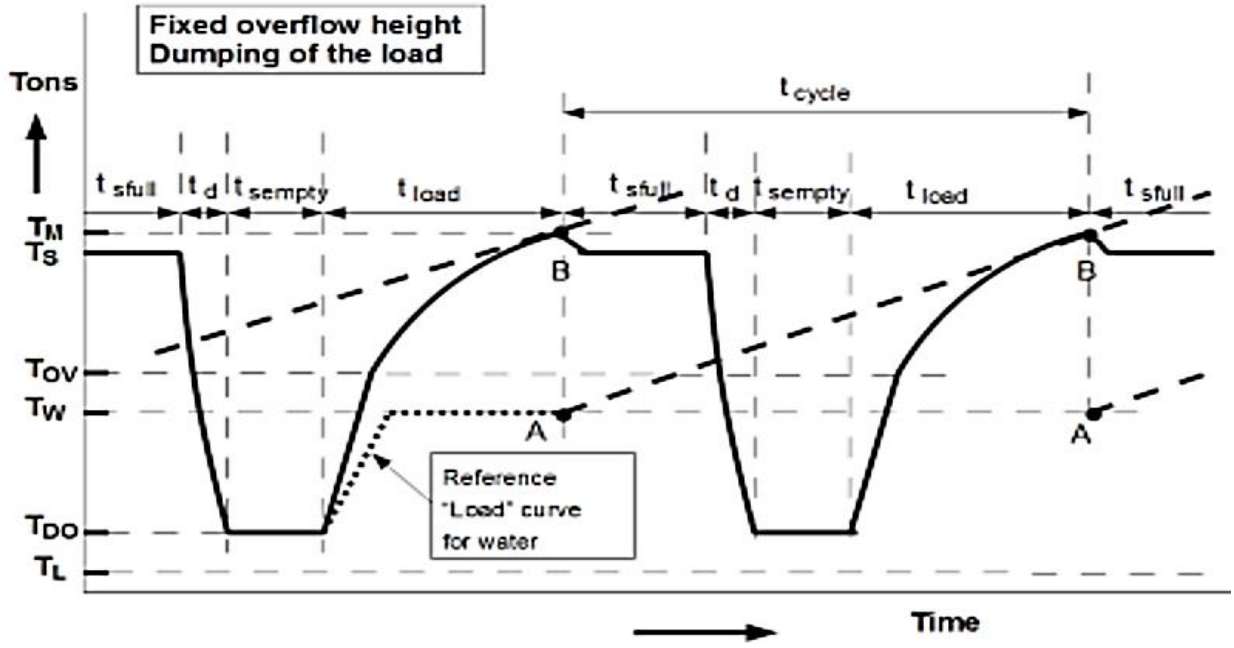

Figure 9: Timeline Volume Hopper TSHD [8]

Legend:

T_M	Max. loaded ship weight	t_{sfull}	Time sailing full (transit loaded)
T_S	Ship weight full after water sheet above overflow level has run off	t_d	Time discharging (unloading)
T_{OV}	Ship weight at start of overflow	t_{sempty}	Time sailing empty (transit empty)
T_W	Ship weight with load to overflow consisting of water alone	t_{load}	Time loading
T_{DO}	Ship weight with 'water load' up to external water level	t_{cycle}	Time cycle ($t_{sfull} + t_d + t_{sempty} + t_{load}$)
T_L	Ship weight of empty vessel		

Loading

The cycle begins when the dredge starts to load at t_{load}, the tonnage increases rapidly up until the mix of water and sand fills the hopper. From that point (T_{ov}) the loading takes longer. The overflow of water slowly flows away as the soil settles in the hopper. To acquire a constant flow of loading, the speed of the vessel is constant. TSHDs sail over the borrow area where soil is available or an area that has to be deepened. With the dragarms lowered, the dragheads excavate the bottom and the loosened soil is sucked up by dredge pumps. The soil is pumped up to the chute and spread in the hopper by a diffusor [8]. To reduce the settling time of the soil, the diffusor is mounted at the end of the chute. With a reduction of the settling time, the loading time therefore decreases. The overflow of the TSHD enables the redundant water to flow out of the hopper. The more water the hopper can drain off, the larger the volume of material is loaded, the more efficient the operation is. Once the hopper reaches its maximum capacity, the vessel sails to the discharge location.

Transit Loaded

At t_{sfull}, the transit to the discharge area begins. The soil continues to settle and the redundant water floats on top of the soil. The speed of the vessel increases to cruise speed, TSHDs are mainly designed to carry heavy loads and sail at moderate speeds. As the power increases quadratically related to the speed, a lower speed can save fuel. The trade-off is to be made whether this result in a reduction of the total operation cost or not. At the start of t_d, the next phase begins.

Connecting

The connecting phase starts when the dredge connects to the pipeline if discharge is by a pipeline to the shore. The dredge sails slowly to the connection pipe. The discharge pipe at the bow of the dredge should be directly above the connection end of the pipeline. The connection of the dredge and the pipe takes place. The dredge maintains position the whole time a discharge takes place. This connection phase takes just several minutes. In Figure 10: Dodge Island Connection Phase the floating components of the pipeline are visible. The Dodge Island is approaching the pumpkin (1) to connect it to the discharge pipe at the bow. The pumpkin is connected to the float hose (2) which is connected to the cube (3). The cube is connected to the pipeline which goes to the shore.

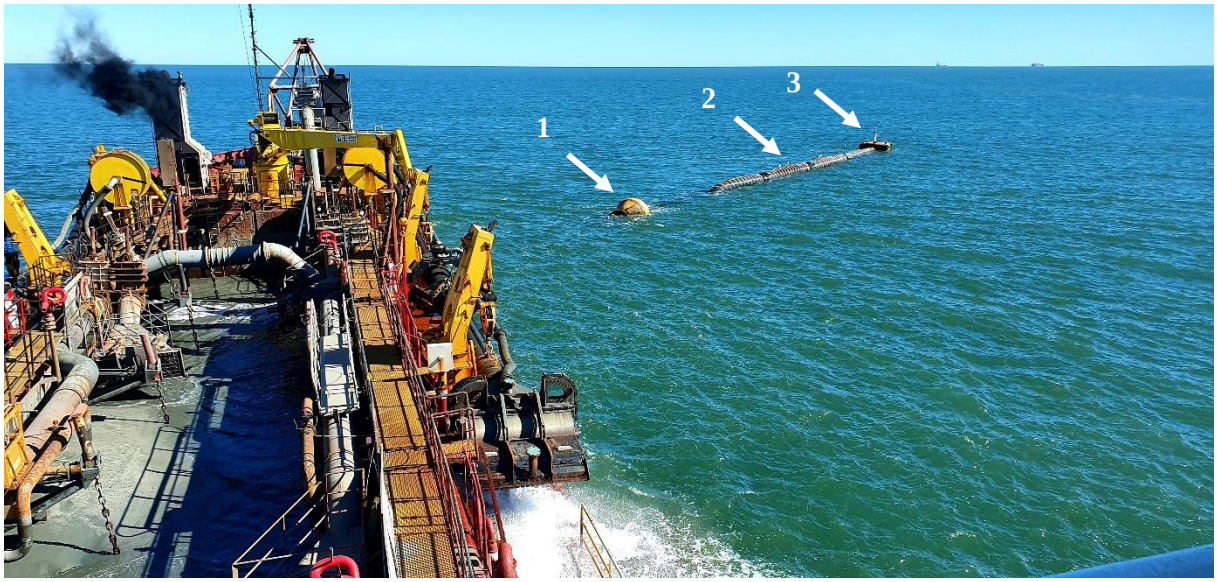

Figure 10: Dodge Island Connection Phase

Source: Photo by Dylan de Roode, 2019

Discharge

At the discharge time (t_d), the discharging begins. As previously mentioned, the time can vary depending on the discharge method. The rainbowing method and discharging by pipeline are the slowest. Discharging by splitting the hull (opening the bottom dump doors) is the fastest. Discharging by pipeline takes more time to unload. The soil is being pumped up from the bottom and exits the dredge through the bow connection. At the location there are multiple options to discharge. The TSHD can connect to a discharge pipe and pumps out the load. Some TSHDs are able to split their hulls where the load is being dropped all at once. Another option is discharging the load by a pump on the bow into the dropping area, this is called rainbowing (see Figure 11: Discharge by Rainbowing). When the TSHD has discharged the cargo, it sails back to the dredging area. The dredging cycle can start over from the beginning until the job is done. For discharging via a pipeline, the discharge pump is connected to the pipe. For rainbowing, no connecting actions are required. For discharging by splitting the hull also no connecting method is required. There are two different connection types used within GLDD for direct pump. The first one is the cube setup, which allows the dredge to be able to rotate around the connection

with current, wind and waves. The second setup is the traditional setup, where the dredge can dispose in shallow water but it requires a tender tug or stern anchor to hold the dredge in position [9].
In terms of weather conditions during operations, THSDs are capable of dredging within waves up to a height of 2 metres. They are able to dredge in rougher conditions compared to most other types of dredges. The limiting factor is the direct pump connection as waves of approximate 1.5 metres will cause trouble. As safety is of the utmost importance, operations will cease in rough weather conditions [9].

Figure 11: Discharge by Rainbowing

Source: https://images.app.goo.gl/tvoq6Z35WhAhmY9K9

Disconnecting

Disconnection would occur only after the discharge is complete. Logically, disconnection is only necessary if the dredge was connected. This phase takes a short amount of time, same as the connecting phase. Connecting and disconnecting can be completed within 7 minutes.

Transit Empty

After the dredge empties the hopper, it is time to sail back to the dredging area. The speed while sailing back is higher than the transit while loaded. The draught and thus displacement are less and with equal power, the dredge can sail faster. This phase is denoted in the diagram as T_{sempty}. When the dredge arrives at the dredging area, the operation can start from the beginning (loading) again until the job is complete.

2.1.3.5 Power Arrangements for a TSHD

On board a TSHD, there are multiple different large energy consumers. The dredge has to perform multiple actions for each phase. The power arrangement can have a large effect on the fuel consumption and the performance of the dredge. This chapter gives an overview of the available power arrangements for TSHDs. There are trade-offs to be made for providing energy on board of a dredge. Factors that should be considered are the environment, cost, space on board, weight of equipment and machinery, redundancy and manoeuvrability.

Propulsor

In terms of types of propulsor there are two main options: The fixed pitch propeller (FPP) and the controllable pitch propeller (CPP). As the name suggests, the fixed pitch propeller is a solid propeller with a fixed pitch angle. The open water diagram of such propeller is fixed as well and the propeller has got an optimal advance ratio (J). The advance ratio is expressed with the incoming speed (v_a) of the water divided by the rotations of the propeller (n) multiplied by the propeller's diameter (D).

$$J = \frac{v_a}{n * D} \tag{1}$$

For each value of the advance ratio, a FPP operates with a certain efficiency. This efficiency is determined by tests and is plotted into a diagram. When the ratio of pitch divided by diameter varies, the efficiency of the propeller also varies. These efficiencies can be plotted into a diagram, known as an open water diagram as shown in Figure 12. The x-axis represents the advance ratio and the y-axis represents the propeller efficiency, thrust coefficient and torque coefficient. The thrust and torque coefficient are used to determine the available thrust and torque at a certain advance ratio with the following equations.

For thrust:

$$K_T = \frac{T_o}{\rho * {n_p}^2 * D^4} \quad (2)$$

For torque:

$$K_Q = \frac{Q_o}{\rho * {n_p}^2 * D^5} \quad (3)$$

A FPP is solely depending on the advance ratio in terms of efficiency. When a dredge is equipped with a FPP, the loading phase becomes highly inefficient. The incoming flow of the water to the propeller is low as the dredging process produces high trailing forces. High amounts of thrust is required by low speeds. Because of that, it is not uncommon that the efficiency drops to 10%. Controllable pitch propellers are more efficient at low speeds and high thrust and torque demands. As the efficiency curve shifts by rotating the blades, the efficiency changes at a certain advance ratio. The diameter of the propeller affects the efficiency as well. The larger the diameter, the higher the propeller efficiency. There are limitations to maximum diameter of the propeller. The larger the diameter, the more power one rotation requires. Available power to the propeller is one of the limitations. Another one is related to the available space between the propeller and the hull. The hull limits the maximum diameter together with the angle of the shaft to the propeller.

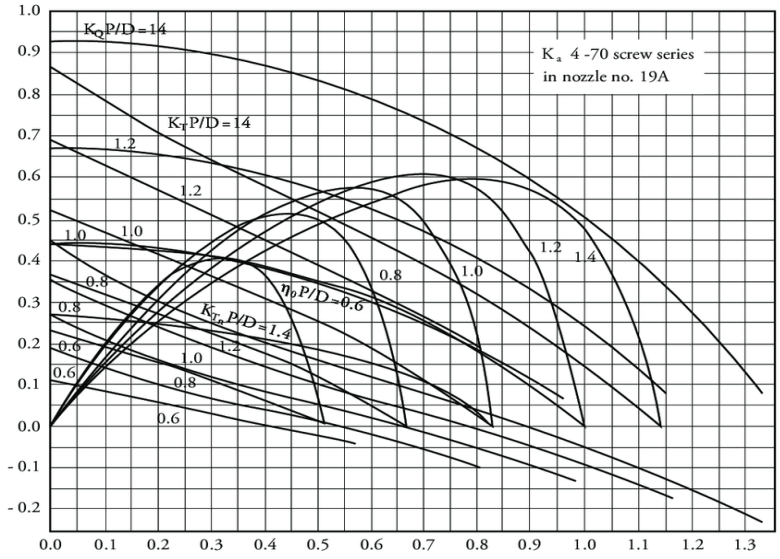

Figure 12: Open Water Diagram for a K4-70 Propeller with Nozzle 19A

Driving Machines

Mechanical energy produced by driving machines is provided to the propulsor and are called a mover. Movers are called primary movers when the energy that is provided is created by primary energy such as fossil fuel or gas. Within the maritime industry, the diesel engine is a widely used prime mover. Other providers of energy is an electric motor. Often the electric driver is separated from the electric power generation. This segregation increases the functional redundancy of the vessel. A combination of the prime mover and the electric mover is convenient. With a power take-off (PTO), the electricity is produced to power energy consumers. One of the advantages of electricity is the usability as it can be easily transferred through cables throughout the dredge.

Transmission

The power transfer between the driving machines and the propeller is through a transmission. The optimal propulsor rotation speed and the rotation speed of the mover can differ. In this case a gearbox is recommendable. A direct drive is possible when the rotational speed of the mover equals the rotational speed of the propulsor. Whether a direct drive or gearbox is fitted within the vessel depends on the optimal rotational speed of both propulsor, mover and the design speed of the dredge. The transmission connects the driver to the propulsor and is designed for the both of them for optimal efficiency. A clutch is used within the transmission to provide an easy start-up for the mover(s) after they have been shut off. A gearbox can combine two movers and convert the energy into one output. The output of the transmission is driven by one or multiple movers with the use of the clutch.

Mechanical Propulsion Arrangements

These types of arrangements are the most direct and less complex arrangements. In a full mechanical power arrangement, the propulsion and all pumps are mechanically driven. Each pump and propulsor is powered by an individual prime mover. This is shown in Figure 13. An advantage of this specific setup is the controllability of the movers. Each mover is controlled separately which increases the precision while operating. The soil density can be kept at a more constant value with more precision during loading. The density of the soil is controlled by variating the power to the pumps.

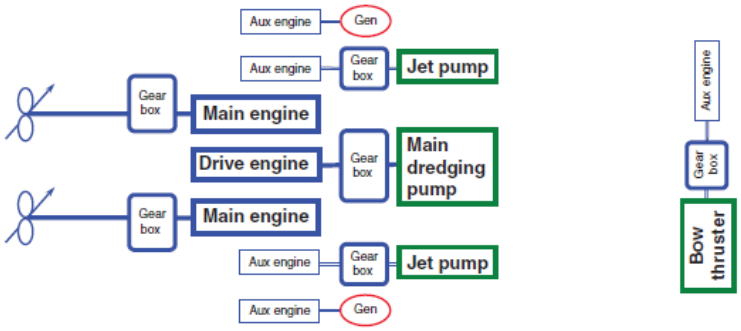

Figure 13: Fully Mechanical Power Arrangement [58]

Another variation of a mechanical power arrangement is shown in Figure 14: Mechanical Power Arrangement with PTO. Through a PTO from the main engines, the dredge pumps, jet pumps and bow thruster are electrically driven. The generators driven by the PTO convert mechanical energy into electrical energy, which is distributed by a switchboard to the pumps and bow thruster. A wide variety of mechanical power arrangements are possible. As mentioned at the beginning of this chapter, the most convenient arrangement depends on several factors including the factor of risk. The acceptance of a certain risk of a non-operational dredge is ultimately determined by human intuition and not necessarily by equations.

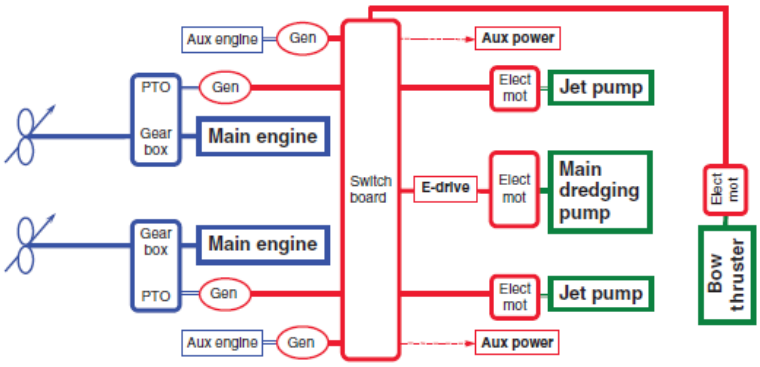

Figure 14: Mechanical Power Arrangement with PTO [58]

Electrical Concepts

A fully electrical dredge is rarely used. GLDD performed in the past a beach nourishment within the state of California. State Authorities require dredges to operate without emissions for most of the jobs. GLDD made one of their cutter suction dredges fully electrical especially for that job in California. The required power to dredge was delivered through a cable which was connected to a power source on the shore. This is one way to operate a fully electrically driven dredge. Electrical concepts offer some advantages over the traditional mechanical power arrangement. As electricity is easily transferable, location of engines, pumps and other energy consumers are flexible. With this flexibility, important dimensions such as draft of the dredge and hopper size can be optimised as less space restrictions apply. Electrical energy is more direct in comparison with energy from prime movers, this can increase the controllability of the dredge pumps which result in a higher dredge efficiency. This efficiency can also result in fuel saving which is another advantage. Figure 15: Integrated Electrical Power Arrangement shows a power arrangement where cruise and main engines provide energy to the generators which convert the mechanical energy into electrical energy. The switchboard transfers the electrical power to the electric motors. A more advanced power arrangement is shown in Figure 16: Integrated Electrical Power Arrangement with Energy Storage. In addition to the previous power arrangement, an energy storage has been included. An overproduction of electrical energy produced by the main engines is stored into batteries. Within this arrangement, the propulsor is provided by energy of both the batteries and the main engines. When peak power is required, all the stored energy of the batteries is used in addition to the energy of the main engines.

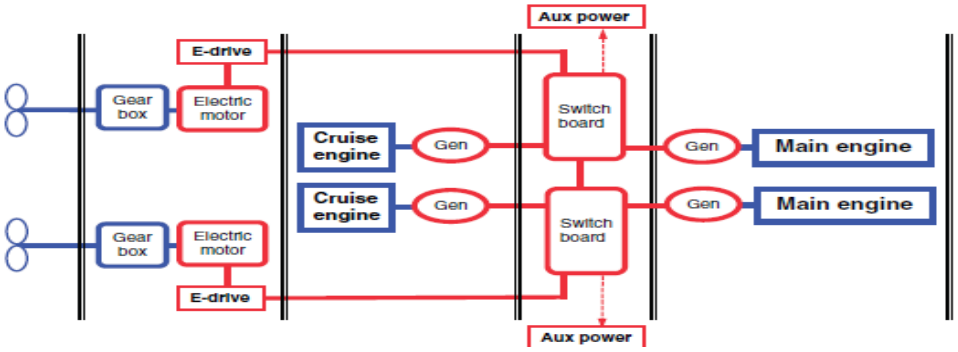

Figure 15: Integrated Electrical Power Arrangement [58]

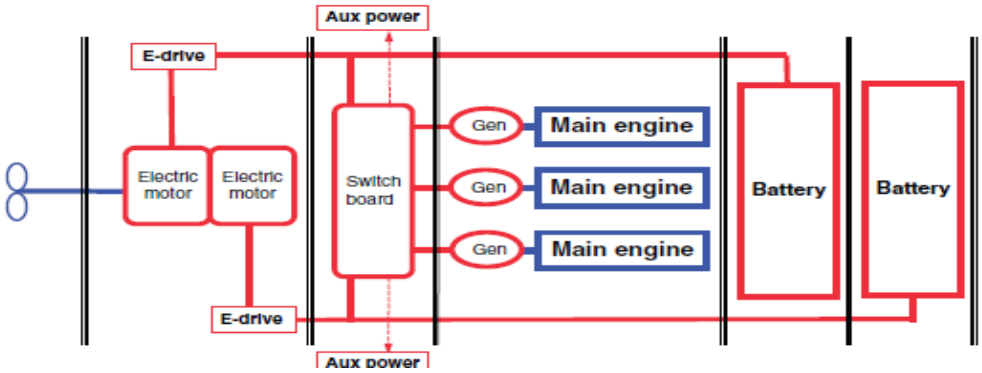

Figure 16: Integrated Electrical Power Arrangement with Energy Storage [58]

Hybrid Concepts

A combination between a mechanical and electrical power arrangement is the hybrid power arrangement. Some pumps and propulsors are driven by electrical power, some are driven by mechanical power. Figure 17: Hybrid Power Arrangement shows a hybrid concept. Two main engines and two auxiliary engines provide electrical energy to the switch board. This energy powers the propulsors and the jet pumps. The dredge pump and bow thruster are provided with mechanical energy.

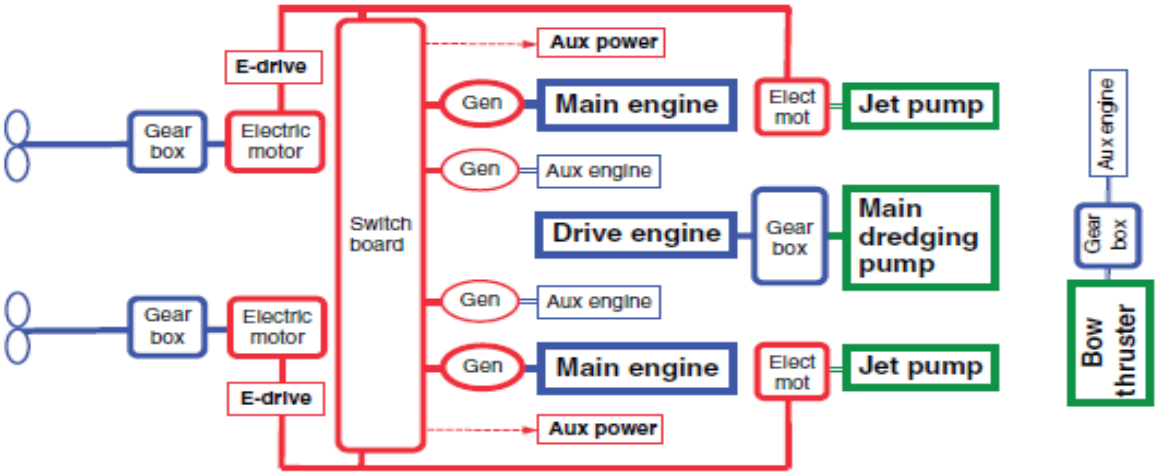

Figure 17: Hybrid Power Arrangement [58]

2.1.3.6 Soil Specifications

TSHDs are capable of dredging different types of soil. The draghead that is used plays a big role for the ability to cut through the soil. The emission model is only capable to calculate the emissions with multiple grain sizes of saturated sand. Therefore, saturated sand is the elaborated on.

Grain Size Distribution

Natural soil consists of many different sizes and shapes of grain. To describe the type of soil a grain size distribution is researched by Roberts et al in 1998. The soil behaviour is mostly dominated by the smaller particles. Three different percentages were introduced: 10%, 50% and 80%. These percentages were bounded to the grain size. As result, the effective size, the size of the particles consisting of 10% of the total particles (d_{10}) can be determined. In other words, when the d_{10} is for example 0.1 millimetre, this means that 10% of the grain size of the soil is smaller or equal to 0.1 millimetre. The same principle applies for d_{50} and d_{80}.

Porosity

The ratio between the voids within the material to the actual material is known as the porosity. For sand, it means the empty space between the grains. The porosity depends on the shape of the grains, the size of the grains and the distribution between the shape and the size. The porosity is expressed in a percentage, the volume of the void space (V_v) is divided by the total volume of the material (V_s):

$$n = \frac{V_V}{V_S + V_V} \tag{4}$$

Dilatation

When cutting through saturated sand it increases in volume and that is the result of dilatancy. Dilatancy is the pore volume change as a result of shear in the sand. The dilatancy can be found with the following equation:

$$\varepsilon = \frac{n_{max} - n_i}{1 - n_{max}} \tag{5}$$

The maximum (n_{max}) and initial porosity (n_i) of the material determine the dilatancy.

Internal Friction Angle

The angle of Mohr's Circle for a given soil can determine the angle of internal friction. In practise, the angle of internal friction is being determined by the number of blows into the material. This is called a standard penetration test (SPT) [10]. A pipe with a certain diameter and length is laid vertical on the material and is driven a 150 millimetre into the material. A slide hammer with a determined weight is dropped from a certain height onto the pipe. The pipe forces its way through the material with each blow of the slide hammer. The number of blows is counted until the pipe reaches a depth of 450 millimetre. As the material that has to be dredged is pressurized by the water at a certain depth, the result of the SPT has to be adapted. With a water depth of 10 metres, the internal friction angle relates to the number of blows as follows [11]:

$$\varphi = 51.5 - 25.9 * e^{-0.01753 * SPT_{10}} \tag{6}$$

In practise, for preparation of the bidding process to acquire a job, the to be dredged material is being investigated. One of those tests of the material is the standard penetration test.

Permeability

In geology, permeability can be described as the capability of a sediment to allow liquids or gases to pass through its pore spaces [12]. The permeability of sand is estimated from the Kozency-Carman equation:

$$k = 8.3 * 10^{-3} * \frac{g}{\nu_1} * \frac{n^3}{(1-n)^2} * d_{10}^2 \tag{7}$$

The g represents the gravitational force, the viscosity as ν_1, the porosity as n, and the d_{10} as the effective size of the sediment grains. The limit for this equation for soil is the effective size between 0.1 and 3.0 millimetre.

2.2 Greenhouse Gasses

Basic information and importance about the GHG are covered in the first sub chapter. The effect of the GHG is touched up upon and historical data of GHG is presented. In the second sub chapter, the past and the future effects of global warming are explained. The emissions of a diesel engine are discussed in the last sub chapter.

2.2.1 Importance of the GHG to the Planet

Greenhouse gasses can be defined as "any of various gaseous compounds that absorb infrared radiation, trap heat in the atmosphere and contribute to the greenhouse effect." [13]. To maintain an average habitable temperature on the Earth, greenhouse gasses are one of the main attributors. Problems occur when the concentration of gasses in the atmosphere is out of balance. This causes a too big or a too small greenhouse effect. The concentration of GHG has been on a steady incline over the last 40 years due to the burning of fossil fuels. Burning fossil fuels produces among other gasses CO_2, which is the most harmful gas as it is released in large quantities.

Each greenhouse gas absorbs a certain wavelength. Greenhouse gasses absorb heat provided by the sun and the Earth's surface (land and sea). Gradually over time, the absorbed heat is radiated to the surface of the Earth. The specific wavelengths per GHG is known which makes it possible to determine the concentration of the gasses in the atmosphere [14]. CO_2 and the water vapour in the atmosphere have a close relation. Water vapour evaporates more when the CO_2 concentration increases, this amplifies the greenhouse effect. This phenomenon increases the importance of the contribution of CO_2 in the atmosphere.

The following gasses are recognised as GHG:

1. Carbon dioxide (CO_2)
2. Methane (CH_4)
3. Nitrous oxide (N_2O)
4. Fluorinated gasses (F-gasses)

2.2.2 The Past and the Future Effects of Global Warming

The average temperatures and concentration of molecules in the atmosphere are traced back to several thousands of years. According to historical data, the relative fast increase of temperature on the Earth is globally noticed.

The Past

The average temperature of the Earth is increasing. The graph in Figure 18 provided by NASA shows the temperature rise of the global mean based on land and ocean data since 1880. Most of the climate changes are caused by a small variation of the Earth's orbit. The Earth endured a dynamic variation in temperature over the last million years based on oxygen isotope thermometry of deep-ocean sediment cores [15]. Temperature swings are not uncommon when looking back a million years. The rise in temperature over the last 200 years can be the effect of humans or be just a natural phenomenon. According to the IPCC Climate Change Synthesis Report, it is "extremely likely" that the increase of global temperature is cause by anthropogenic increase of GHG [16].

Over the period of 800,000 years, the highest concentration of CO_2 in the atmosphere is around 300 ppm [17]. For a visualisation, see Figure 19: CO2 Concentration over the Past 800,000 Years. More than 3 million year ago, the temperature of the surface of the Earth was 2-3 degrees Celsius higher in comparison with today's temperature. The sea level was higher as well, with 15-25 meter. The higher temperature and sea level occurred with a concentration of CO_2 that was equal to today's concentration. Whether these facts are directly related to the concentration of CO_2 is unknown.

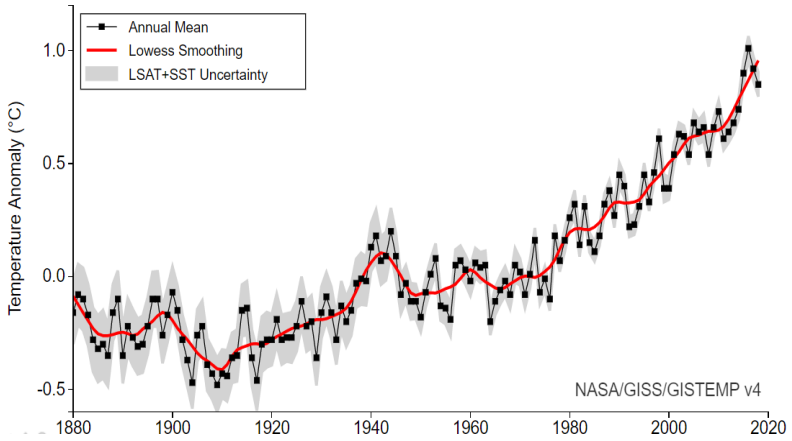

Figure 18: Global Mean Estimates Based on Land and Ocean Data [59]

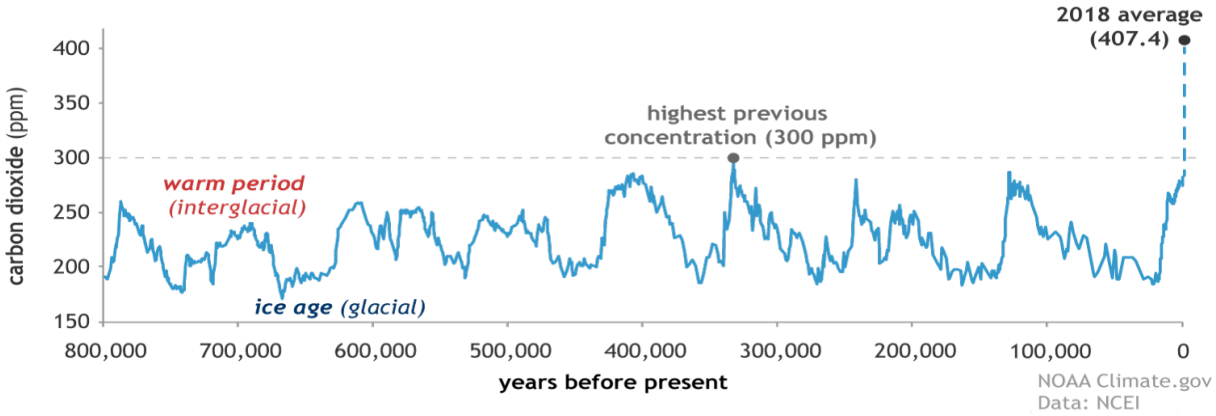

Figure 19: CO_2 Concentration over the Past 800,000 Years [19]

The Future

The IPCC forecasts a global temperature rise of 1 to 4 degrees Celsius [18]. According to the Third and Fourth National Climate Assessment Report this rise in temperature produces some significant changes to the conditions on the Earth. The strength of the hurricanes and other storms will likely become stronger over the years. Large parts of the U.S. will face a higher risk of extremely long droughts by 2100 that can last for decades. These droughts have the potential to last for decades and will diminish the amount of fresh water available agriculture and cattle. With regard to flora and fauna, the plants that use CO_2 to produce O_2 will become less nutritious. Animals move to habitats where they are most comfortable. This means that they move up north, following their ideal temperature. Species that are not able to adapt or move are likely to become extinct.

Global warming increased the average temperature of the ocean [19]. Currently, the oceans provide 50% of the Earth's oxygen. One of the consequences of the increased temperature of the ocean is acidification. Acidification occurs when the salt water from the ocean absorbs the CO_2 from the atmosphere and the water becomes more acidic because an increased number of hydrogen ions are produced. The increase in ions means a decrease in carbonate ions. The pH levels dropped by 0.1 since the pre-industrial revolution times [20]. For the flora and fauna in the ocean, this results in calcification for shellfish and corals. This shifts the marine ecosystem that rely on the shellfish and the coral. Acidification can have catastrophic consequences to our marine life and the people who rely on it.

2.2.3 Contribution of Exhaust Gasses of Diesel Engines to the Environment

Using ultra-low sulphur diesel (ULSD) reduces the SOx emission to the limit set by the IMO. The composition of exhaust gasses from a diesel engine is given in Figure 20. The pollutant emissions are less than 1% and consist of CO, HC, NOx, SOx and PM [21]. The content of sulphur in ULSD is lowered, this is beneficial for the environment. The reduction brings also some negative effects. The natural lubricity of the fuel is reduced, which increases the wear of the engine. A fluid that increases the lubrification of the engine can be added to reduce the wear. The energy density of ULDS is less than MDO or HFO, this affects the fuel consumption as less energy is available per unit of volume of diesel.

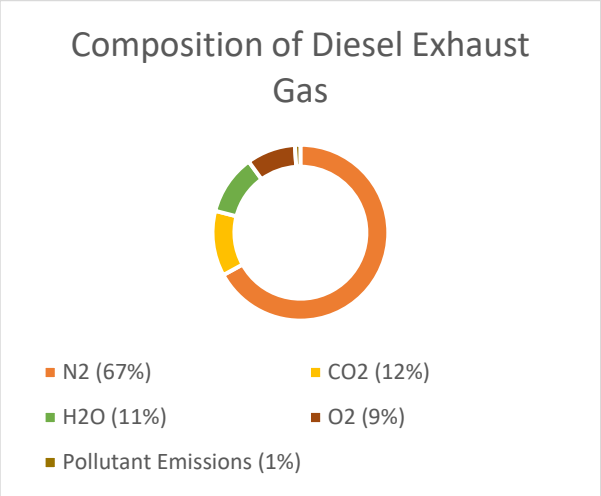

Figure 20: Composition of Diesel Exhaust Gas [23]

2.2.3.1 Effect of Nitrogen Oxide

Multiple causes can lead to the production of NOx. Such causes are: improper air and fuel ratio for combustion, high temperature in cylinder, heavy load on the engine and bad quality of fuel [22]. The highest concentrations of the NOx family consist of nitric oxide (NO) and nitrogen dioxide (NO_2) [23]. NOx contributes to various health and environmental issues. When NOx come in contact with UV rays, the composition breaks apart and form ozone (O_3). Ozone at ground level affects human health. It has the potential to cause pre-mature mortality and asthma, among various other issues. In the atmosphere, ozone reduces the amount of UV radiation from the sun that reaches the Earth's surface [24]. Nitric acid is formed in presence of water molecules like rain. The nitric acid contributes to acid rain.

2.2.3.2 Effect of Sulphur Oxide

The more fuel gets refined, the lower the sulphur content is. The large engines that dredges use for propulsion and dredging use low grade fuel with high concentrations of sulphur. Due to the sulphur cap, as is explained in Chapter 2.3.1.3 SOx Emission Reduction, more refined fuels are made available for maritime purposes. Sulphur dioxide (SO_2) is part of the SOx family. SO_2 contributes to acidic deposition together with NOx mentioned in the previous chapter. Furthermore, SO_2 is a precursor to particular matter, to be more precise, PM2.5. Fine particular matter, such as PM2.5, is harmful as they are small enough to be inhaled. Particular matter can cause serious health problems when they get into the lungs or even bloodstream.

2.3 Environmental Rules and Regulations for Dredges

The first subchapter focusses on worldwide rules and regulations. How independent companies and agencies influence the shipping industry and therefore, the dredging industry is discussed. In the US there are different regulations per district, which is explained in the second sub chapter.

2.3.1 Current Rules and Regulations Worldwide

The IMO is a specialized agency with the responsibility for safety and security of shipping and the prevention of marine and atmospheric pollution by ships [25]. The Marine Environment Protection Committee (MEPC) is the department within the IMO concerned with the prevention and control of pollution from ships [26]. One of the conventions is the International Convention for the Prevention of Pollution from Ships (MARPOL).

2.3.1.1 CO_2 Emission Reduction

The relevant Annex regarding reduction of the GHG and thus the CO_2 emission is Annex VI Prevention of Air Pollution from Ships. This Annex attempts to reduce the GHG by applying a Ship Energy Efficiency Plan (SEEMP) and an Energy Efficiency Design Index (EEDI). On 1 January 2013 it is made mandatory to all ships over 400 gross tonnage to have a SEEMP. For new ships the EEDI went into force. However, an Administration may waive the requirement for new ships from complying with the EEDI [15]. As the regulations to reduce air pollution are applicable to all vessels, dredges have to comply to the standards as well. On the 13th of April 2018 the resolution MEPC.304 (72) was adopted. The MEPC includes a reduction of GHG emissions consistent with the Paris Agreement temperature goals. The aim is to reduce the total annual GHG emissions by at least 40% by 2030 and 50% by 2050 compared to 2008 [2].

Within the shipping industry, few GHG stand out. The CO_2 emission is the largest contributor of the GHG. As mentioned, the biggest cause of the excess of CO_2 is burning fossil fuels. The shipping industry emits around 940 million tonnes of CO_2 per year [27]. This is equal to 2.5% of the total emitted CO_2. This percentage is a result of the Third IMO GHG Study of 2014 of period 2007 – 2012 [28]. The IMO plotted multiple scenarios which all show an increase in CO_2 emissions of between 50% and 250%. The study is based on international shipping, so the scenarios for future emissions are also based on international shipping. Dredges are outside the scope of research of the IMO. Nevertheless, dredges need to comply with the rules and regulations adopted by the nation, country and/or district.

2.3.1.2 NOx Emission Reduction

Vessels with a diesel engine that can produce more than 130 kW are subjected to the NOx control requirements. Over the years, since the first of January 2000, a limit was determined of the amount of NOx that was allowed to be produced. This was known as tier I, which limits the NOx according to a certain engine speed (rpm) and engine power output. In January 2011, tier II was introduced. Five years later tier III appeared. Every tier limits the NOx emission further. Figure 21 shows the NOx limits of tier I, II and III in grams per kilowatt-hours to the rpm of the engine. The year the construction of the ship was finished determines the tier and thus the NOx limit the diesel engines have to comply with. Tier I and II are applicable globally, tier III only applies within ECAs (see Chapter 2.3.2). For each NOx certified diesel engine, a NOx Technical Code 2008 must be present on the vessel. The flag State of the vessel test the limit of the NOx and provides an Engine International Air Pollution Prevention (EIAPP) Certificate.

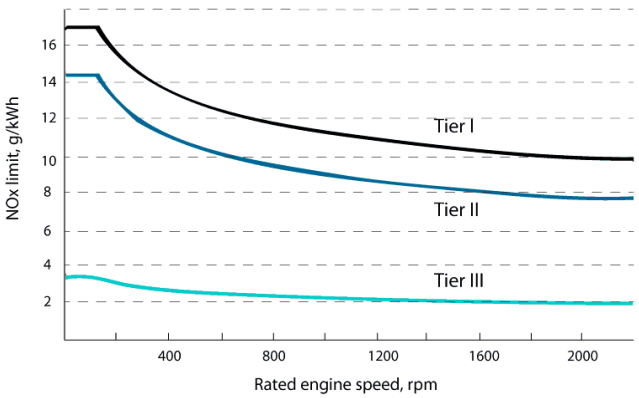

Figure 21: NOx limit for Engine Tier I, II and III [61]

2.3.1.3 SOx Emission Reduction

Different limits for SOx emissions are set for inside and outside an ECA zone. Outside an ECA zone, the limit went from 4.50% m/m (mass per mass) prior to 1 January 2012 to 3.50% m/m after 1 January 2012 [29]. The new limit has been set at 0.50% m/m after 1 January 2020. Inside the ECA, prior ships to July 2010, the limit was 1.50% m/m, after July 2010 1.00% m/m and from 1 January 2020 0.10% m/m. For to comply with the new limit, ULSD is widely used. ULSD is the cheapest short-term option. Ships which operate inside and outside the ECA can use blends of fuel to reduce the cost and still comply to the set limit. Another option, which requires a higher investment and more space on the ships is the use of scrubbers. Exhaust gasses pass through a scrubber where a mixture of chemicals and water react to the SO_2. The reaction removes the SO_2 up to 95% or more [30]. Scrubbers are explained in more detail in Chapter 4.2.4.

2.3.2 Rules and Regulations in the U.S. and the Individual States

The United States law that implements the MARPOL and the Annex VI is the Act to Prevent Pollution from Ships [31]. This act is applicable to vessels operating within 200 nautical miles of the coast or in U.S waters. Because of the APPS, it is a crime for any person to knowingly violate the MARPOL, the APPS or regulations under the APPS [32].

The EPA is an independent agency formed in 1970 as result of the necessity to protect the environment of the United States. In that time, President Nixon sent to Congress a plan to form a new agency. From then on, the environment was the responsibilities of the federal government and the EPA was formed. The EPA and the USCG will mutually cooperate to implement the MARPOL Annex VI as adopted in June 2011 [33]. In the ECA of North America, as shown in Figure 22, pollution limits of both SOx and NOx apply. The Annex VI limits the NOx emissions from marine diesel engines with a power output of more than 130 kW. The sulphur content of marine fuels is also limited accordingly to the Annex VI. To ensure diesel engines comply to the emission standards, the EIAPP certificate is required. This is issued by the EPA. For certain vessels, an International Air Pollution Prevention Certificate (IAPP) is required and issued by the USCG. Individual States can have more stringent regulations than the federal regulations. Texas, for example, states the following: No authorization or notification is required for any project that haves an increase of GHG if the requirements of the Texas Administrative Code § 116.164(a)(1) or (a)(2) are met. The TAC § 116.164(a)(1) states that new sources of GHG that have the potential or can emit 75.000 tons per year (CO_2e) are subjected to the Prevention of Significant Deterioration (PSD). Dredges have the potential to emit more than the given amount of CO_2e which means they are subjected to the PSD. Contractors take the liberty of setting limits to the emissions according to the regulations. In the future, the U.S. are dependent on the decisions of the IMO as the EPA adopted the Annex IV. The States are therefore dependent on the regulatory decisions of the IMO.

Figure 22: ECAs of the World [60]

2.4 Great Lakes Dredge and Dock Company

This sub chapter provides information about the Great Lakes Dredge and Dock Company and is divided into three sub chapters. The development of GLDD is presented within the first chapter. From the very beginning up until 2019, major events are described. The next chapter describes the current market of the company and the expectations for the future. The design philosophies are presented in the last sub chapter. These philosophies give guidelines to the viability of the methods previously presented to reduce the emissions.

2.4.1 Development of GLDD

The first job of the Lydon & Drews dredging company was to construct a tunnel in Chicago [34]. The tunnel would reach from a crib to the submerged water intake offshore in Lake Michigan. This crib is now known as the Two-Mile Crib. In 1894, the company built the first rig, Dredge No. 1. On the 2nd of May 1905, the company's name was changed to Great Lakes Dredge & Dock Company.

In the 70s, GLDD started to experience growth and began trading on the New York Stock Exchange (1971). The first Manhattan class hopper dredge was constructed in 1977, the Manhattan Island, soon to be followed by the Dodge Island and the Padre Island (1979). GLDD moved to their new headquarters (1978) and a holding company was formed (1979). Since the 70s, GLDD was bought by several companies and the fleet expanded with hopper, cutter and clamshell dredges. Projects were accepted around the world and GLDD became the largest American dredging contractor [35]. The Water Resources Development Act of 1986 provided GLDD with a large number of port deepening projects [36]. Four years later, in 1990, the first international job was successfully completed, a harbor at Jebel Ali in Dubai. Work in the Middle East continued with multiple jobs. For the year of 2000, several high-profile contracts were completed in multiple countries, including Denmark and Egypt. Within the U.S., GLDD expanded two California terminals, created Pier 400 in Los Angeles and improved the Port of Long Beach. After suffering from financial health from 2014, the company executed a plan to regain financial health in 2018. This turned out to be a success. During 2018 the company focused on winning, executing and completing five large, complex port deepening projects. To date, the company's fleet is the largest of all dredge companies in the States. In total GLDD owns 23 dredges, currently two are deployed internationally. The fleet exists of 13 hydraulic dredges, 6 hopper dredges and 4 mechanical dredges.

2.4.2 Dredging Market Future Outlook

The dredging market is divided into different types of operations. Dredging operations in the U.S. is divided into four types: coastal protection, maintenance, capital and rivers & lakes [37].

Coastal protection

Moving sand from the sea floor to the shore is the most general way of describing coastal protection. Due to erosion, the width of the shoreline decreases over time. It is an everlasting problem and therefore creates a continues workflow for dredging companies. 28% of GLDDs revenue of 2018 consisted of coastal protection work [37]. Over the years, erosion of the shoreline happens at a higher frequency. Beach nourishment (part of coastal protection), has shown to be the best solution to maintain the shoreline. Some other options are building sea walls, moving assets or relocating buildings.

Maintenance

Jobs that require maintaining waterways and canals where dredging already took place are called maintenance jobs. The main reason for maintenance work is river sedimentation. Other reasons are the underwater currents, ships with large drafts that stir up the bottom floor or rough weather conditions. Dredges deepen out the channel once again to maintain the depth. Every one to three years channels need maintenance and this creates a recurring source of dredging work.

Capital
Port expansions are the main project within the capital type of dredging. These projects consist of deepening channels and berthing basins. Other projects that would be categorized here are land reclamation, trench digging for pipeline and construction of breakwaters. Jetties or other marine structures are also within the capital type of dredging operations. What these operations all have in common is the immediate economic benefit to the ports and nearby communities. Capital work is mainly impacted by budgetary constraints and economic conditions.

River & Lakes
This type of dredging relates to a variety of dredging operations including construction dredging, environmental restoration and habitat improvements within rivers and lakes. GLDD found her very first foundation by dredging in areas of lakes and rivers (see previous chapter). The name of the company is related to those operations.

Clients
The largest domestic customer of GLDD is the U.S. Corps of Engineers (further mentioned as the "Corps"). In addition, GLDD completes projects for State and Local Governments and Port operators. The Corps is the largest federal provider of outdoor recreation [38]. One of the Corps' responsibilities is that of improving and maintaining navigation channels and harbors in the United States. The Corps uses its own dredging equipment as well as contracting with dredging firms.

The Corps operates more than 12,000 miles of commercial inland navigation channels, which is beneficial for GLDD as its customer. While the Corps is GLDD's largest customer they must win their work through a competitive bidding process. Multiple influences will affect the costs and therefore the outcome of the bidding process. Project site conditions, seasonality, location, complexity of a project contribute to the total cost of a project and the likelihood of winning a contract. According to the Annual Report of 2018, the most significant operating cost is the diesel fuel [37]. Approximately 9% of the contract revenues is the fuel.

Future Market
The future market is determined by the size and complexity of the job as well as government regulations and certification requirements. Focussed on the beach nourishment jobs, the number of jobs will increase as mentioned. With the rising sea levels and stronger storms, especially on the east coast, beach nourishment jobs are expected to increase. The sand on the beaches gets washed away faster because of the rough weather conditions.

2.4.3 Design Philosophy
Before a final design of a new dredge is created, many factors and trade-offs are taken into account. The design philosophy is formed with the future outlook and those factors and trade-offs. The factors that influence the design philosophy are split up into internal and external factors and are both guidelines to the path of designing a new dredge. To get a better understanding of the process of designing a dredge, a summary of the designing process of the Ellis Island is given. The trade-offs are based on multiple variables which are discussed at the end of this sub chapter.

External Factors

There are a few external factors that impact decisions of GLDDs investment decisions and the technology they choose. By law, the dredges must be built within the States. This brings both opportunities and restrictions. Companies in need for a vessel are restricted to what American shipyards have to offer. As there are no U.S. shipyards with extensive dredge-building experience, it is expensive and time-consuming to build modern dredges. The height of the building costs is another obstacle that influences the modernisation of dredges. Another external factor which has to be taken into account before designing a dredge is the expectations of the market. For the most reasonable prediction of the market, a market analysis is executed. For specialised dredges such as TSHDs which are mainly used for beach nourishments, the market is already determined.

Internal Factors

Next to the uncontrollable external factors, the internal factors are determined. GLDD aims to keep their dredges as simple as possible in order to reduce unnecessary costs and stay on budget. They try to maintain a fleet of dredges that use interchangeable parts to reduce the quantity of parts that need to be stored. This reduces the storage costs and the quantity of parts to store. The specifications of the dredges are determined mainly by the market and accumulated experience withing GLDD from the past. Experience of the past contributes by improving the dredge performance based on past flaws. On what market the company wants to focus depends and on what the company predicts what will happen and whether opportunities arise. Another internal factor that influences the design of new dredges is the available budget. The design process is related to the available budget and decisions are made with that in mind. In order to operate new dredges, the knowledge how to operate a dredge should be present just as the number of employees to operate the dredge. This might be a minor factor within the choice making of the design. To conclude, the following factors influence the design process:

External factors

1. Availability of knowledge within a shipyard to build a dredge
2. Expectations market
3. Availability technology
4. Height of building costs

Internal factors

1. Interchangeable parts
2. Focus on market

Ellis Island

The last constructed TSHD that GLDD added to the fleet is the Ellis Island. This part explains how the specifications of the Ellis Island were determined within the company. The dimensions, available power and dredge set-up (barge and tug combination) of the Ellis Island are determined by the past operational experience combined with the future expectations for the market. The goal of the Ellis Island being built was to be able to complete a wide variety of jobs. The need for a larger TSHD was noticeable as the capacity of the current TSHDs were barely enough to compete with competitive dredging companies. The past experiences of the crew on board the dredges and the experiences of the office employees are taken into account with the design. As the Ellis Island was going to be a large capacity TSHD, the number of required crewmembers increased. To decrease the required number of crewmembers operating on a large dredge, the decision was made to create a tug and barge combination. Regulations for this configuration allows the required number of crewmembers to be reduced. In addition, the separation into a separate tug and barge would provide less construction risk than a single large vessel.

3

EMISSION MODEL: TSHD IN OPERATION

Source: Photo by Dylan de Roode, 2019

3. Emission Model: TSHD in Operation

This chapter describes the steps that are taken to determine the total energy requirement and the emissions of a TSHD per operation. The basis of the emission model is made with the specifications of the Dodge Island. The first sub chapter presents the specifications of the Dodge Island. The description of the model is given in the second sub chapter. Within that sub chapter, structure and the used formulas of the model are presented. The accuracy of the model is tested and verified in the third sub chapter with operations of the Dodge Island that are already completed. A conclusion regarding the emission model is given in the last sub chapter.

3.1 Specifications of the Dodge Island

This sub chapter is divided into three parts. An introduction of the Dodge Island is given in the first part. In the second part, the energy producers on board of the Dodge Island are described. In the third part, the power arrangement of the dredge is presented.

3.1.1.1 Introduction Dodge Island

One of the oldest dredges within the fleet of GLDD is the Dodge Island. The dredge is one of the six TSHDs in operation. At around 1980 the dredge is built and it is still operational. See Figure 23: The Dodge Island for an image of the Dodge Island. The engines, equipment and system on board are registered in the database of GLDD. The dredge completes multiple jobs yearly and the power arrangement is relatively simple which makes this dredge a good starting point for developing models. The Dodge Island can use the bottom dumping system as it has a split hull. The starboard and portside part of the hull is hydraulically split. This is the fastest way to discharge. Either the discharge is by splitting the hull or by connecting the discharge pump to a pipeline that guides the soil to the dumping area. Table 13 in Appendix 7.1.1 shows the specifications of the Dodge Island required for the emission model.

Figure 23: The Dodge Island [41]

3.1.1.2 Energy Producers

On board the dredge there are multiple energy users, energy producers provide energy to supply the users. Five main energy producers are defined:

1. Main engines
2. Generators
3. Pump engines
4. Jet pump engines
5. Bowthruster engine

Within each phase, multiple energy producers are necessary to execute the work or in other words, execute actions. The three main actions, providing auxiliary power, providing pumping power and manoeuvring, are powered by energy producers. Table 1 shows in which phase which action is being powered by which energy producer. The auxiliary prime movers consist of two generators (Gen), the pumping prime movers are the jet pump engines (JP) and pump engines (DP). The main engine (ME) is the prime mover for the manoeuvring. To maintain position with (dis)connecting, the bowthruster (BT) is also used which is part of manoeuvring.

Phases	Auxiliary	Pumping	Manoeuvring
Loading	Gen	JP & DP	ME
Transit Loaded	Gen		ME
Connection	Gen		ME & BT
Discharge	Gen	JP & DP	ME
Disconnect	Gen		ME & BT
Transit Empty	Gen		ME

Table 1: Actions of the Dredge in Operation

3.1.1.3 Power Arrangement

The Dodge Island is designed with a mechanical power arrangement with a direct drive. This is visualised in Figure 49: Power Arrangement Dodge Island in Appendix 7.1.2. Every pump or propulsor is connected to a single engine. The main engine is connected to a gearbox which takes care of the propulsion. While dredging the dredge engines produce the power for the dredging pump whereas the jet engines produce the power for the jet pumps. The generators are responsible for all the energy to the auxiliary equipment. Lastly, the bowthruster is powered by a similar engine as for the jet pumps.

3.2 Description of the Emission Model

The purpose of the emission model is to show the amount of CO_2 per dredged volume of soil. This sub chapter describes the structure and explains the formulas that are used to determine the emissions per operation. It is divided into ten parts, where the first part gives an overview of the inputs and results. The next eight chapters describe the model per calculation part of the model. First, the hull resistance is described in part two. The resistance due to trailing is explained in the third part. The matching of the propeller and the main engine is presented in the fourth part, followed up by the fuel consumption calculations in the fifth part. How the emissions are determined is presented in the sixth part. The power requirements of the engines on board, pumps and auxiliary equipment are described in the seventh, eighth and ninth part. In the last part, it is explained to which phase of operation which calculations are used.

3.2.1 Total Emission Profile

On the first page of the model an overview is given where job and dredge specific information is filled in and results are shown. Figure 24 visualises the first part of the overview with inputs (green font) and the results. Choices of the discharge method, visor type, dredge and power arrangement are also made within the overview. Two discharge methods are implemented, discharging with a pipeline and discharging with splitting the hull. The option of the type of dredging with a visor is given, a fixed visor or a floating visor can be chosen. Two dredges are implemented in the model, the Dodge Island and the Padre Island. Multiple dredges can be added to the inventory of the model with their own specifications. The model supports one type of power arrangement which is a mechanical power arrangement with a direct drive.

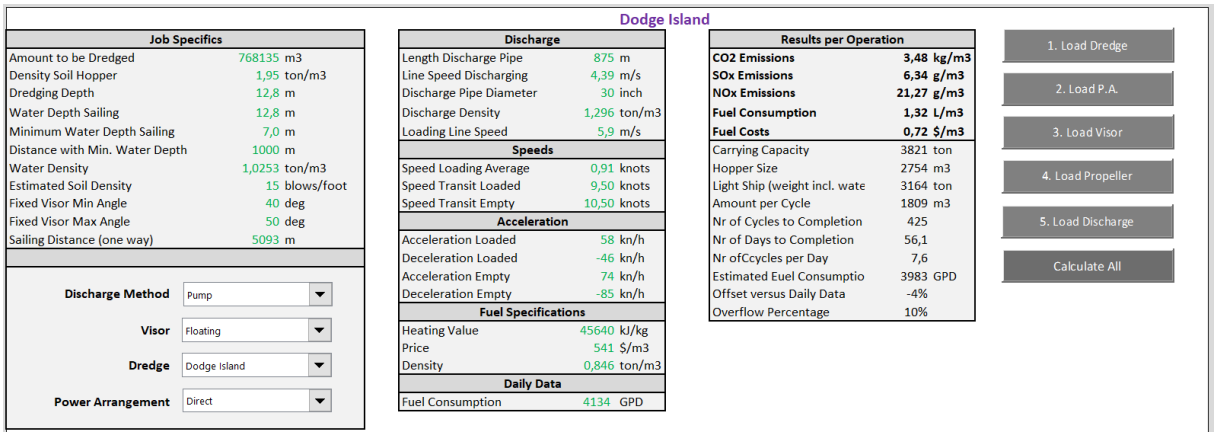

Figure 24: Overview of the Inputs and Results of the Emission Model

The other part of the overview is shown in Figure 25 on the next page. This table shows the power usage, fuel consumption, costs and CO_2 emission per phase per engine. On the left, the time per phase is visible as well as the relevant speed. This table shows the results of all the calculations done within the model and clearly presents them.

				Generator				Main Engines				Dredge Engines				Jet Engines				Bowthruster Engine				Total			
	Time	Time	Speed	Power	Fuel Consumption	Cost	CO2 emission	Power	Fuel Consumption	Cost	CO2 emission	Power	Fuel Consumption	Cost	CO2 emission	Power	Fuel Consumption	Cost	CO2 emission	Power	Fuel Consumption	Cost	CO2 emission	Power	Fuel Consumption	Cost	CO2 emission
	min	h/day	kn	kW	L/day	$/day	kg/day	kW	L/day	$/day	kg/day	kW	L/day	$/day	kg/day	kW	L/day	$/day	kg/day	kW	L/day	$/day	kg/day	kW	L/day	$/day	kg/day
Loading 1	57	6,8	0,91	396	930	503	2450	1160	2601	1407	6853	1388	2934	1587	7728	738	1754	949	4622	0	0	0	0	3682	8219	$4.447	21653
Transit loaded 2	28	3,4	9,50	345	401	217	1057	1207	847	458	2232	0	0	0	0	0	0	0	0	0	0	0	0	1552	1248	$ 675	3289
Connecting 3	9	1,1	0,00	328	121	65	318	73	23	13	62	110	37	20	96	8	3	2	8	164	61	33	161	684	245	$ 132	645
Discharge 4	57	6,7	0,00	345	801	433	2109	73	147	80	389	1727	3607	1951	9501	738	1734	938	4567	33	77	42	203	2916	6365	$3.444	16769
Disconnecting 5	7	0,8	0,00	328	94	51	247	73	18	10	48	110	28	15	75	8	2	1	6	164	48	26	125	684	190	$ 103	502
Transit empty 6	25	2,9	10,50	345	346	187	912	1156	831	460	2240	0	0	0	0	0	0	0	0	0	0	0	0	1501	1177	$ 647	3152
Turn time 7	9	1,0	9,50	345	121	66	320	1690	257	139	676	110	32	17	84	8	1	1	2	0	0	0	0	2154	411	$ 222	1082
Other 8	10	1,2	0,00	328	134	73	353	73	26	14	69	110	41	22	107	8	3	2	9	0	0	0	0	520	204	$ 110	538
Total	202	24		2759	2948	1595	7767	5506	4751	2581	12567	3557	6678	3613	17592	1509	3498	1892	9215	361	186	100	489	**13692**	**18060**	**9781**	**47630**

Figure 25: Overview of the Used Power, Fuel Consumption, Costs and CO_2 Emission per Phase per Engine

In Figure 24, the inputs for the model are shown. Below, the inputs and results are written down and explained.

Inputs

Job Specific:

- **Amount to be Dredged**: The total amount of soil for the job that is to be dredged up (m^3)
- **Density Soil Hopper**: This represents the density of the soil within the hopper after it is settled (ton/m^3)
- **Dredging Depth**: The average depth from the surface of the water to the sea bottom of the borrowing area (m)
- **Water Depth Sailing**: The average depth from the surface of the water to the sea bottom during the sailing phases (m)
- **Minimum Water Depth Sailing**: The minimum depth from the surface of the water to the sea bottom the dredge encounters (m)
- **Distance with** Min. **Water Depth**: An approximation of the distance the dredge is sailing with the minimum water depth (m)
- **Water Density**: The density of the water the dredge is operational (ton/m^3)
- **Estimated Soil Density**: The result of a SPT is to be entered here, expressed in the numbers of blows (blows/foot)
- **Fixed Visor Min Angle**: The minimum visor angle where the visor is fixed (degree)
- **Fixed Visor Max Angle**: The maximum visor angle where the visor is fixed (degree)
- **Sailing Distance (one way)**: The average one-way sailing distance from the borrowing area to the dumping area (m)

Discharge:

- **Length Discharge Pipe**: The average length of the discharge pipe (m)
- **Line Speed Discharging**: The average line speed of the slurry within the discharge pipe (m/s)
- **Discharge Pipe Diameter**: The diameter of the discharge pipe (inch)
- **Discharge Density**: The average density of the slurry going through the discharge pipe (ton/m^3)
- **Loading Line Speed**: The average line speed within the suction pipes while loading (m/s)

Speeds:

- **Speed Loading Average**: The average speed of the dredge while loading (knots)
- **Speed Transit Loaded**: The maximum constant speed of the dredge while sailing in loaded condition (knots)
- **Speed Transit Empty**: The maximum constant speed of the dredge while sailing in empty condition (knots)

Acceleration:

- **Acceleration Loaded**: The average acceleration of the dredge in loaded condition (kn/h)
- **Deceleration Loaded**: The average deceleration of the dredge in loaded condition (kn/h)
- **Acceleration Empty**: The average acceleration of the dredge in empty condition (kn/h)
- **Deceleration Empty**: The average deceleration of the dredge in empty condition (kn/h)

Fuel Specifications:

- **Heating Value**: The heating value of the used fuel (kJ/kg)
- **Price**: The price of the used fuel ($/m^3)
- **Density**: The density of the used fuel (ton/m^3)

Daily Data:

- **Fuel Consumption**: The average amount of fuel that is burned per day at a working rate of 100% according to the daily data (GPD)

Results

Results per Operation:

- **CO_2 Emissions**: the total amount of CO_2 emitted as result of the model (kg/m^3)
- **SOx Emissions**: the total amount of SOx emitted as results of the model (g/m^3)
- **NOx Emissions**: the total amount of NOx emitted as results of the model (g/m^3)
- **Fuel Consumption**: The fuel consumption as result of the model (L/m^3)
- **Fuel Costs**: The cost of the fuel as result of the model ($/m^3)
- **Carrying Capacity**: The capacity the dredge is able to transport (ton)
- **Light Ship (weight incl**. water and fuel): The weight of the light ship including full water and fuel tanks (m^3)
- **Hopper Size**: The capacity of the hopper (ton)
- **Amount per Cycle**: The amount of soil the dredge transport with each cycle, taken into account the overflow percentage minus the amount of soil that is not discharged (residue) (m^3)
- **Nr of Cycles to Completion**: the number of cycles the dredge needs to complete the job at a working rate of 100% (-)
- **Nr of Days to Completion**: the number of days the dredge needs to complete the job at a working rate of 100% (-)
- **Nr of Cycles per Day**: The number of cycles the dredge can complete at a working rate of 100% (-)
- **Estimated Fuel Consumption**: The estimated fuel consumption by the model per day at a working rate of 100% (GPD)
- **Offset versus Daily Data**: This percentage represents the offset of the daily data versus the estimated fuel consumption (%)
- **Overflow Percentage**: The overflow of the hopper expressed in percentage (%)

To determine the results of the emission profile, the calculations are split into eight parts which are presented in the following eight parts of this sub chapter:

1. Hull resistance
2. Trailing resistance
3. Matching propeller and the main engine
4. Fuel consumption
5. Emissions
6. Engine power requirement
7. Pump power requirement
8. Auxiliary power requirement

The hull resistance is calculated with the statistically approach of Holtrop and Mennen [39] and extended with air and shallow water resistance. The trailing resistance consist of three main parts: The force and moment equilibrium of the dragarm (suction pipes and draghead), the determination of the cutting force and the method to determine the cutting depth. The force equilibrium is implemented according to the master thesis by Gijs ter Meulen: Drag Analysis and Model for Forces and Production [40]. The cutting forces are implemented according to the book The Delft Sand, Clay and Rock Cutting Model by Sape Miedema [41]. The cutting depths are calculated according to the paper Production Estimation of Water Jets in Dragheads by Sape Miedema [42]. With the known total resistance of the dredge, the matching of the propeller with the main engine is done according to the method published by Hans Klein Woud and Douwe Stapersma in their book Design of Propulsion and Electrical Power Generation Systems [43]. The fuel consumption, emission calculations and engine power requirement are also determined according to the book Design of Propulsion and Electrical Power Generation Systems. The main document used to determine the pump power requirement is the paper The Mathematics of Pumping Water by Mathew Milnes [44]. To determine the auxiliary power requirement, measurement on board a dredge in operation are personally under supervision executed.

3.2.2 Hull Resistance

There are eight contributors for the hull resistance used within the model [39] [43]:

1. Frictional or viscous resistance (R_V)
2. Wave resistance (R_W)
3. Model-ship correlation resistance (R_A)
4. Air resistance (R_{AA})
5. Additional pressure resistance of immersed transom stern (R_{IT})
6. Appendages resistance (R_{APP})
7. Bulbous Bow resistance (R_B)
8. Shallow water resistance

The total hull resistance is calculated by adding up the individual resistant components:

$$R_{tot} = R_V + R_W + R_A + R_{AA} + R_{IT} + R_B + R_{APP} \quad (8)$$

When the dredge is loading, the trailing resistance (R_{TR}) is added to the total resistance:

$$R_{tot} = R_V + R_W + R_A + R_{AA} + R_{IT} + R_B + R_{APP} + R_{TR} \quad (9)$$

3.2.2.1 Frictional or Viscous Resistance

When a body moves through the water, the surface of the body creates a resistance between the surface and the water. The roughness of the hull increases the frictional resistance as well as the surface of the hull (wetted surface).

The total viscous resistance is determined with the following equation:

$$R_V = C_V * \frac{1}{2} * \rho * v^2 * S \tag{10}$$

Four variables have to be determined to calculate the total viscous resistance. The velocity (v) of the vessel is taken as a variable. The density of the sea water is presented as ρ. The wetted surface (S) and the viscous coefficient (C_v) are elaborated on below. The wetted surface of the hull of the dredges is approached when the actual data is not available. Holtrop and Mennen have developed a formula to approach the wetted surface:

$$S = L(2T + B)\sqrt{C_M}(0.453 + 0.4425C_B - 0.2862C_M - 0.003467B/T + 0.3696C_{WP}) + 2.38A_{BT}/C_B \tag{11}$$

C_m represents the midship coefficient, C_b the block coefficient, C_{wp} the waterline coefficient, A_{bt} the transverse sectional area of the bulb and T the average draught of the vessel. When no bulb is attached to the vessel, this part of the equation equals zero and is neglected within the model. All the components to determine the wetted surface relate to the dimensions of the vessel. The viscous resistance is a combination of the viscous pressure drag (K), friction coefficient (C_f) and the correlation coefficient (C_A). The equation to determine the viscous resistance is the following:

$$C_V = K * C_f + C_A \tag{12}$$

The first component of the viscous resistance is the viscous pressure drag [45]:

$$K = 19 * (\frac{\nabla}{Lwl * B * T} * \frac{B}{Lwl})^2 \tag{13}$$

The correlation coefficient (C_A) required to determine the viscous coefficient is calculated with the following formula:

$$C_A = 0.006(L + 100)^{-0.16} - 0.00205 + 0.003\sqrt{\frac{L}{7.5}}C_B{}^4\ c2(0.04 - c4) \tag{14}$$

The length between perpendiculars of the ship is given as L. The coefficients c2 and c4 are determined with the following equations.

$$c2 = \exp(-0.89 * \sqrt{c3}) \tag{15}$$

For $T_F/L < 0.04$, c4 is calculated with the following formula:

$$c4 = \frac{T_F}{L} \tag{16}$$

When $T_F/L > 0.04$, c4 is set at a value of 0.04. T_F is the forward draft of the vessel in metres. The coefficient c3 is only applicable if the vessel is equipped with a bulbous bow. If not, the coefficient equals zero, which makes the outcome of the coefficient c2 equal to 1.

$$c3 = 0.56 * A_{BT}^{1.5}/(BT(0.31 * \sqrt{A_{BT}} + T_F - h_B)) \tag{17}$$

The h_B is the position of the centre of the transverse area (A_{BT}) above the keel line. The last unknown to determine the total friction resistance is the friction coefficient. The friction coefficient is determined with the ITTC-57 formula:

$$Cf = \frac{0.075}{(Log(Re) - 2)\text{^}2} \tag{18}$$

Rn is the abbreviation for the Reynolds number. It consists of three variables: the velocity and the characteristic length of the object and the kinematic viscosity of the fluid surrounding the object. The characteristic length for a vessel is the length of the waterline (L). The viscosity of the fluid is denoted as υ and the velocity is v. The outcome of the Reynolds number determines whether the flow around the hull is turbulent (Re > $1x10^6$), transient ($5x10^5$< Re < $1x10^6$) or laminar (Re < $5x10^5$) [46].

$$Re = \frac{v * L}{\nu} \tag{19}$$

3.2.2.2 Wave Resistance

When the vessel sails, it pushes the surrounding water away. On the water surface this creates waves and thus resistance. Depending on the velocity of the vessel, the length of the waves variate and create a non-linear resistance curve versus the velocity. The total wave resistance is determined with the following equation:

$$R_W = c1 * c2 * c5 * \nabla\rho g * \exp\left(m1 * F_n^{-0.9} + m2 * \cos(\lambda F_n^{-2})\right) \tag{20}$$

The displacement of the vessel (∇) is in unit m^3, g the gravitational acceleration, m1 and m2 are variables which is stated below. The breadth of the vessel is denoted as B. With coefficient c1 and its variables:

$$c1 = 2223105 * c_7^{3.78613} * \left(\frac{T}{B}\right)^{1.07961} * (90 - i_E)^{-1.37565} \tag{21}$$

The following equation to determine coefficient c7 is valid when 0.11 < B/L < 0.25:

$$c7 = \frac{B}{L} \tag{22}$$

The half angle of entrance (i_E) is the angle of the waterline at the bow of the vessel with reference to the centre plane but neglecting the local shape at the stern [39]. This angle is determined with the following equation:

$$i_E = 1 + 89 * \exp\left(-\left(\frac{L}{B}\right)^{0.80856} * \left(1 - C_{wp}\right)^{0.30484} * \left(1 - C_p - 0.0225 * lcb\right)^{0.6367} * \left(\frac{L_R}{B}\right)^{0.34574} * \left(100 * \frac{\nabla}{L^3}\right)^{0.16302}\right) \tag{23}$$

Variables that are not yet mentioned are lcb and L_R. The form-factor formula to determine L_R reflects the length of the run with the following equation:

$$L_R = L * (1 - C_p + 0.06 * C_p * lcb/(4 * C_p - 1)) \tag{24}$$

The lcb is expressed as the longitudinal position of the centre of buoyancy forward of 0.5*L as percentage of the waterline length. Before the lcb is determined, the centre of buoyancy has to be known. To simplify the model, the centre of buoyancy is assumed constantly to have a value of zero.

With lcb is zero, L_R becomes:

$$L_R = L * (1 - C_p) \tag{25}$$

The coefficient c5 is determine with the following equation:

$$c5 = 1 - 0.8 * A_T/(BTC_m) \tag{26}$$

A_T represents the immersed part of the transverse area of the transom at zero speed. Lambda is a constant which is expressed when L/B < 12 in:

$$\lambda = 1.446 * C_p - 0.03 * L/B \tag{27}$$

When L/B > 12 then Lambda becomes:

$$\lambda = 1.446 * C_p - 0.036 \tag{28}$$

M1 and m2 are calculated with the following equations:

$$m1 = 0.0140407 * L/B - 1.75254 * \nabla^{\frac{1}{3}}/L - 4.79323 * B/L \ - c16 \tag{29}$$

$$m2 = c15 * C_p^2 * \exp(-0.1F_n^{-2}) \tag{30}$$

When the C_p > 0.80 then c16 is determined by:

$$c16 = 1.73014 - 0.7067 * C_p \tag{31}$$

For values of L^3/∇ < 512, c15 is equal to -1.69385. The Froude number (Fn) is the ratio of flow speed to wave speed. The Fn is calculated with the following equation:

$$Fn = \frac{v}{\sqrt{g * L}} \tag{32}$$

Where v is the velocity of the vessel, g the gravitational acceleration and L the length of the vessel. The length of the waves alongside the hull and the length of the ship have an influence to the total resistance. By plotting the total resistance to the Froude number for a certain velocity, the relation between the length of the waves and the ships are shown. Figure 50 in Appendix 7.1.3 shows that relation for the Dodge Island fully loaded. With Froude number 0.300 the wavelength is roughly half of the ship's length; this cancels the stern wave and reduces the wavemaking. At a Froude number of around 0.365, the resistance reaches a top. This occurs with a wavelength of 2/3 of the ship length. The bow wave creates a trough at the stern which increases the wavemaking. With a Froude number of 0.420, the length of the wave equals the length of the ship. This is also known as the hull speed, if the speed still increases the ship is starting to plane and requires a lot of energy. For ships that are not build to plane, by increasing the speed, the resistance increases dramatically.

3.2.2.3 Appendages Resistance

Appendages are attached to the hull of the vessel and increase the total resistance. All appendages have different magnitudes of resistance and can be approached. The resistance of the appendages is expressed in the following formula:

$$R_{APP} = 0.5 * \rho * v^2 * S_{APP}(1 + k_2)_{eq} * C_F \quad (33)$$

The density of the water, velocity of the vessel and the friction coefficient are known. The wetted area (S_{APP}) of the appendix and the $1+k_2$ values are to be calculated. By testing the following values are known for different types of appendages, these are shown in Table 14 in Appendix 7.1.4. The wetted surface of the appendages is approximated with drawings of the researched vessels. The equivalent $1+k_2$ is determined with:

$$(1 + k_2)_{eq} = \frac{\sum((1 + k_2) * S_{APP})}{\sum S_{APP}} \quad (34)$$

3.2.2.4 Air Resistance

The area of the vessel above the water surface is subjected to the resistance of the air flow. As one of the boundaries is that the vessel is not subdue to weather conditions, at standstill, the vessel has no air resistance. The air resistance is roughly approached by a percentage of 6% over the rest of the contributors to resistance:

$$R_{AA} = 0.06 * (R_V + R_{APP} + R_W + R_{TR} + R_A) \quad (35)$$

R_A is the model-ship correlation resistance and R_{TR} is the additional pressure resistance of an immersed transom stern.

3.2.2.5 Model-Ship Correlation Resistance

This resistance is due to the differences in resistance between tested models and full-scale ships. The coefficient C_A is found from analysis of the results of speed trials, which are corrected to ideal trial conditions.

$$R_A = 0.5 * \rho * v^2 * S * C_A \quad (36)$$

3.2.2.6 Pressure Resistance of Immersed Transom Stern

The additional pressure resistance due to the immersed transom is determined with the following equation:

$$R_{IT} = 0.5 * \rho * v^2 * A_T * c6 \quad (37)$$

With coefficient c6 when $F_{nT} < 5$:

$$c6 = 0.2 * (1 - 0.2 * F_{nT}) \quad (38)$$

F_{nT} is expressed in:

$$F_{nT} = v/\sqrt{2 * g * A_T/(B + B * C_{WP})} \quad (39)$$

3.2.2.7 Bulbous Bow Resistance

At a certain speed a bulbous bow creates a lower wave resistance. At all other speeds, the bulbous bow only increases the total resistance. Whether a bulbous bow is beneficial is determined by a trade-off between the time the ship sails at the resistance reducing speed and the time the ship does not sail at that speed. Holtrop and Mennen includes a bulbous bow accordingly:

$$R_{BB} = 0.11 \exp\left(-3 * {P_B}^{-2}\right) * {F_{ni}}^{3} * {A_{BT}}^{1.5} * \rho * g/(1 + {F_{ni}}^{2}) \tag{40}$$

With P_B:

$$P_B = 0.56 * \sqrt{A_{BT}}/(T_F - 1.5h_B) \tag{41}$$

and F_{ni}:

$$F_{ni} = v/\sqrt{g\left(T_F - h_B - 0.25 * \sqrt{A_{BT}}\right) + 0.15 * v^2} \tag{42}$$

3.2.2.8 Shallow Water Resistance

TSHDs are ocean-going vessels and capable of working in non-ideal water and weather conditions. Even with that capability it is not uncommon that discharging or even loading happens in shallow water. Whether water is shallow or not is not only determined by water depth within this model. It is a combination of vessel speed and water depth. When a ship encounters shallow water, the waves created by the hull shorter and grow steeper which increases the resistance. The resistance as result of a vessel sailing at a certain speed in shallow water is expressed in a percentage of speed loss. The method that is used to determine the effect of sailing in shallow water is the Schlichting method. The Depth Froude Number (DFN) is to be defined as:

$$DFN = \frac{v}{\sqrt{g * D}} \tag{43}$$

Where D represents the water depth in feet, g is the gravitational acceleration and v is the velocity in miles per hour. Within the model, the conversion of the units to the metric system is taken into account. For the following values the speed loss is estimated:

DFN < 0.4 there is no speed loss
DFN = 0.6 there is a 1% speed loss
DFN = 0.8 there is a 4% speed loss
DFN = 1.0 there is a 14% speed loss

3.2.3 Trailing Resistance

The total trailing resistance is determined by three main components, the penetration depth of the jets and visor, the resistance of the draghead and the resistance of the suction pipes. The penetration depth is used as a variable to determine the cutting forces. To determine the total trailing resistance, a force and moment equilibrium is made which includes the cutting forces, resistance of the draghead and the resistance of the suction pipes. In the first part of this sub chapter, the forces of the suction pipes are calculated. In the second part the forces of the draghead are determined which include the method to calculate the cutting forces. In the third part the penetration depth of the jets and the visor is determined. The total trailing resistance is presented in the last part.

3.2.3.1 Forces in the Suction Pipes

The suction pipe is split up into two parts: the upper and the lower part of the suction pipe. As the draghead is attached to the end of the lower part of the suction pipe, the created forces are implemented within the calculations of the forces in the suction pipes. The suction pipes are subdued to several forces: Gravity force, drag force, forces in the joints, forces in the cables and forces from the draghead. Within the following sketch, the lengths of the suction pipe and the components are shown.

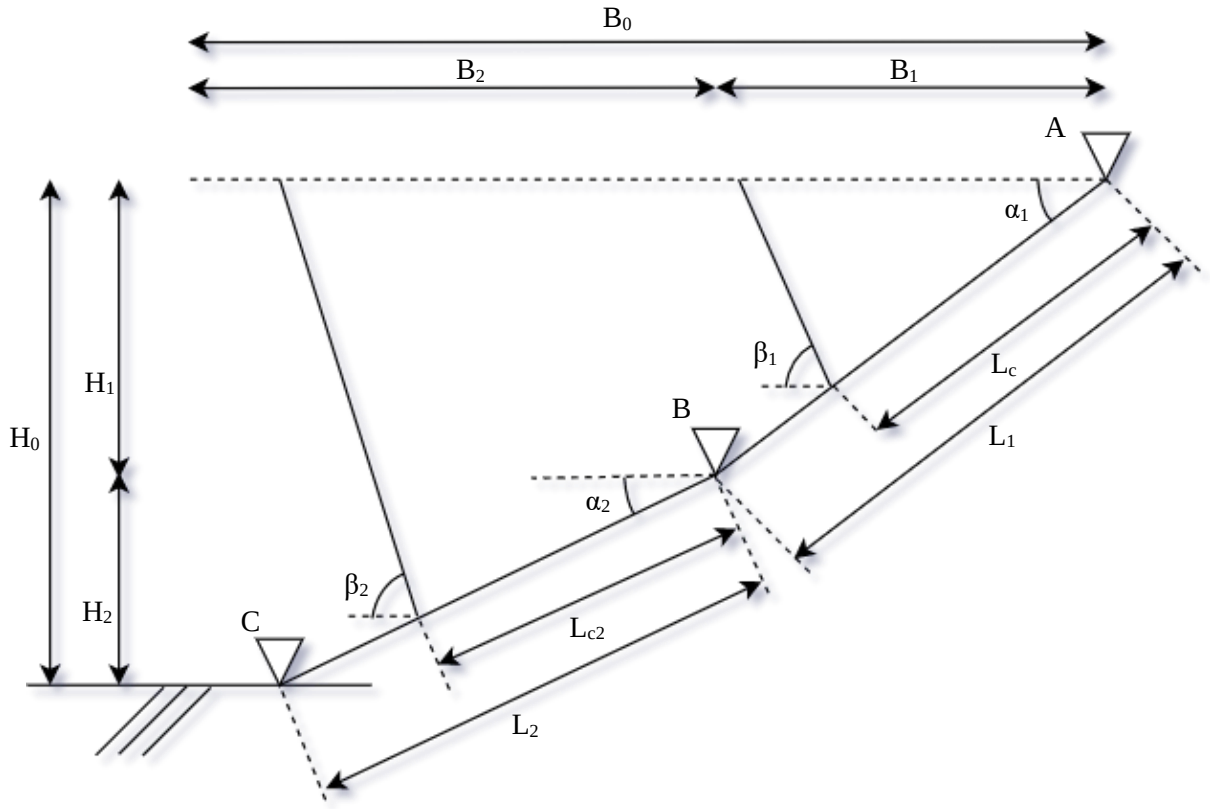

Figure 26: Lengths of the Suction Pipes

Gravity Force

Objects that are completely submerged in a fluid have a different magnitude of gravity force in comparison with objects in the everyday atmosphere. The magnitude of gravity force on an object submerged in water is calculated with the following equation:

$$F_{g,sub} = g * \left(\rho_{object} - \rho_w\right) * V \tag{44}$$

The masses and volumes are determined according to the provided drawings (PDF and AutoCAD). The volumes, if not present, are calculated according to the drawings. For more accuracy, measurements of the volume and weight are taken from drawings. The weights and volumes of the suction pipes are presented in Table 15 in Appendix 7.1.5.

Drag Force

As the suction pipes move through water, a drag force is created. The magnitude of the drag force depends on the velocity of the fluid, density of the fluid and shape of the body. The drag force of the suction pipe and the draghead are determined for the calculation of the trailing forces. The drag force for a pipe is calculated with the following equation:

$$F_D = \frac{1}{2} * \rho_w * {v_f}^2 * C_d * L_{pipe} * D_{pipe} \tag{45}$$

The coefficient of the drag force depends on the regime, whether it is laminar or turbulent. The regime is calculated and determined with the formula of Reynolds:

$$Re = \frac{v * L}{\nu} \tag{46}$$

The velocity of the fluid is multiplied by the length of the body. This is divided by the viscosity of the fluid. The flow is turbulent for Re > $1x10^6$, transient for $5x10^5$< Re < $1x10^6$ and laminar for Re < $5x10^5$. For pipes the formula of Reynolds becomes:

$$Re = \frac{v_f * D_{pipe}}{\nu} \tag{47}$$

For the draghead the formula of Reynolds becomes:

$$Re = \frac{v_f * w_{dh}}{\nu} \tag{48}$$

As the suction pipes are situated in an angle the drag force in practise varies per pipe. In practise, a horizontal approach of a circle under an angle takes the form of an ellipse. Within the calculations it is assumed that the pipes maintain the circle shape. The velocity of the water flowing around the suction pipe is taken perpendicular. Therefore, the velocity is multiplied by the sinus of the angle of the suction pipe. The Reynolds number variates with the angle of the pipes and the trailing velocity, which creates a variation in the drag force. The perpendicular velocity on the pipes is determined as follows:

$$v_{f\perp} = v_f * \sin(\alpha) \tag{49}$$

The parallel velocity to the suction pipes is determined by multiplying the velocity with the cosine of the angle of the pipes. The perpendicular velocity can now be used to determine the new Reynolds number and the new drag force. Within those formulas, v_f becomes v_{fL}.

Static Situation

Four iterations are made to obtain the required forces. The first iteration is a static situation at standstill without soil forces. The second one is a static situation with compensated vertical soil forces at standstill. The third iteration is a static situation with compensated vertical soil forces with increasing trailing velocity. The last iteration is a static situation with compensated excavation soil forces and increasing trailing velocity.

The figure below shows the existing forces on the suction pipe in static condition without soil forces of the draghead.

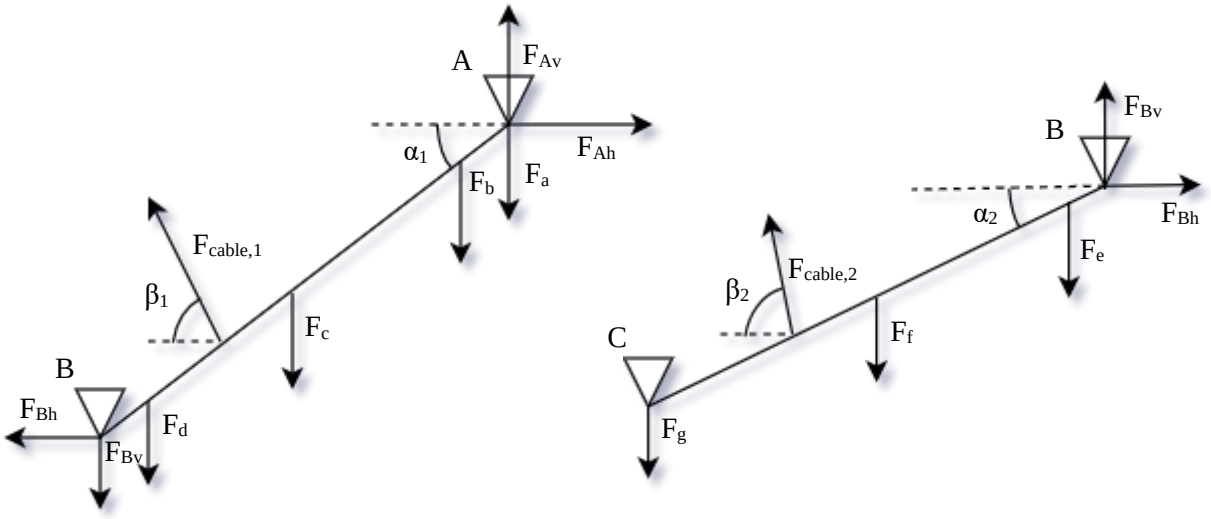

Figure 27: Force Overview Static Situation for Upper (left) and Lower (right) Suction Pipe

Three equations are set up from the figure, with three unknown variables. The drag forces are zero, as the there is no velocity. The centre of the moment is taken in point B with counter-clockwise as positive direction. Furthermore, the up and right direction are taken positive as well.

Lower Suction Pipe

$$\sum M_{B,l} = F_e * B_e + F_f * B_f + F_g * B_g - F_{drag,2} * L_{d2} - F_{cable,2} * \sin(\beta_2) * B_{c2} - F_{cable,2} * \cos(\beta_2) * H_{c2} = 0 \quad (50)$$

$$\sum F_{v,l} = F_{Bv} + F_{drag,2} * \cos(\alpha_2) + F_{cable,2} * \sin(\beta_2) - F_e - F_f - F_g = 0 \quad (51)$$

$$\sum F_{h,l} = F_{Bh} - F_{drag,2} * \sin(\alpha_2) - F_{cable,2} * \cos(\beta_2) = 0 \quad (52)$$

The three unknown variables: F_{cable2}, F_{Bv} and F_{Bh} are calculated with the three equations.

$$F_{cable,2} = \frac{F_e * B_e + F_f * B_f + F_g * B_g - F_{drag,2} * L_{d2}}{B_{c2} * \sin(\beta_2) + H_{c2} * \cos(\beta_2)} \quad (53)$$

$$F_{Bv} = -F_{drag,2} * \cos(\alpha_2) - F_{cable,2} * \sin(\beta_2) + F_e + F_f + F_g \quad (54)$$

$$F_{Bh} = F_{drag,2} * \sin(\alpha_2) + F_{cable,2} * \cos(\beta_2) \quad (55)$$

Static Situation with Vertical Soil Force

Cable 2 (or draghead cable) is attached to the draghead davit, which uses a swell compensator. This means that the force on this cable is held constant. The compensator has to be included in the calculations and is introduced as a ‘c’ subscript. The compensation factor is set at 50% as the soil is saturated sand. With the swell compensator, a vertical soil reaction force of the draghead is created. The vertical soil

reaction force of the draghead and the swell compensator are introduced which creates new unknown variables. The compensated force in the cable is expressed with the following equation:

$$F_{cable,2,v,c} = F_{cable,2} * \sin(\beta_2) * \mathrm{c} \tag{56}$$

$$F_{cable,2,h,c} = F_{cable,2} * \cos(\beta_2) * \mathrm{c} \tag{57}$$

$$F_{cable,2,c} = \sqrt{{F_{cable,2,v,c}}^2 + {F_{cable,2,v,c}}^2} \tag{58}$$

Lower Suction Pipe

The goal of the second iteration, is to calculate the vertical soil reaction force onto the draghead (F_{cv}). This is solved by equalising the sum of the moments around point B of the lower suction pipe:

$$\sum M_{B,l,c} = F_e * B_e + F_f * B_f + F_g * B_g - F_{drag,2} * L_{d2} - F_{cable,2,v,c} * B_{c2} - F_{cable,2,h,c} * H_{c2} - B_2 * F_{cv} = 0 \tag{59}$$

$$F_{cv} = \frac{F_e * B_e + F_f * B_f + F_g * B_g - F_{drag,2} * L_{d2} - F_{cable,2,v,c} * B_{c2} - F_{cable,2,h,c} * H_{c2}}{B_2} \tag{60}$$

With the introduced vertical soil reaction force, the reaction forces in the lower suction pipe have to be recalculated:

$$\sum F_{v,l,c} = F_{cv} + F_{Bv,c} + F_{drag,2} * \cos(\alpha_2) + F_{cable,2,v,c} - F_e - F_f - F_g = 0 \tag{61}$$

$$\sum F_{h,l,c} = F_{Bh,c} - F_{drag,2} * \sin(\alpha_2) - F_{cable,2,v,c} = 0 \tag{62}$$

For the lower suction pipe, the two unknown variables $F_{Bv,c}$ and $F_{Bh,c}$ can now be calculated with the two equations:

$$F_{Bv,c} = -F_{cv} - F_{drag,2} * \cos(\alpha_2) - F_{cable,2,v,c} + F_e + F_f + F_g \tag{63}$$

$$F_{Bh,c} = F_{drag,2} * \sin(\alpha_2) + F_{cable,2,h,c} \tag{64}$$

Upper Suction Pipe

The reaction forces within the upper suction pipe can also be determined:

$$\sum M_{A,u,c} = F_a * B_a + F_b * B_b + F_c * B_c + F_d * B_d + B_1 * F_{Bv,c} - H_1 * F_{Bh,c} - F_{drag,1} * L_{d1} - F_{cable,1,c} * \sin(\beta_1) * B_{c1} - F_{cable,1,c} * \cos(\beta_1) * H_{c1} = 0 \tag{65}$$

$$\sum F_{v,u,c} = -F_{Bv,c} + F_{drag,1} * \cos(\alpha_1) + F_{cable,1,c} * \sin(\beta_1) + F_{Av,c} - F_a - F_b - F_c - F_d = 0 \tag{66}$$

$$\sum F_{h,u,c} = -F_{Bh,c} - F_{drag,1} * \sin(\alpha_1) - F_{cable,1,c} * \cos(\beta_1) + F_{Ah,c} = 0 \tag{67}$$

For the upper suction pipe, there are three unknown variables ($F_{cable,1,c}$, $F_{Av,c}$, $F_{Ah,c}$) and three equations:

$$F_{cable,1,c} = \frac{F_a * B_a + F_b * B_b + F_c * B_c + F_d * B_d + F_{Bv,c} * B_1 - F_{Bh,c} * H_1 - F_{drag,1} * L_{d1}}{B_{c1} * \sin(\beta_1) + H_{c1} * \cos(\beta_1)} \quad (68)$$

$$F_{Av,c} = F_{Bv,c} - F_{drag,1} * \cos(\alpha_1) - F_{cable,1,c} * \sin(\beta_1) + F_a + F_b + F_c + F_d \quad (69)$$

$$F_{Ah,c} = F_{drag,1} * \sin(\alpha_1) + F_{cable,1,c} * \cos(\beta_1) + F_{Bh,c} \quad (70)$$

Figure 51 in Appendix 7.1.6 shows an overview of the forces of the suction pipes.

Static Situation with Increasing Velocity

With the third iteration, the trailing velocity is introduced. The drag forces will now affect the force equilibrium. The vertical force of the draghead, the force in the cables and the forces in the connections are affected by the increasing velocity. The subscript vt is introduced to indicate the relation to the increasing velocity.

Lower Suction Pipe

$$\sum M_{B,l,c,vt} = F_e * B_e + F_f * B_f + F_g * B_g - F_{drag,2} * L_{d2} - F_{cable,2,v,c} * B_{c2} - F_{cable,2,h,c} * H_{c2} - F_{cv,vt} * B_2 = 0 \quad (71)$$

$$\sum F_{v,l,c,vt} = F_{Cv,vt} + F_{Bv,c,vt} + F_{drag,2} * \cos(\alpha_2) + F_{cable,2,v,c} - F_e - F_f - F_g = 0 \quad (72)$$

$$\sum F_{h,l,c,vt} = F_{Bh,c,vt} - F_{drag,2} * \sin(\alpha_2) - F_{cable,2,h,c} = 0 \quad (73)$$

The three unknown variable are $F_{Cv,vt}$, $F_{Bv,c,vt}$ and $F_{Bh,c,vt}$, they are calculated with the three equations:

$$F_{cv,vt} = \frac{F_e * B_e + F_f * B_f + F_g * B_g - F_{drag,2} * L_{d2} - F_{cable,2,v,c} * B_{c2} - F_{cable,2,h,c} * H_{c2}}{B_2} \quad (74)$$

$$F_{cv,vt} = F_{cv,draghead,vt} \quad (75)$$

$$F_{Bv,c,vt} = -F_{Cv,vt} - F_{drag,2} * \cos(\alpha_2) - F_{cable,2,v,c} + F_e + F_f + F_g \quad (76)$$

$$F_{Bh,c,vt} = F_{drag,2} * \sin(\alpha_2) + F_{cable,2,h,c} \quad (77)$$

Upper Suction Pipe

$$\sum M_{A,u,c,vt} = F_a * B_a + F_b * B_b + F_c * B_c + F_d * B_d + F_{Bv,c,vt} * B_2 - F_{Bh,c,vt} * H_2 - F_{drag,1} * L_{d1} - F_{cable,1,c,vt} * \sin(\beta_1) * B_{c1} - F_{cable,1,c,vt} * \cos(\beta_1) * H_{c1} = 0 \quad (78)$$

$$\sum F_{v,u,c,vt} = -F_{Bv,c,vt} + F_{drag,1} * \cos(\alpha_1) + F_{cable,1,c,vt} * \sin(\beta_1) + F_{Av,c,vt} - F_a - F_b - F_c - F_d = 0 \quad (79)$$

$$\sum F_{h,u,c,vt} = -F_{Bh,c,vt} - F_{drag,1} * \sin(\alpha_1) - F_{cable,1,c,vt} * \cos(\beta_1) + F_{Ah,c,vt} = 0 \quad (80)$$

$F_{cable,1,c,vt}$, $F_{Av,c,vt}$ and $F_{Ah,c,vt}$ are the three unknown variables, they are solved with three equations:

$$F_{cable,1,c,vt} = \frac{F_a * B_a + F_b * B_b + F_c * B_c + F_d * B_d + F_{Bv,c,vt} * B_2 - F_{Bh,c,vt} * H_2 - F_{drag,1} * L_{d1}}{B_{c1} * \sin(\beta_1) + H_{c1} * \cos(\beta_1)} \quad (81)$$

$$F_{Av,c,vt} = F_{Bv,c,vt} - F_{drag,1} * \cos(\alpha_1) - F_{cable,1,c,vt} * \sin(\beta_1) + F_a + F_b + F_c + F_d \quad (82)$$

$$F_{Ah,c,vt} = F_{drag,1} * \sin(\alpha_1) + F_{cable,1,c,vt} * \cos(\beta_1) + F_{Bh,c,vt} \quad (83)$$

Figure 52 in Appendix 7.1.7 shows the force overview of the static situation with compensated vertical soil reaction force and increasing velocity.

Static Situation with Compensated Soil Excavation Forces and Increasing Velocity

In this last iteration, with the calculations done for the forces within the draghead, the complete force equilibrium is determined. For the result of the forces within the draghead see chapter 3.2.3.2. Those forces resulted in $F_{Cv,soil,vt}$ and $F_{Ch,soil,vt}$.

Lower Suction Pipe

$$\sum F_{v,l,soil,c,vt} = -F_{Bv,soil,c,vt} - F_{Bv,c,vt} - F_{Cv,soil,vt} = 0 \quad (84)$$

$$\sum F_{h,l,soil,c,vt} = -F_{Bh,soil,c,vt} - F_{Bh,c,vt} - F_{Ch,soil,vt} = 0 \quad (85)$$

$$F_{Bv,soil,c,vt} = F_{Bv,c,vt} + F_{Cv,soil,vt} \quad (86)$$

$$F_{Bh,soil,c,vt} = F_{Bh,c,vt} + F_{Ch,soil,vt} \quad (87)$$

The force in the cable of the lower suction pipe is constant as the swell compensator levels out the tension.

Upper Suction Pipe

$$\sum M_{A,u,soil,c,vt} = F_a * B_a + F_b * B_b + F_c * B_c + F_d * B_d + F_{Bv,soil,c,vt} * B_2 - F_{Bh,soil,c,vt} * H_2 - F_{drag,1} * L_{d1} - F_{cable,1,soil,c,vt} * \sin(\beta_1) * B_{c1} - F_{cable,1,soil,c,vt} * \cos(\beta_1) * H_{c1} = 0 \quad (88)$$

$$\sum F_{v,u,soil,c,vt} = -F_{Bv,soil,c,vt} + F_{drag,1} * \cos(\alpha_1) + F_{cable,1,soil,c,vt} * \sin(\beta_1) + F_{Av,soil,c,vt} - F_a - F_b - F_c - F_d = 0 \quad (89)$$

$$\sum F_{h,u,soil,c,vt} = -F_{Bh,soil,c,vt} - F_{drag,1} * \sin(\alpha_1) - F_{cable,1,soil,c,vt} * \cos(\beta_1) + F_{Ah,soil,c,vt} = 0 \quad (90)$$

The three unknown variables are: $F_{cable,1,soil,c,vt}$, $F_{Av,soil,c,vt}$ and $F_{Ah,soil,c,vt}$. These are solved with the three equations.

$$F_{cable,1,soil,c,vt} = \frac{F_a * B_a + F_b * B_b + F_c * B_c + F_d * B_d + F_{Bv,soil,c,vt} * B_2 - F_{Bh,soil,c,vt} * H_2 - F_{drag,1} * L_{d1}}{B_{c1} * \sin(\beta_1) + H_{c1} * \cos(\beta_1)} \quad (91)$$

$$F_{Av,soil,c,vt} = F_{Bv,soil,c,vt} - F_{drag,1} * \cos(\alpha_1) - F_{cable,1,soil,c,vt} * \sin(\beta_1) + F_a + F_b + F_c + F_d \quad (92)$$

$$F_{Ah,soil,c,vt} = F_{drag,1} * \sin(\alpha_1) + F_{cable,1,soil,c,vt} * \cos(\beta_1) + F_{Bh,soil,c,vt} \quad (93)$$

Figure 53 in Appendix 7.1.8 shows the force overview of the static situation with compensated soil excavation forces and increasing velocity.

3.2.3.2 Forces in the Draghead

To complete the equilibrium of the forces within the suction pipe, the total resulting force in the draghead is determined. The cutting force is determined by the cutting depth of the jets. The force exerted by the jets are discussed in 3.2.3.2 Penetration Depth and Production Jets. Results of the calculations of the jets are used within this chapter to complete the force equilibrium for the draghead. The method to calculate the forces within the draghead is based on the method that Gijs ter Meulen used in his master thesis: Draghead Analysis [40]. The following main forces exist in the draghead while dredging:

1. Gravity Force
2. Drag Force
3. Jet Force
4. Impulse Force
5. Vacuum Force
6. Sled Force (incl. TED)
7. Friction Force
8. Cutting Force

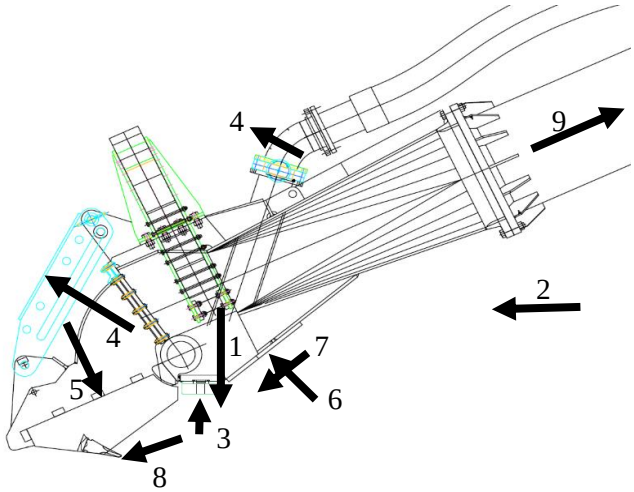

Figure 28: Forces on the Draghead

Source: GLDD Tame Dragon Draghead

Gravity Force

The gravity force of the draghead is determined with equation 45 explained in chapter 3.2.3.1. The total submerged force of the draghead is 85,866 N.

Drag Force

To determine the drag force of the draghead, the draghead is approximated as a block. The theory of the drag force is presented is chapter 3.2.3.1. The drag force for the draghead is approximated with the following equation where A represents the frontal surface of the draghead and Cd the drag coefficient:

$$F_D = \frac{1}{2} * \rho_w * {v_f}^2 * C_d * A \tag{94}$$

Jet Force

The water being forced out of the nozzles by the jet engine create a force. The direction of the force depends on the lower arm angle (LAA) as the draghead is fixed to the lower suction pipe. With a lower arm angle of 25°, the force of the jets is vertical.

$$F_j = \rho_w * A_n * {u_j}^2 * n_j \tag{95}$$

The area of the nozzle (A_n) is multiplied by the exit velocity of the water (u_j) squared by the density of the water and the number of nozzles (n_j) to determine the total forces exerted by the jets (F_j). The exit velocity of the water is calculated by taking the root of two times the differential pressure of the jets.

Impulse Force

The bend of the visor to the lower suction pipe causes an impulse force when the soil is being sucked up. The energy of accelerating the soil creates an impulse force when the direction of travel changes. This direction changes where the suction pipe within the draghead bends. The horizontal, vertical and total impulse force is determined respectively with the following equation:

$$F_{imp,h} = \rho_m * A_{sp} * {v_s}^2 * (1 - \cos(\beta_b)) \tag{96}$$

$$F_{imp,v} = \rho_m * A_{sp} * {v_s}^2 * \sin(\beta_b) \tag{97}$$

$$F_{imp} = \sqrt{{F_{imp,h}}^2 + {F_{imp,v}}^2} \tag{98}$$

To determine the impulse force, the density of the mixture (ρ_m) is needed, as well as the area of the suction pipe (A_{sp}) within the draghead, the trailing speed (v_s) and the bending angle (β_b).

Vacuum Force

Dredging pumps create a low pressure which enables the suction of the excavated soil. At the opening of the visor a vacuum force is created as result of the low pressure. The draghead is pulled towards the ocean bottom as the dredge moves along. This vacuum force is determined by a few factors. The dimensionless coefficient ξ is a correction for the seal and shape of the suction pipe entrance and also for the geometry inefficiency of the inside of the draghead. The density of the mixture, velocity of the dredge and the area of the visor where the soil is sucked up ($A_{suction}$) are the other factors. This result in the following equation to determine the vacuum force:

$$F_{vac} = \frac{1}{2} * \xi * \rho_m * {v_s}^2 * A_{suction} \tag{99}$$

Sled Force

Because of the weight of the draghead, it sinks into the sand at the bottom. The cables do not fully support the dragheads weight. Dragging along the draghead while it is partly buried in the sand creates a dragging force, also known as a sled force (F_{sled}). With the specific compaction force method by Koolen and Kuipers in 1983, the settlement depth is calculated:

$$h_{settle} = \sqrt{\frac{2 * Q * \sin(\alpha_2)}{w_{sup} * q_{soil} * g}} \tag{100}$$

The w_{sup} is the width of the area that makes contact with the bottom. q_{soil} represents the specific compaction force. This force is set at 6 kg/cm^3 which is for heavy soil determined by Bernacki and Haman in 1973. The last unknown is the resultant force Q of the draghead on the bed. That force is determined by a moment equilibrium around point B with all the existing forces and becomes:

$$\begin{aligned}\sum M_B = &-Q * l_2 - \left(F_{c,visor,h} + F_{imp,bend,visor,h}\right) * l_2 * \sin(\alpha_2) \\ &+ \left(F_{c,dh,v} - F_{jet} + F_{c,visor,v} - F_{imp,bend,visor,v}\right) * l_2 * \cos(\alpha_2)\end{aligned} \tag{101}$$

With Q:

$$\begin{aligned}Q = &-\left(F_{c,visor,h} + F_{imp,bend,visor,h}\right) * \sin(\alpha_2) \\ &+ \left(F_{c,dh,v} - F_{jet} + F_{c,visor,v} - F_{imp,bend,visor,v}\right) * \cos(\alpha_2)\end{aligned} \tag{102}$$

All the represented forces are made clear in the following chapters. The Q can only be determined with all the other forces known.

Friction Force

Dragging the draghead along the bottom also creates a friction force of the sand with the bottom of the draghead. An external friction angle (δ) is known for two materials making contact. With that angle, the friction coefficient (μ) is calculated:

$$\mu = \tan(\delta) \tag{103}$$

The external friction angle is 10° which makes the friction coefficient 0.176. This is according to Butterfield and Andrawes (1972b). They found a friction coefficient of 0.17 for a fine particle soil with a porosity of 43.7%. The total friction force is determined by multiplying the friction coefficient with the sled force (Q) calculated in the previous chapter.

$$F_{fr} = 0.176 * Q \tag{104}$$

The total friction force is decomposed into a vertical and horizontal component respectively:

$$F_{fr,v} = F_{fr} * \sin(\alpha_2) \tag{105}$$

$$F_{fr,h} = F_{fr} * \cos(\alpha_2) \tag{106}$$

3.2.3.1 Turtle Excluder Device

Dredging areas are chosen to where the most production can be achieved. It is possible that dredging can interfere with the marine life even though dredging companies try to avoid that. One of the species that are actively protected from being harmed are the turtles. When danger approaches, turtles have the tendency to dig themselves into the ground. The green sea turtle is an endangered sea turtle that dredges have to avoid. The turtle excluder device (TED) is developed in the 70s In the U.S. the device was made mandatory for trawling shrimping boats in 1987. In most States dredges are obliged to use TEDs attached to the dragheads to avoid turtles being sucked up in the draghead. The TED, circled in red in Figure 29, has the form of a wedge to push aside any turtles. A draghead equipped with a TED increases the trailing resistance significantly. The weight of the TED also increases the trailing resistance.

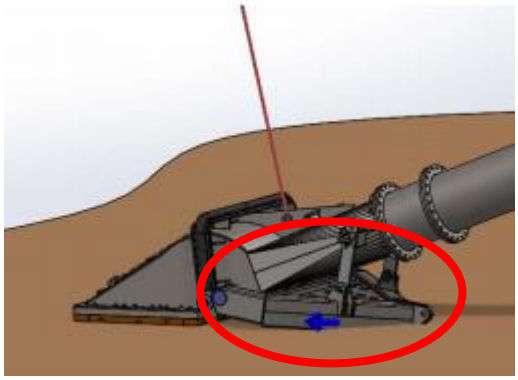

Figure 29: Representation of a TED [62]

The TED is included in the resistance of the draghead with the following specifications:

Specifications TED

Mass	mTED	982	kg
Depth	hTED	0.152	m
Angle	αTED	45	deg
Width	wTED	2.00	m

Table 2: Specifications TED

The resistance of the TED is determined with the same method as the sled resistance of the draghead by using the settlement depth. The settlement depth of the TED is a constant. Therefore, the resistance at a certain depth is calculated as follows:

$$F_{sled,TED} = \frac{h_{TED,settle}{}^{2} * w_{TED} * q_{soil} * g}{2 * \sin(\alpha_{TED})} \quad (107)$$

The friction of the TED is then calculated with the following equation:

$$F_{fric,TED} = \tan(\delta) * F_{sled,TED} \quad (108)$$

The horizontal and vertical components of the friction and sled resistance are added up to the force equilibrium of point C (total draghead force).

Cutting Force

The penetration depth of the teeth (h_i) which is needed to calculate the cutting forces are determined in chapters 3.2.3.2 and 3.2.3.3. The cutting forces of the draghead are determined according to the theory of The Delft Sand, Clay and Rock Cutting Model [41]. For determining the cutting forces, saturated sand is used as the soil type. This method is based on a certain penetration depth (h_i) at variable speeds. However, the penetration depth of the teeth variate with the speed can also be calculated within the model. The total equilibrium of the horizontal and vertical forces is calculated with the following equations:

$$\sum F_h = K1 * \sin(\beta + \varphi) - W1 * \sin(\beta) + W2 * \sin(\alpha) - K2 * \sin(\alpha + \beta) = 0 \quad (109)$$

$$\sum F_v = -K1 * \cos(\beta + \varphi) + W1 * \cos(\beta) + W2 * \cos(\alpha) - K2 * \cos(\alpha + \beta) = 0 \quad (110)$$

The W1 represents the result of the water under pressure in the shear zone and W2 the pressure on the blade. The figures below show the forces on the layer cut and blade in water saturated sand.

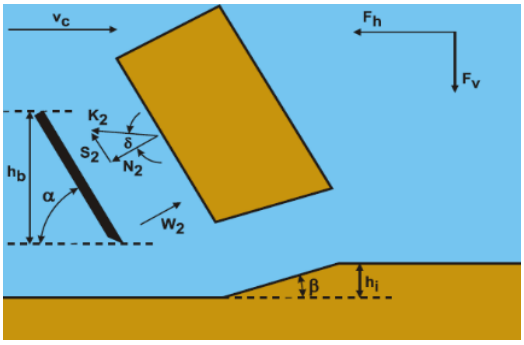

Figure 31: Forces on the Layer Cut in Water Saturated Sand

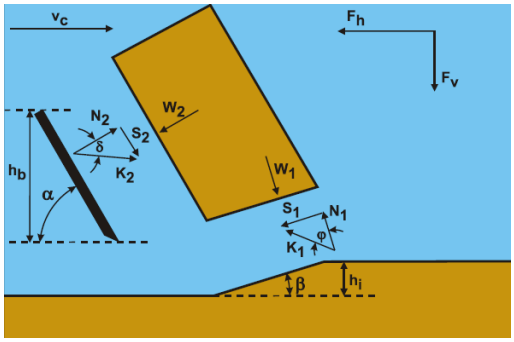

Figure 30: Forces on the Blade in Water Saturated Sand

The normal force (N1) and shear force (S1) are expressed in the resulting grain force K1 of the shear plane:

$$K1 = \sqrt{N1^2 + S1^2} \quad (111)$$

The resulting force K2 is calculated in the same way but with the normal and shear force of the blade. Combining the equilibrium of forces and the equation to determine the resulting grain force (K), forces K1 and K2 are expressed as follows:

$$K1 = \frac{W2 * \sin(\varphi) + W1 * \sin(\alpha + \beta + \delta)}{\sin(\alpha + \beta + \delta + \varphi)} \quad (112)$$

On the blade, the force K2 is expressed as follows:

$$K2 = \frac{W2 * \sin(\alpha + \beta + \delta) + W1 * \sin(\delta)}{\sin(\alpha + \beta + \delta + \varphi)} \quad (113)$$

The horizontal and vertical forces on the blades can now be derived with the following formula:

$$F_h = -W2 * \sin(\alpha) + K2 * \sin(\alpha + \delta) \tag{114}$$

$$F_v = -W2 * \cos(\alpha) + K2 * \cos(\alpha + \delta) \tag{115}$$

Figure 32 on the right represents the forces on the blade when cutting through water saturated sand.

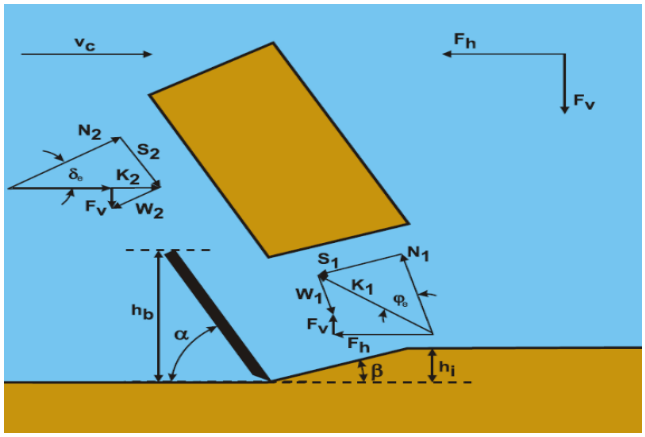

Figure 32: Forces on the Blade when Cutting through Water Saturated Sand

In order to determine the forces on the blades, the pore pressures in the shear plane and the pore pressures of the material on the blade have to be calculated. When the teeth of the draghead cut through the sand, the volume of the sand changes as a result of the shear stresses. The following equation represents the increase in pore volume per unit of blade length:

$$\Delta V = \varepsilon * \Delta A = \varepsilon * \Delta x * \Delta h_i = \varepsilon * \Delta x * \Delta l * \sin(\beta) \tag{116}$$

The figure below shows the distribution of the particles before and after the material is cut. After the cutting the porosity of the particles increases.

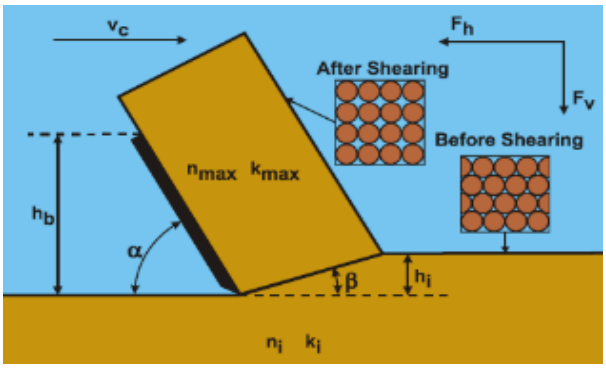

Figure 33: Particles Distribution Before and After Shearing

The space created by the disorientation of the particles will fill up with the fluid it is situated. For sand the equation below represents the volume flow rate flowing to the created space:

$$\Delta Q = \frac{\partial V}{\partial t} = \varepsilon * \frac{\partial x}{\partial t} * \Delta l * \sin(\beta) = \varepsilon * v_c * \Delta l * \sin(\beta) \tag{117}$$

When including Darcy's Law, the following equation is derived to determine the specific flow rate perpendicular to the deformation zone:

$$q = \frac{\partial Q}{\partial L} = q1 + q2 = \varepsilon * v_c * \sin(\beta) \tag{118}$$

The flow lines for the analytical method are shown in the figure below:

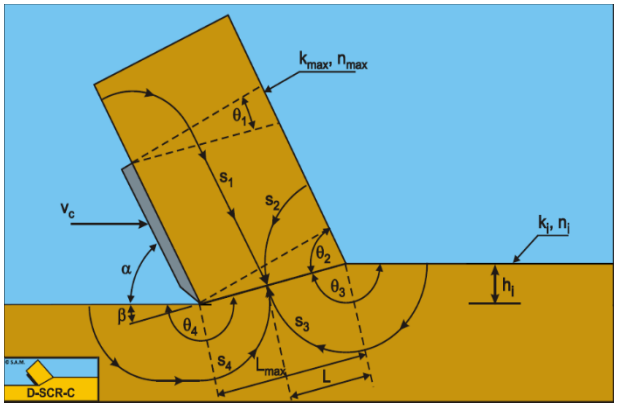

Figure 34: Flow Lines of the Analytical Method

The variables for the shear plane and the total resistance of the flow lines are defined in Appendix 7.1.9. The total resistance replaces the h_i/k_{max} part of the water under-pressure equations. This results in the following equation to determine the pore vacuum pressure of the point on the shear zone:

$$\Delta p = \rho_w * g * v_c * \varepsilon * \sin(\beta) * R_t \tag{119}$$

The average pore vacuum pressure is determined by the summation of the pore vacuum pressure of each point:

$$p_{1m} = \frac{1}{n} * \sum_{i=0}^{n} \Delta p_i \tag{120}$$

The pore pressures on the blade are determined with different equations as there is no dilatation the blade. This is shown in Appendix 7.1.10. When the number of intervals for entrainment and the geometry are taken into account the R2 is written as follows:

$$R'_2 = N * 1.75 * \left(\frac{h_i}{\sin(\beta)} * \frac{\sin(\alpha)}{h_b} \right) * R_2 \tag{121}$$

The flows over the blade can now be determined with the three equations below:

$$q_0 = \frac{\Delta p_{tip}}{\rho_w * g * R_{t,0}} \tag{122}$$

$$q_{1,0} = \frac{\Delta p_{tip}}{\rho_w * g * R_{1,0}} \tag{123}$$

$$q_{2,0} = \frac{\Delta p_{tip}}{\rho_w * g * R'_2} \tag{124}$$

Each iteration step of the pore vacuum pressure over the blade are determined by:

$$q_i = q_{i-1} - q_{2,i-1} \tag{125}$$

$$\Delta p_i = \rho_w * g * q_i * R_{t,i} \tag{126}$$

The average pore vacuum pressure can now be determined by summation of each point with:

$$p_{2m} = \frac{1}{n} * \sum_{i=0}^{n} \Delta p_i \tag{127}$$

The boundary conditions in which the water under-pressures are calculated are shown in Figure 35. The pressure distribution equals zero if the height difference over the blade is neglected.

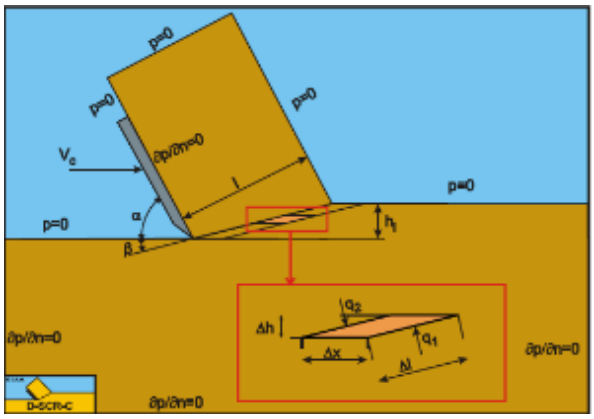

Figure 35: Volume Balance over the Shear Zone

With physical modelling it has been assumed that the tip of the teeth (or cutting blade) is always sharp, whereas in practise the sharpness of the blade wears off quickly. The equations below show the water pressure forces without cavitation:

$$W1 = \frac{p_{1m} * \rho_w * g * v_c * \varepsilon * {h_i}^2 * w}{k_{max} * \sin(\beta)} \tag{128}$$

$$W2 = \frac{p_{1m} * \rho_w * g * v_c * \varepsilon * h_i * h_h * w}{k_{max} * \sin(\alpha)} \tag{129}$$

Cavitation occurs when the pore pressures reach the water vapour pressure. At a water temperature of 15 °C the vapour pressure is 1.7056 kPa. The following equations of the water pressure forces are valid when cavitation occurs:

$$W1 = \frac{\rho_w * g * (z + 10) * h_i * w}{\sin(\beta)} \tag{130}$$

$$W2 = \frac{\rho_w * g * (z + 10) * h_b * w}{\sin(\alpha)} \tag{131}$$

The cutting forces can now be determined with the following equations. The first horizontal and vertical force are used in situations without cavitation, the second set of equations are used for a cavitating cutting process.

$$F_h = \frac{c_1 * \rho_w * g * v_c * \varepsilon * {h_i}^2 * w}{k_{max}} \tag{132}$$

$$F_v = \frac{c_2 * \rho_w * g * v_c * \varepsilon * {h_i}^2 * w}{k_{max}} \tag{133}$$

When in cavitating condition the following equations are to be used:

$$F_h = d_1 * \rho_w * g * (z + 10) * h_i * w \tag{134}$$

$$F_v = d_2 * \rho_w * g * (z + 10) * h_i * w \tag{135}$$

The unknown c_1 and c_2 are calculated as follows:

$$c_1 = \left(\frac{\left(p_{1m} * \frac{\sin(\phi)}{\sin(\beta)} + p_{2m} * \frac{h_b}{h_i} * \frac{\sin(\alpha+\beta+\phi)}{\sin(\alpha)} \right) * \sin(\alpha+\beta)}{\sin(\alpha+\beta+\delta+\phi)} - p_{2m} * \frac{h_b}{h_i} * \frac{\sin(\alpha)}{\sin(\alpha)} \right) * \frac{(a_1 * k_i + a_2 * k_{max})}{k_{max}} \tag{136}$$

$$c_2 = \left(\frac{\left(p_{1m} * \frac{\sin(\phi)}{\sin(\beta)} + p_{2m} * \frac{h_b}{h_i} * \frac{\sin(\alpha+\beta+\phi)}{\sin(\alpha)} \right) * \cos(\alpha+\beta)}{\sin(\alpha+\beta+\delta+\phi)} - p_{2m} * \frac{h_b}{h_i} * \frac{\cos(\alpha)}{\sin(\alpha)} \right) * \frac{(a_1 * k_i + a_2 * k_{max})}{k_{max}} \tag{137}$$

With for a weighted average permeability k_m:

$$a_1 + a_2 = 1 \tag{138}$$

$$k_m = a_1 * k_i + a_2 * k_{max} \tag{139}$$

The values of d_1 and d_2 for the cavitating cutting process are calculated as follows:

$$d_1 = \frac{\left(\frac{\sin(\phi)}{\sin(\beta)} + \frac{h_b}{h_i} * \frac{\sin(\alpha+\beta+\phi)}{\sin(\alpha)} \right) * \sin(\alpha+\delta)}{\sin(\alpha+\beta+\delta+\phi)} - \frac{h_b}{h_i} * \frac{\sin(\alpha)}{\sin(\alpha)} \tag{140}$$

$$d_2 = \frac{\left(\frac{\sin(\phi)}{\sin(\beta)} + \frac{h_b}{h_i} * \frac{\sin(\alpha+\beta+\phi)}{\sin(\alpha)} \right) * \cos(\alpha+\delta)}{\sin(\alpha+\beta+\delta+\phi)} - \frac{h_b}{h_i} * \frac{\cos(\alpha)}{\sin(\alpha)} \tag{141}$$

This approach gives an approximation of the vertical and horizontal forces. Results show that the cutting forces are linear with the given speed with the other variables constant. For every variation in speed the calculations have to be repeated. The result of the horizontal cutting force with a fixed visor is shown in Figure 36. In Figure 37, the horizontal cutting force with a floating visor is shown.

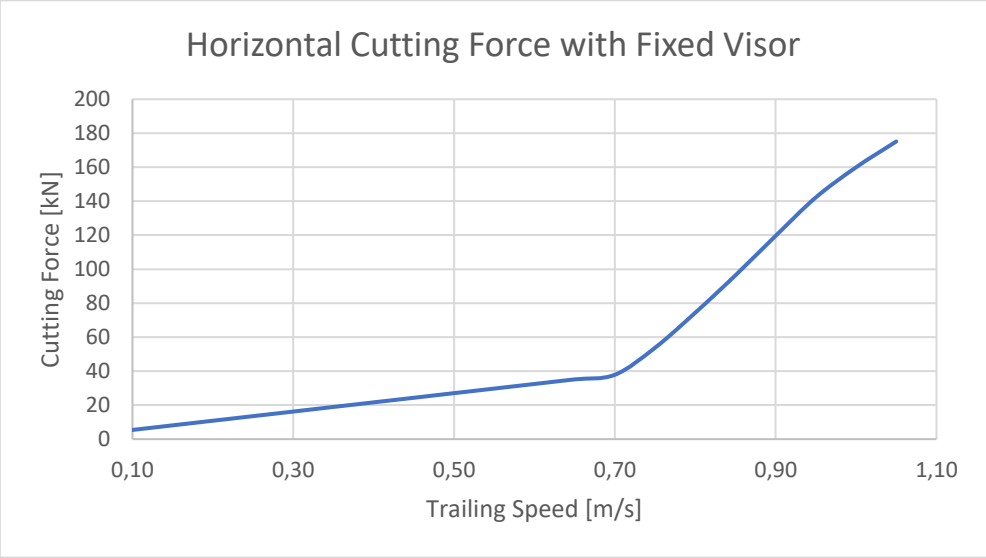

Figure 36: Horizontal Cutting Force with a Fixed Visor

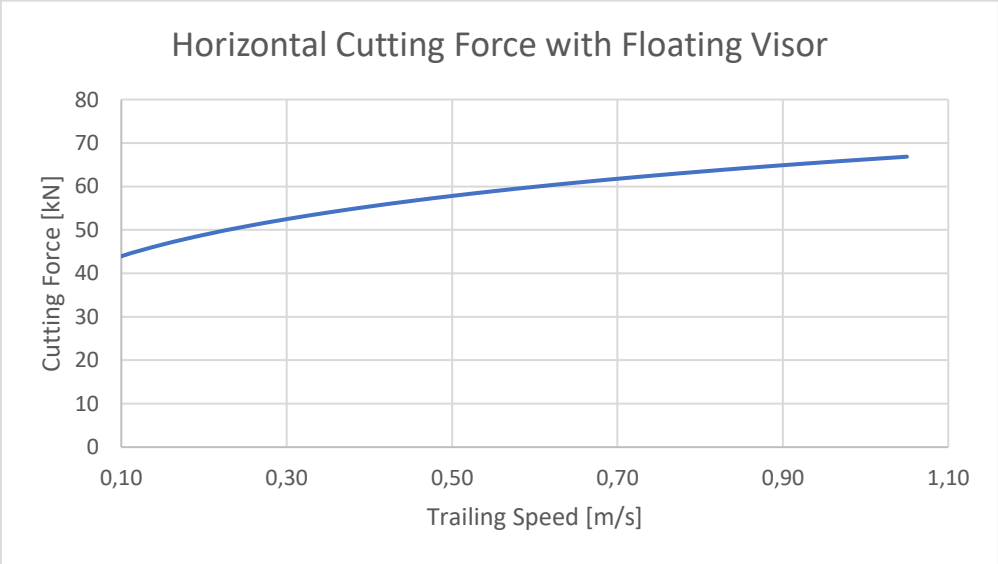

Figure 37: Horizontal Cutting Force with a Floating Visor

3.2.3.2 Penetration Depth and Production Jets

The water exerted by the jets forces its way into the soil and penetrates through the soil up to a certain depth. This depth is dependent on multiple factors, such as the speed of the water pushed through the nozzles, the number of nozzles, the exit diameter of the nozzles and the grain size of the soil. As the jets inject water into the soil, the density of the soil changes. With the paper 'Production Estimation of Water Jets in Dragheads' written by S.A. Miedema [42], the penetration depth of the jets and the density of the mixture at variable trailing speeds is calculated.

The penetration depth of one nozzle is given by the following equation:

$$h_{i,j} = \sqrt{\frac{(\Delta p_j * \frac{2 * \Delta p_j}{p_1})^{\frac{1}{2}} * \frac{\pi}{4} * (\alpha * D_j)^2}{c_1 * \rho_1 * g * {v_c}^2 * w_j}} * \frac{k_m}{\varepsilon} \tag{142}$$

The situ production of one nozzle (Q_s)is calculated with the following formula:

$$Q_s = \frac{(\Delta p_j * \frac{2 * \Delta p_j}{p_1})^{\frac{1}{2}} * \frac{\pi}{4} * (\alpha * D_j)^2}{E_{sp}} \tag{143}$$

The specific energy (E_{sp}) is approached with the assumption that the specific energy for jetting equals the specific energy for non-cavitating cutting:

$$E_{sp} = c_1 * \frac{\rho_1 * g * h_{i,j} * v_c * \varepsilon}{k_m} \tag{144}$$

To determine the penetration height, the equation to determine the specific energy is implemented. The mean permeability (k_m) is the average of the maximum (k_{max}) and initial permeability (k_i). The mean permeability is calculated as follow:

$$k_m = \frac{k_i + k_{max}}{2} \tag{145}$$

The dilatation is expressed in:

$$\varepsilon = \frac{n_{max} + n_i}{1 - n_{max}} \tag{146}$$

The maximum porosity (n) is set at 0.5. The initial porosity is a result a soil sample. In the estimation phase of bidding on a job, GLDD takes samples of the to be dredged soil. The soil is studied and one of the results is the porosity. The initial permeability is determined with the following equation and is only valid in a laminar flow:

$$k = 8.3 * 10^{-3} * \frac{g}{v_1} * \frac{n^3}{(1-n)^2} * {d_{10}}^2 \tag{147}$$

As result of using the Kozency Carman equation for the permeability the ratio of km to ε is found:

$$\frac{k_m}{\varepsilon} \approx 10 * k_i \tag{148}$$

The penetration depth and width are used to determine the production of the jets. The penetration width is dependent on the trailing speed. To calculate the width for a certain trailing speed, the following equation is used:

$$w_j = (\frac{v_c}{v_1})^{\beta} * h_i \tag{149}$$

The β and v_1 are both about unity according to the results based on the experiments of van Rhee [47] [48] [49]. Therefore, the penetration depth and width is expressed into the following equations:

$$h_{i,j} = 2 * \frac{\Delta p_j{}^{1/2} * D_j{}^{2/3} * k_i{}^{1/3}}{v_c} \tag{150}$$

$$w_j = 2 * \Delta p_j{}^{1/2} * D_j{}^{2/3} * k_i{}^{1/3} \tag{151}$$

A limit has been set to the penetration depth of the jets to make the situation more realistic as these calculations are an approach to the reality. The situ production with the jets of one nozzle becomes:

$$Q_s = h_{i,j} * w_j * v_c \tag{152}$$

The density of the saturated sand changes with the injected water by the jets. To determine the density of the mixture, the mixture concentration (C_{VS}), density of the water and quartz has to be known. The $Q_{s,dh}$ is determined by multiplying the Q_s with the number of nozzles on the draghead. The production of the suction pipe (Q_m) influences the mixture concentration. The C_{VS} is calculated as follows:

$$C_{VS} = \frac{Q_{s,dh} * (1 - n_i)}{Q_m} \tag{153}$$

The density of the quartz is known by the type of sand, the density of the water is also known. Now, the density of the mixture is determined:

$$\rho_m = C_{VS} * \rho_q + (1 - C_{VS}) * \rho_w \tag{154}$$

The first layer is cut by the jets, the layer underneath is cut by the teeth. The total penetration depth also depends on the penetration depth of the visor which is explained in the following chapter.

3.2.3.3 Penetration Depth and Production Visor and Jets Combined

The penetration depth of the jets is known. Two different types of dredging is used within the model. Dredging with a fixed visor and dredging with a floating (free) visor. When dredging occurs with a fixed visor, the minimum and maximum angle of the visor is fixed. The visor is therefore forced into the soil which creates in theory a constant penetration depth at a certain trailing speed. The interaction between trailing speed, penetration depth of the jets and soil grain size determine the penetration depth of the teeth and thus the forces. The cutting force by the teeth are the biggest contributor of resistance during the loading condition.

The other option to dredge is with a floating visor. The angle of rotation of the visor is free and the cutting depth of a free visor is determined by the created moment of the visor. With a free visor, higher trailing speeds can be obtained, but the production per time unit is lower in comparison with a fixed visor.

Fixed Visor

Within the model the minimum ($\gamma_{1,min}$)and maximum angles ($\gamma_{1,max}$) of the visor is an input. The minimum depth of the visor ($h_{v,min}$) is calculated as follows:

$$h_{v,min} = l_v * \sin(\gamma_{1,min} + LAA - 45°) + D_t \tag{155}$$

The maximum depth of the visor ($h_{v,max}$) is calculated with the same equation as above only with maximum visor angles instead of minimum. The minimum penetration depth of the visor is equal to the

total penetration depth ($h_{p,fi}$). The penetration depth of the teeth (D_t) is dependent on the length of the teeth (l_t), the angle of the teeth to the visor (γ_2) and the nozzle height:

$$D_t = l_t * \sin(\gamma_2 - \sin(\gamma_1 + LAA - 45°)) - h_{nozzle} \quad (156)$$

The lower arm angle (LAA) is the angle between the bottom of the ocean and the lower suction pipe. The angle of the draghead to the lower suction pipe is fixed at an angle of 25°. The dredge master variates the lengths of the cables to the suction pipes in a way that the LAA is at an angle of 25°. For the production with a fixed visor, the cutting depth of the teeth has to be known. The total penetration depth is known as the visor is fixed. This means that the cutting depth by the teeth are the total penetration depth minus the jet penetration depth.

The situ production of the draghead with a fixed visor ($Q_{s,vi,fi}$) becomes:

$$Q_{s,\mathrm{vi},fi} = h_{p,fi} * w_{vi} * v_c \quad (157)$$

To determine the cutting depth of the fixed visor ($h_{c,fi}$), the total penetration depth ($h_{p,fi}$) must be subtracted by the penetration depth of the jets ($h_{c,j}$). The mixture concentration is determined as follows:

$$C_{VS,t,fi} = \frac{Q_{s,\mathrm{vi},fi} * (1 - n_i)}{Q_m} \quad (158)$$

The total density of the mixture is determined accordingly:

$$\rho_{m,t,fi} = C_{VS,t,fi} * \rho_q + \left(1 - C_{VS,t,fi}\right) * \rho_w \quad (159)$$

Floating Visor

To determine the cutting depth of a floating visor for non-cavitational cutting forces the following equation is used:

$$h_{c,fl} = \sqrt{\frac{F_G * L_G * k_i}{v_c * w_{vi} * (c_2 * L_h - c_3 * L_v)}} \quad (160)$$

The constants c_2 and c_3 are determined with the equations below:

$$c_2 = 0.0427 * e^{0.0509*\varphi} \quad (161)$$

$$c_3 = 0.0343 * e^{0.0341*\varphi} \quad (162)$$

The angle of internal friction is dependent on the blow count as explained in chapter 2.1.3.6 Soil Specifications. The width of the draghead (w_{dh}) and the trailing speed are known, this leaves the moment of the visor to be calculated. The gravitational force of the visor submerged is determined as follows:

$$F_G = g * m_v - (V_v * \rho_w) \quad (163)$$

The L_G is the horizontal distance of the point of gravity of the visor to the rotation point (visor bearing). L_h represents the horizontal distance of the point of the teeth to the visor bearing and L_v the same distance but vertically. The cut production of the floating visor ($Q_{c,fl}$) can be calculated with:

$$Q_{c,fl} = h_{c,fl} * w_{vi} * v_c \quad (164)$$

The total production of the draghead for the floating visor, so the production of the jets and visor ($Q_{s,dh,fl}$) is adding up the two separate productions. The total density mixture of the jets combined with the teeth can now be determined with first the mixture concentration ($C_{VS,t}$):

$$C_{VS,t,fl} = \frac{(Q_{s,\mathrm{dh}} + Q_{c,fl}) * (1 - n_i)}{Q_m} \tag{165}$$

Next the density mixture of the total production ($\rho_{m,t}$):

$$\rho_{m,t,fl} = C_{VS,t} * \rho_q + \left(1 - C_{VS,t}\right) * \rho_w \tag{166}$$

When the weight of the draghead is included, the total depth that the draghead creates is determined with the following equation with either the floating or fixed visor:

$$h_{tot} = h_c + h_j \tag{167}$$

The cutting depth of the teeth and the jets create the total penetration depth. As the trailing speed increases the total cutting depth remains constant with a fixed visor as shown in Figure 38 below.

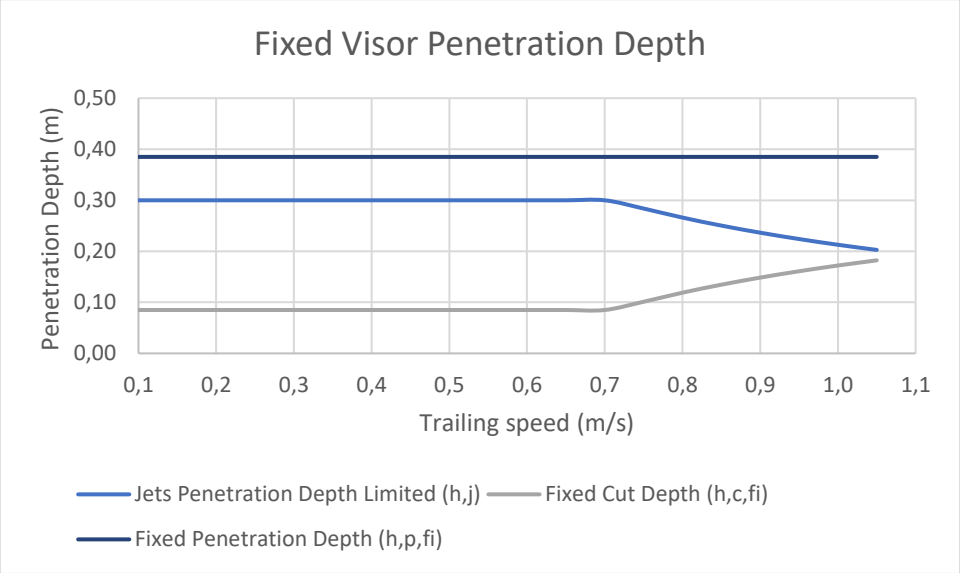

Figure 38: Fixed Visor Penetration Depth

With a floating visor, the total penetration depth decreases as the trailing speed increases as shown below. The penetration depth of the floating visor is independent to the jet penetration.

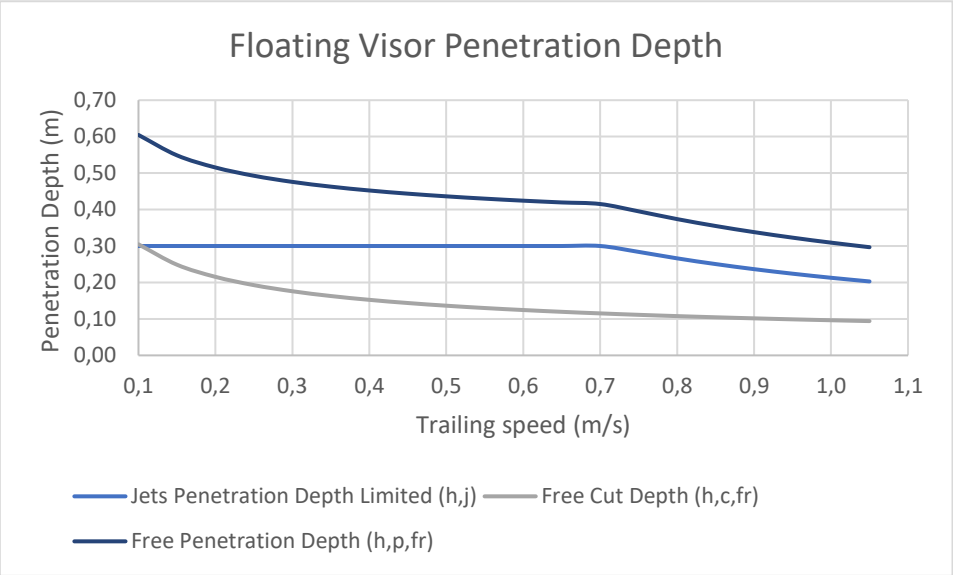

Figure 39: Floating Visor Penetration Depth

3.2.3.1 Hopper Settlement

The duration of the loading of the hopper depends on either the maximum load or the maximum volume of the soil. When one of these reaches the limit, the hopper is considered full. Both variables are calculated and the shortest time to load decides whether the hopper is full by weight or volume. The emission model is based on fine saturated sand. Within this scenario, the hopper is considered fully loaded when it reaches the maximum load weight. The time to reach the maximum weight (T_f) is determined by the production of the jets (Q_j) and the production of the teeth (Q_t). This production is multiplied by the percentage volume of the quartz (C_{VS}) for both jets and teeth. The suction velocity (Q_p) determines the volume of the quartz is dropped into the hopper. The maximum weight allowed in the hopper (V_H) is divided by the production rate:

$$T_f = V_H / \left((Q_j * C_{VS,j} + Q_t * C_{VS,t}) * Q_p \right) \tag{168}$$

The time to full load variates with the dredging velocity, total penetration depth, percentage volume of the quartz, suction volume and the hopper size. The overflow is taken into account as a variable in the time to load. The total time for the hopper to be full is multiplied by the percentage of overflow losses.

3.2.3.2 Total Draghead Force

The total force of the draghead can now be determined. This force is used to determine the total forces in the suction pipes (see chapter 3.2.3).

$$\sum F_{h,draghead} = -F_{c,visor,h} - F_{fric,draghead,h} - F_{sled,draghead,h} - F_{imp,bend,visor,h} - F_{sled,TED,h} - F_{fric,TED,h} + F_{c,soil,h} = 0 \tag{169}$$

$$\sum F_{v,draghead} = F_{jet} - F_{c,visor,v} - F_{c,draghead,v} - F_{fric,draghead,v} + F_{sled,draghead,v} + F_{imp,bend,visor,v} + F_{sled,TED,v} - F_{fric,TED,v} + F_{c,soil,v} = 0 \tag{170}$$

Which gives for the $F_{c,soil}$ horizontal and vertical:

$$F_{c,soil,h} = F_{c,visor,h} + F_{fric,draghead,h} + F_{sled,draghead,h} + F_{imp,bend,visor,h} + F_{sled,TED,h} + F_{fric,TED,h} \quad (171)$$

$$F_{c,soil,v} = -F_{jet} + F_{c,visor,v} + F_{c,draghead,v} + F_{fric,draghead,v} - F_{sled,draghead,v} - F_{imp,bend,visor,v} - F_{sled,TED,v} + F_{fric,TED,v} - F_{c,soil,v} \quad (172)$$

3.2.3.1 Total Trailing Resistance

The total trailing resistance that the dredge has to overcome by propulsion power are calculated with the following equation:

$$F_{h,total,trailing} = F_{Ah,soil,c,vt} - F_{Ah,c} \quad (173)$$

The cutting forces, draghead forces and the forces on the suction pipes are combined to determine the total trailing resistance. Figure 41 shows the trailing force with a fixed visor with an increasing trailing speed. The change of increase rate at a speed of 0.7 m/s is cause by the decreasing penetration depth of the jets. Figure 40 shows the total trailing force with an increasing speed with a floating visor. As the visor does not dig into the sea bottom, the trailing force encounters a slight increase as the trailing speed increases.

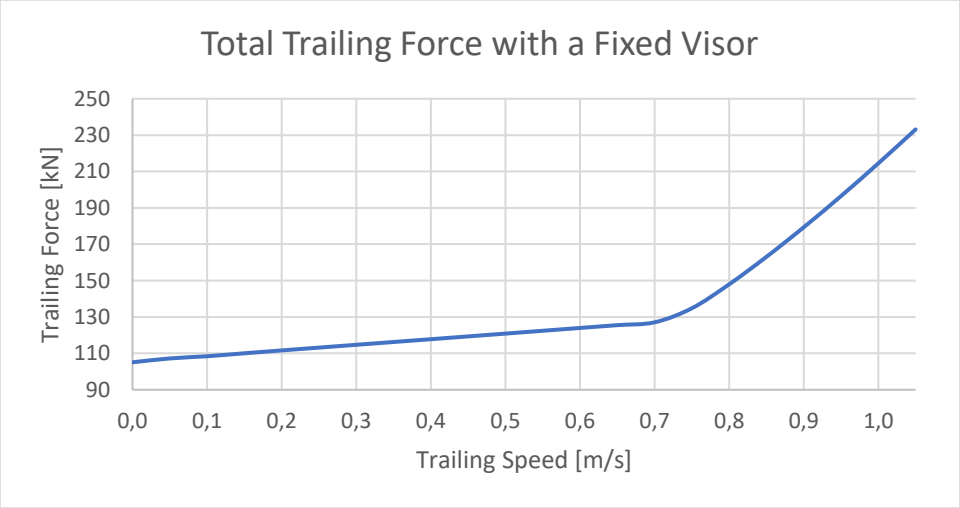

Figure 41: Total Trailing Force with a Fixed Visor

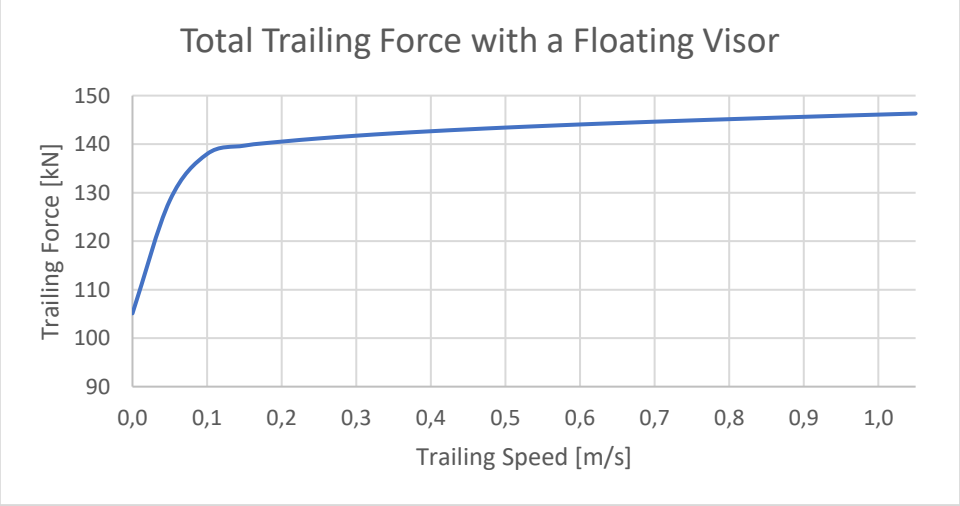

Figure 40: Total Trailing Force with a Floating Visor

3.2.4 Matching the Propeller and the Main Engine

The background information of the efficiency of the propeller is given in chapter 2.1.3.5. With the total resistance known the power to overcome the resistance (also known as the effective towing power (P_E)) is calculated with the following equation:

$$P_E = R_{tot} * v_s \tag{174}$$

The power of the engine has to be transferred to the propulsor. The propulsor transfers the mechanical energy to propel the ship. The type and specifications of the propulsor have a large impact on the performance and efficiency. Figure 42 shows the components that are calculated to determine the engine power to propel the vessel. The effective towing power is now known. The thrust power (P_T) is determined next by dividing the P_E to the number of propulsors. The propulsor power (P_P), power to the shaft (P_S) and finally the required brake power of the engine (P_B) are to be calculated. Within the model, a FPP is used to determine the required power of the engine. The velocity of the flow to the propeller is different than the velocity of the vessel. The velocity of the fluid right before the propeller is called the advance velocity (v_A). The hull of the vessel determines the flow to the propeller, especially the shape of the aft part of the vessel. The wake-factor is the difference between the velocity of the vessel and advance velocity as a ratio of the velocity of the vessel. The advance velocity is influenced by the wake of the vessel. The wake-factor is approached by the following equation to eventually determine the advance velocity. This equation is valid for twin screw ships:

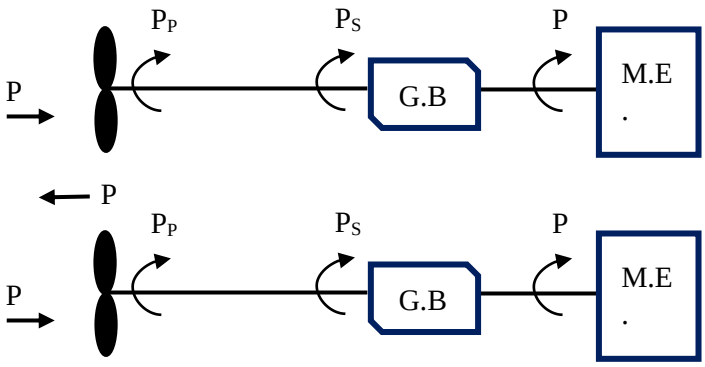

Figure 42: Propulsion Power Plant with Two Propellers and Two Engines

$$w = 0.3095 * C_B + 10 * C_V * C_B - 0.23 * D/\sqrt{BT} \tag{175}$$

The advance velocity can now be determined with:

$$v_A = (1 - w) * v_S \tag{176}$$

Not all the produced thrust is used to overcome the total resistance of the vessel. A reduction of the thrust must be taken into account. The thrust deduction factor (t) is approached with the following equation:

$$t = 0.325 * C_B - 0.1885 * D/\sqrt{BT} \tag{177}$$

With the thrust deduction factor and the wake factor known, the hull efficiency is expressed:

$$\eta_H = \frac{1 - t}{1 - w} \tag{178}$$

With the hull efficiency and the effective towing power (P_E) known, the thrust power (P_T) is calculated:

$$P_T = \frac{P_E}{(\eta_H * k_p)} \tag{179}$$

The number of propellers is denoted as k_p. With twin screw vessels, the thrust power shows the amount of power that has to be delivered per propeller. The power arrangement now determines the engine power. To determine the engine brake power, the following steps are valid for a mechanical power arrangement. The propellers are both directly driven by one propulsion engine. The propeller efficiency, thrust coefficient and torque coefficient can be determined for a certain propeller. The curves of the efficiency and coefficients are dependent on the advance ratio and the pitch diameter ratio. In chapter 2.1.3.5, more information is given about the propeller and the open water diagram. Figure 12 on page 18 shows the efficiency and coefficients curves. In loading conditions, the propeller efficiency is very low due to the low advance ratio. In order to achieve higher efficiencies, a CPP is recommended for dredges. The pitch diameter ratio can be adjusted which shifts the efficiency curve. At low advance ratio's, higher efficiencies can thus be achieved.
The amount of torque and power required by the propeller is determined by combining the propeller rotational speed and the open water diagram with the advance ratio. The total required thrust to overcome the resistance (P_T) and the propeller specifications to calculate the required power at the end of the shaft (P_O). This is called the open water power and is determined by dividing the thrust power per propeller by the open water propeller efficiency and:

$$P_O = \frac{P_T}{\eta_O} \tag{180}$$

For a TSHD with a fixed pitch propeller at design speed, the propeller efficiency can reach more than 50%. In loading conditions as the resistance due to trailing is very high and the actual speed of the vessel is very low, the efficiency of the propeller can drop to just 12%.
The total propulsive efficiency (η_D) is determined by multiplying the hull, open water propeller and relative rotative efficiency:

$$\eta_D = \eta_H * \eta_O * \eta_R \tag{181}$$

The hull and open water propeller efficiencies are known. The relative rotative efficiency is assumed to be 0.99 as it is normally constant. With the total propulsive efficiency known, the delivered power to all propellers is calculated:

$$P_D = \frac{P_E}{\eta_D} \tag{182}$$

The propeller law states the relation between the power delivered to a propeller and the shaft speed and is calculated with the following equation:

$$P_p = \frac{P_D}{k_p} \tag{183}$$

With an assumed shaft efficiency of 99%, the power at the shaft is calculated. The shaft power is determined by dividing the power to the propeller (P_p) by the shaft efficiency (η_S)

$$P_S = \frac{P_p}{\eta_S} \tag{184}$$

The power loss of the gearbox (η_{GB}) now has to be taken into account to determine the required brake power of the engine:

$$P_B = \frac{P_S}{\eta_{GB}} \tag{185}$$

The efficiency of the gearbox is assumed to be 0.98. The required power that the engine has to produce is now known. The next step is to match the engine specifications with the required power.
In the case where the propeller and the engine are both known, the propeller power curve and the engine power curve should match. In the designing process of the dredge the engine is chosen according to the required power of the propeller. The thrust curve of the propeller is known. Open water diagrams are the result of tests of the propeller operating in a water tank. The thrust curve of the ship can be calculated with the resistance at a certain speed. This is expressed in ship coefficient 1:

$$sc1 = R_t * {v_s}^2 \tag{186}$$

The unit of sc1 is in ton/m as the unit of the density of water is given in ton/m^3. with sc1 known, ship coefficient 7 is determined accordingly:

$$sc7 = \frac{1}{\rho_w * D^2} * \frac{sc_1}{k_p * (1-t) * (1-w)^2} \tag{187}$$

The thrust curve of the ship can now be calculated and plotted within the open water diagram of the propeller. The thrust curve of the ship is determined with the following equation:

$$K_{T,ship} = sc7 * J^2 \tag{188}$$

The required rotational speed of the propeller (n_p) is determined with the advance speed, advance ratio and the diameter of the propeller:

$$n_p = \frac{v_a}{J * D} \tag{189}$$

This gives the revelations per second (rps) of the propeller. For each speed, there is a unique thrust curve of the ship. The thrust of the propeller (K_T) has to match the required thrust of the ship ($K_{T,ship}$). This point of intersection is visible within the open water diagram. At the point of intersection, the curves have the same advance ratio (J). This advance ratio determines the torque coefficient (K_Q) and the propeller efficiency (η_O) according to the open water diagram. Figure 43 shows within the open water diagram the thrust curve of the ship at 10 knots. The black vertical line clarifies the intersection point which helps determining the K_T, K_Q, η_O and J. In case of the shown figure, the intersection point is at an advance ration of approximately 0.56.

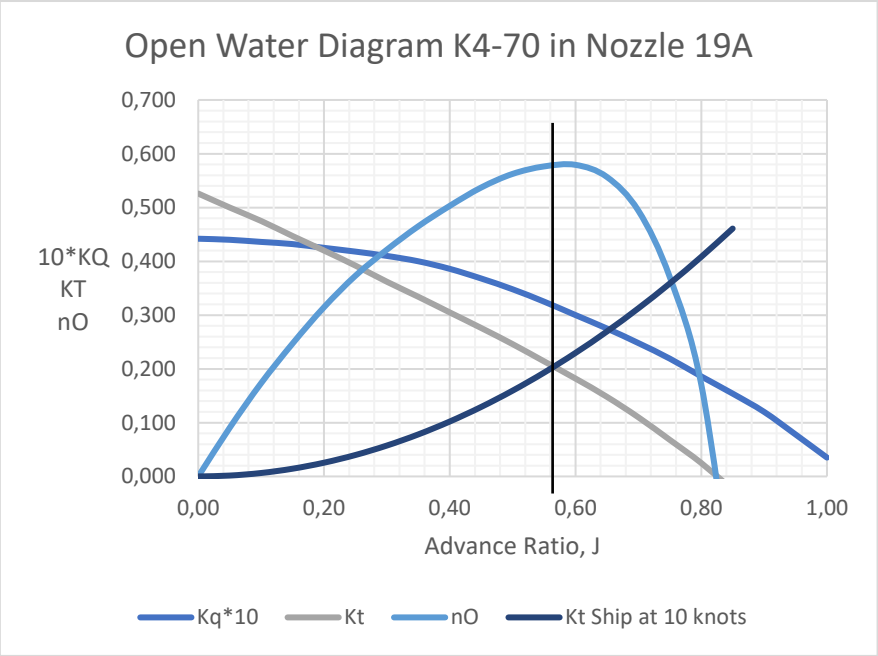

Figure 43: Open Water Diagram for a K4-70 Propeller in a Nozzle 19A with P/D = 1.0

The required thrust, torque and power of the propeller can now be determined with the coefficients from the open water diagram with the rotational speed of the propeller:

$$T_p = K_T * \rho_w * {n_p}^2 * D^4 \tag{190}$$

$$M_p = K_Q * \rho_w * {n_p}^2 * D^5 \tag{191}$$

$$P_p = M_p * 2\pi * n_p \tag{192}$$

The required torque must match the torque of the engine. The gearbox ratio (i) and gearbox efficiency (η_{GB}) determine the torque required by the engine (M_B):

$$M_B = \frac{M_p}{i * \eta_{GB}} \tag{193}$$

The speed of the engine (n_e) is calculated with the propeller speed times the gearbox reduction:

$$n_e = n_p * i \tag{194}$$

The required power of the engine is calculated with the required torque of the engine with the following equation:

$$P_B = M_B * 2\pi * n_e \tag{195}$$

The characteristic power and torque curve at a certain rpm of the engine is given by the manufacturer of the engine. Figure 45 shows the power curve of an EMD L12-645-E7, Figure 44 shows the torque curve of the same engine. The four curves in each graph represent the amount of throttle given in percentage. With low load, the engine can run at 900 rpm but at just 25% of the throttle is needed to provide the required power. The same is true for the required amount of torque. The engine curves are plotted against the required power and torque curves of the propeller (load). The available power and torque are related to the amount of fuel that is used per combustion cycle. The power available by the engine is called the

drive. The power required by the propeller is called the load. The drive and load characteristics have to match. The percentage of throttle is determined at the intersection of the drive and load curve.

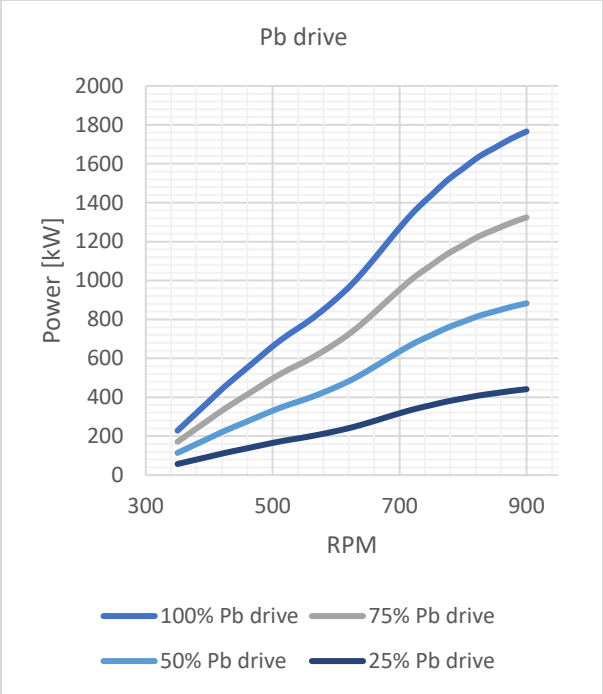

Figure 45: Power Curve EMD L12-645-E7

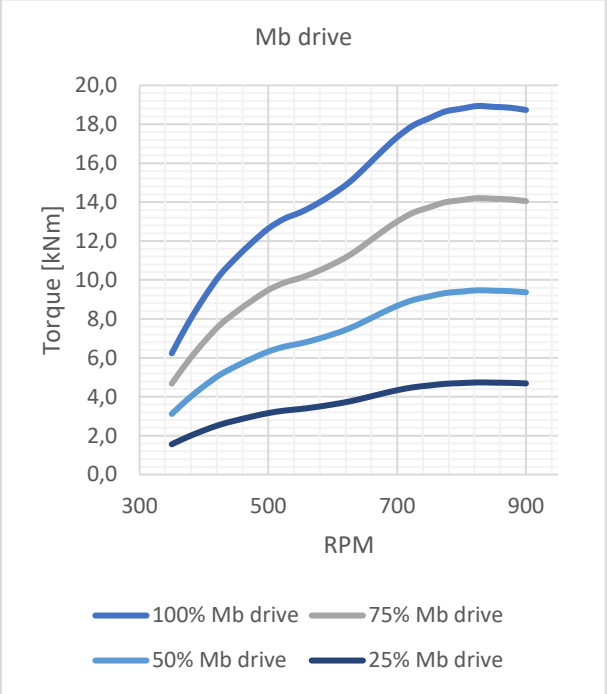

Figure 44: Torque Curve EMD L12-645-E7

The three phases where the engine is matched with the propulsion power required are transit loaded, loading and transit empty. The graphs in Figure 54 and Figure 55 in Appendix 7.1.11 show the combined drive and load characteristics of the loading phase. The amount of throttle that is given during loading determines the amount of rpm the engine runs and the amount of power generated. For example, if 75% of throttle is given, according to the intersection of the graphs, the engine runs at approximately 635 rpm and delivers 11.4 kNm of torque and 765 kW of power. The intersection between the load and drive curve is the operational point of the dredge. The drive curve depends on the engine characteristics and the load curve depends mostly on the resistance of the dredge and type of propeller. The speed limit of the emission model is set at 1 m/s, otherwise the load curve for both the torque and power would have continued. Figure 56 and Figure 57 in Appendix 7.1.12 represent the combined power and torque curve for loaded condition. In Appendix 7.1.13, Figure 58 and Figure 59 show the combined power and torque curve for empty condition. The load curve in loaded and empty condition is outside the drive curve which means the engine cannot run at full throttle as it is limited to the maximum rpm. In these conditions the engine is too powerful, however the power is needed in the loading condition.

3.2.5 Fuel Consumption

The specific fuel consumption (sfc) as well as the engine efficiency variates with the rpm. The sfc is expressed in gram of fuel per kilowatt-hour (g/kWh). In general, the higher the rpm the more efficient the engine runs and the sfc decreases. The sfc values are given by the manufacturer who tested the engine at certain rpms under a certain load. The engine efficiency is determined with the heating value of the used fuel times the sfc. The engine efficiency gives a percentage of how much of the available energy in the fuel is effectively be converted into mechanical energy.

The fuel consumption of the engine is calculated by multiplying the total required power output of the engine(s) by the sfc.

$$\dot{m}_f = sfc * P_{B,load} \tag{196}$$

The power required to propel the dredge is equal to the power the engine has to deliver. The required RPMs are similar as well but at the operational point the percentage of fuel injection is determined. With the density of the fuel and the fuel consumption in gram per minute, the fuel consumption in litre per minute is calculated.

$$\dot{m}_f(\frac{L}{\min}) = \frac{\dot{m}_f\ (\frac{g}{min})}{\rho_{MDO}\ (\frac{ton}{m^3})} * 10^{-3} \tag{197}$$

When the amount of time of the phase is known, the amount of litre per day is determined. The cost of the fuel can also be determined at this stage. The cost of fuel per litre is multiplied by the fuel consumption. The fuel cost variates per day and has to be updated frequently for accurate results.

3.2.6 Emissions

The amount of emissions depends on the type of fuel that is used. In general, for MDO, measurements resulted in an amount of emission for the fuel that is used. According to the IMO study of 2014, CO_2 has got a per-value of 3114 g/kg. This amount if expressed in gram of emission per kilogram of fuel. The amount of fuel ($\dot{m}_f$) that is used at a certain speed is known. This amount is expressed in ton/h and is multiplied by the per value of the pollutant. The equation below shows the relation between the amount of emissions in the fuel.

$$per = \frac{\dot{m}_{pe}}{\dot{m}_f} \tag{198}$$

When the value of per is known the quantity of emissions can be calculated. Table 3 shows the per values for CO_2, SOx and NOx. The result is an emission quantity per phase. The quantity of the CO_2, SOx and NOx emissions are calculated within the model. The NOx emissions are determined in a different way compared to the CO_2 and SOx emissions. The quantity of NOx emissions is dependent on the load and the rotational speed of the engine. On contour plots, the specific NOx emission is found with the combination of the load and the rpm. This number is expressed in g/kWh, so when multiplied by the running hours and the power demand, the NOx emission is approximated. Figure 46 shows the contour plot of the NOx emission per load an rpm of the engine. This plot is valid for engines installed in the Dodge Island.

Pollutant		per	
Carbon Dioxide	CO_2	3114	g/kg
Sulfur	SOx	4	g/kg

Table 3: per Values Emissions

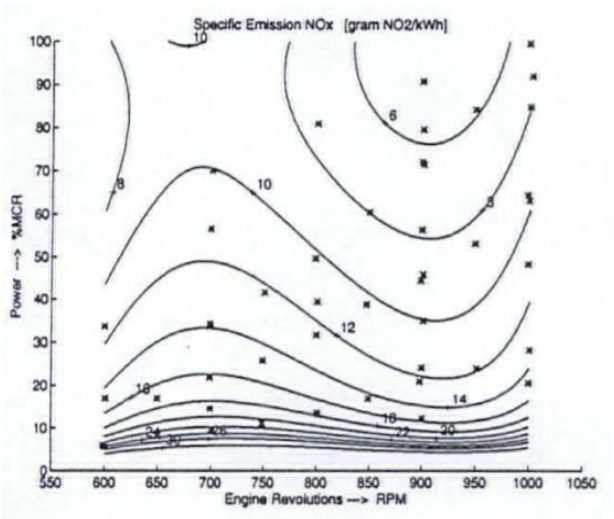

Figure 46: Specific Emission NOx [63]

3.2.7 Other Engine Power Requirement

Within the emission model, the power requirement of the main engine is extensively determined. This is necessary as the power requirement varies as the main engines are used to deliver power to the propulsors. For the other engines on board, which run at a certain rotational speed, a less detailed approach is taken. The other engines on board are the jet engines, bowthruster engine, generators and dredge engines. The sfc per engine at the expected rpm is used to determine the fuel consumption and emissions. The method to determine the fuel consumption and emissions is discussed in the previous two sub chapters. Figure 60 in Appendix 7.1.14 shows the calculation sheet of the emission model where the fuel consumption and the emissions are determined for the generators and the dredge engines.

3.2.8 Pump Power Requirement

The required power to load and discharge is calculated within the emission model with a simplified pump power calculation. The calculated pump power shows a decent representation of the pump power required in real life. The calculated discharge time and the real discharge time vary per job. To simplify the required pumping power, the mathematics of pumping water is used. In practise the pumps require more power as solids are also pumped up into the hopper. The same method to calculate the pumping power is applied to loading conditions and discharge conditions. The total pump power is expressed as follows [44]:

$$Pp = \frac{Q * H * g * \rho}{\eta_p} \tag{199}$$

The total power per pump is the flow through the pipe (Q_p) multiplied by the total head (H), gravitational force (g) and density of the fluid (ρ) divided by the pump efficiency (η_p). Within the model, the density of the mixture is taken as the density of the fluid. The mixture density is determined by the method given in chapter 3.2.3.3. The gravitational force is 9.81 m/s^2. The flow through the pipe is determined with the area of the pipe section (A_p) multiplied by the concentration of solids in volume (C_{VS}) and the line speed (v_l).

$$Q_p = A_p * C_{VS} * v_l \tag{200}$$

The line speed is determined according to the available pump power. In practise, the pump engines operate near full power. The line speed depends on the length of the pipeline and the power used. It is considered an input for the model. The volume concentration of the solids is determined in chapter 3.2.3.3. The total head is split up into two main components, dynamic and static head. The static head is the physical change in elevation between the water level in the hopper and the water level of the ocean. Within the model, it is assumed that the hopper is fully filled with water. The height difference then depends on the depth and draft of the dredge. The difference between the depth and the draft determines the static head, which is merely a small percentage of the dynamic head. The dynamic head is calculated as follows:

$$H_D = \frac{K * {v_l}^2}{2g} \tag{201}$$

The loss coefficient (K) is multiplied by the line speed squared and divided by twice the gravitational force. The loss coefficient is divided into two parts, the loss for the fittings ($K_{fittings}$)and the loss within the pipe (K_{pipe}). The values for the loss of the fittings are shown in Appendix 7.1.15. Each K-value is multiplied by the number of fitting items. The sum of the K-values determines the loss coefficient for the fittings. The loss coefficient of the pipe relates to the straight lengths and is expressed as in equation 203.

$$K_{pipe} = \frac{f * L}{D} \tag{202}$$

The f represents the friction coefficient of the pipe, L the length of the pipe and D the pipe diameter. With a modified version of the Colebrook White equation the friction coefficient is determined:

$$f = \frac{0.25}{\left(log\left(\frac{k}{3.7D} + \frac{5.74}{Re^{0.9}}\right)\right)^2} \tag{203}$$

With the roughness factor k and the Reynolds number (Re). The Reynolds number for a pipe is determined with:

$$Re = \frac{v * D}{\upsilon} \tag{204}$$

The kinematic viscosity of the mixture is taken to determine the Reynolds number. A modified form of the equation by D.G. Thomas to determine the mixture viscosity is used. The viscosity of the mixture (ν_m) is determined as follows [50]:

$$\upsilon_m = \upsilon_w * (1 + 2.5 * C_{VS} + 10.06 * {C_{VS}}^2 + 0.00273 * e^{16.6 * C_{VS}}) \tag{205}$$

Where ν_w is the viscosity of the water. The roughness factor k depends on the material and the finish of the pipe. A commonly used roughness factor for galvanized iron of 0.15 m is used [51]. The friction coefficient, the total loss coefficient and the dynamic head can now be determined.

3.2.9 Auxiliary Power Requirement

An electrical load balance (ELB) is made to show the auxiliary energy usage. This balance shows the load per phase of operation. There are many factors and variables that affect the specific load which causes the balance to be inaccurate. Even so, a decent model is made because of experiences in the past and analytical approaches. The data for the ELB is gathered from multiple sources. There is a database of GLDD which contains all the data of the equipment onboard. The database is mainly used to find specifications of parts when replacement parts are needed. To create the ELB, the database is used to list all the energy consumers of the dredges that consume power from the generators. For most of the equipment, the specific model is known. The maximum required power is found either on the web at product information or it is stated in the database. For the equipment that is unknown, on board investigation is done. The individual equipment is grouped within the column Systems/Components. The following systems/components exist:

- Bilge
- Ballast
- Compressed Air
- Cranes
- Dragarm Hoisting
- Electrical
- Fuel Oil Transfer
- Galley
- Gland Seal
- HVAC
- Hydraulic Service System
- IT Equipment
- Loop Cooling
- Mooring and Anchor
- Navigation
- Potable Water
- Raw Water
- Safety Fire Fighting
- Sanitation System
- Steering
- Valve Flushing

Each system/component contains multiple types of equipment. For each equipment on board, the installed power is stated. For each phase of the operation, a load factor and simultaneity factor are determined. Figure 61 in Appendix 7.1.16 represents a part of the ELB. The product of the installed power, load factor and simultaneity factor are the average absorbed power. The load factor is the average percentage of used power when the equipment is in use, this number variates from 0 to 1. The simultaneity factor represents the amount of time in percentage that the equipment is consuming energy. This number also variates between 0 and 1. As it is nearly impossible to measure the load and simultaneity factor, common sense and experience of chief engineers is used to make assumptions. Chief engineers have worked years on dredges and have completed numerous operations, which makes them the most reliable source next to measurements. The total amount of absorbed power is the sum of each equipment. With the total required power per phase, the load of the generator is calculated. The fuel consumption is determined with the characteristics of the generator. The total amount of power that is used is validated by measuring the fuel consumption per generator. As not all users are dependent to the phase of the operation, a division between night (6 p.m. till 6 a.m.) and day (6 a.m. till 6 p.m.) time is made. Also, a division between the seasons is included. More accurate results are obtained with these variables. For example, lights are only turned on during night time. In summer the heaters are not used, and in winter cooling of the quarters is not operational.
To validate the data for the electrical load balance of the database, a site visit is made to the Dodge and Padre Island in week 43. Multiple days were spent to execute measurements on the dredges and get familiar with the working principles.

Site Visit to the Dodge Island and Padre Island in week 43 of 2019

The horsepower of all pumps given by the database is checked with all the pumps on board. It is registered at what phase which pumps are running while the dredge is operating. Some specification on the plates on the pumps were unreadable, the horse power for those pumps are taken from the database if the type matched.
While operating, the amps of the pumps that were running were measured. The current was measured in the control lockers within the room of the specific pumps. This gives an accurate visualisation of the power the pumps use. Difficulties arose for the measurements in the wheelhouse. Due to safety issues, lack of proper equipment and low accessibility, the usage of the equipment used in the wheelhouse could not be measured. The running times of the energy users in the wheelhouse is based on experience of the chief engineer, captain and crew.
While on board, the dredge operated two full circles of operation. In the control room, the amps and kilowatts of the generator were visible. The data of the amps and kilowatts was recorded multiple time per phase. The output was very constant during the entire operation.
One difference was when the dredge lowered its dragarms into the water and also out of the water. The pumps of the winches consumed almost full power for the lowering and lifting of the dragarms. Furthermore, the load of the generator is dependent on the time of the day (night or day) and the outside temperature (winter or summer). The measurements were taken with an outside temperature of 18°C during the daytime. At night the lighting requires much more energy than during the day. In a cold environment, the heaters of the quarters and wheelhouse are turned on. In a warmer environment, the air conditioning is running instead of the heaters.

How the data is acquired is stated below.

Data Acquired

#	Data	Instrument of Measurement	Place of Measurement
1	Date	Master clock	Wheelhouse
2	Time	Master clock	Wheelhouse
3	Speed ship	GPS	Wheelhouse
4	Rpm main engines	Rpm sensor	Wheelhouse monitor
5	Rpm dredge engines	Rpm sensor	Wheelhouse monitor
6	Rpm bowthruster	Rpm sensor	Wheelhouse monitor
7	Rpm generator	Rpm sensor	Wheelhouse monitor
8	Rpm jet engines	Rpm sensor	Wheelhouse monitor
9	Amps generator	Amp meter	Control room
10	Amps multiple engines	Amp meter	Pump and engine rooms

3.2.10 Phases of the Operation

There are six main phases to describe one operation of a TSHD. In addition to those, two phases are included. The additional phases are the ‘turning time’ and ‘other time’. Which part of the model is executed within the main phase is described within the first part of this sub chapter. The second part covers the details of the turning time. In the last part, the ‘other time’ is described.

3.2.10.1 Main Phases

When the dredge arrives at the borrowing area, the dragarms are lowered into the water. Once the dragheads touch the bottom, the loading phase starts. The loading phase continues until the hopper is reached maximum capacity or loading weight. At this point, the dragarms are hoisted and the loading phase comes to an end. The dredge accelerates and the ‘transit loaded’ phase starts. The connecting phase starts when the dredge has arrived at the connector and starts to attain the connection of the connector floating in the water. The connecting phase takes approximately nine minutes. The connecting phase ends when discharging is possible. When the dredge is connected to the connector, and discharge can begin, the discharge phase starts. Once the hopper is emptied, the discharge phase ends. When the dredging pumps are shut down as the soil is discharged from the hopper, the disconnecting phase starts. This phase, which takes approximately seven minutes, ends when the dredge starts to increase velocity. The dredge now sails to the borrowing area where the cycle of operation can start again till the job is finished.

Only the necessary parts of the model are used per phase. For clarification, Table 4 shows which parts of the calculations are used to determine the energy usage per phase. The ‘x’ represents that the calculation part is used within the corresponding phase. Where no ‘x’ is present, the corresponding calculation part is not used.

Phase	Hull Resistance	Trailing Resistance	Main Engine Matching	Fuel Consumption	Emissions	Engine Power Requirement	Pump Power Requirement	Electrical Load Balance
Loading	x	x	x	x	x	x	x	x
Transit Loaded	x		x	x	x	x		x
Connecting				x	x	x		x
Discharge				x	x	x	x	x
Disconnecting				x	x	x		x
Transit Empty	x		x	x	x	x		x

Table 4: Used Calculation Parts per Phase

3.2.10.2 Turning Time

Within the loading phase, the dredge has to make turns to remain within the borrowing area.
When the dredge is turning, it lifts the dragarms from the bottom, steers into one direction and gives almost full throttle. As there is much variety of power usage within the turns, an approximation is used to calculate the power for the turning time. The power required for the turning time is approximated by increasing the average loading speed of the dredge fully loading with 20%. The duration of the turning time is assumed to be 15% of the total loading time.

3.2.10.3 Other Time

The time the dredge is occupied with anything else than dredging but still part of the operation is included in ‘other time’. This includes for example the time the dredge has to wait before it can discharge when another dredge is discharging. The downtime is not included within this phase. When the weather is too rough and the captain of the dredge decides to wait the storm out, it does not count as ‘other time’. Lastly, when the dredge encounters mechanical issues, the ‘other time’ does not increase, in this case a report is made to verify for the downtime. The total duration of this phase is determined at the end of a job. Depending on the number of cycles the dredge completed, the time for this phase is included. For example, if the ‘other time’ of the dredge during the job was 200 minutes and 100 cycles of operations are completed, then the duration of ‘other time’ per cycle would be 2 (200/100) minute.

3.3 Variations and Results Emission Model

This sub chapter shows the accuracy of the model based on already completed jobs. The Dodge Island is used to validate the results of the emission model. The first part discusses the variations that occur due to the differences between practise and theory. The second part presents the four completed jobs, the third part reviews the results of the comparison.

3.3.1 Variations Emission Model

The calculations within the model are a simplified representation of the outcomes in practise. Numerous reasons exist which causes the offset between the daily data and the emission model. The sub chapters below describe the variables with the most impact to the offset.

Daily Data Variations

There are many reasons why there is an offset between the predicted fuel consumption and the real fuel consumption. The amount of fuel that is refuelled every day varies. This creates an uncertainty of the documented amount of fuel. The time in between every refuel is not exactly 24 hours. The data within the daily data is filled in by the crew, which creates another source of inefficiencies. The exact time the data was recorded can vary and thus the value of the data varies. The method to measure the fuel that is used is done by sticking a stick in the diesel tank, pulling it out and take note of the height the fuel reached on the stick. This can create highly inaccurate results as the dredge should be absolutely flat on the water. The trim of the dredge, the movement on the dredge and the movement of the ocean are the cause of inaccurate measurements.

Draghead Variations

In practise, the bottom of the ocean is not flat and there is a lot of inefficiencies on the bottom floor. This creates and increase and decrease in trailing resistance continuously. The calculations are based on perfect conditions which include sharp teeth and undamaged side plates. Over time the length of the teeth decreases and they become less sharp. The drag resistance of the draghead increases as the side plate and sled become more worn out. This affects the engine power that is needed to overcome the resistance. The drag force of the draghead is different in practise. This also counts for the drag force of the suction pipes. The draghead and the suction pipes have many appendages which are not taken into account within the calculations. The weights of the suction pipes and draghead are in practise different than on paper.

Grain Distribution Variations

The type of soil influences the total trailing resistance and the loading time. Before a job starts, samples of the soil within the borrowing areas are investigated. Some of the outcomes are the grain sizes d10, d50 and d80. The model is only accurate with a minimum d10 size of 0.1 mm to 3.0 mm. Below or above these values, the model becomes more inaccurate. The borrowing areas does not contain the same grain size distribution, it variates. Which means that the cutting resistance of the soil also variates. The different strengths of the soil also create a variation of values.

Dredge Variations

The calculated dredge propulsion resistance contains few assumptions. The gearbox, shaft and relative rotational efficiencies are assumed and influences the total resistance. The specifications of the dredge are calculated with the Holtrop and Mennen method. The equations within this method are based on the average of a large number of ships. For more accurate values of, for example, the wet surface, prismatic coefficient and thrust factor, they are to be taken from model testing or CFD calculations. Organism that are attached to the surface of the hull create a higher friction resistance and disrupts the flow of the water. Assumptions are made to account for those losses, but it brings an inaccuracy. The weather conditions are not taken into account within the model. In practise the weather conditions can influence the fuel consumption greatly.

Model Variations

The operational point is the intersection between the thrust needed to propel the ship and the thrust that is delivered by the engine. The determination of the intersection is done with a linear approach. This means that there is a deviation of the intersection coordinates as the curves are polynomial. This creates an offset for the actual thrust that should be provided by the engine.
The buoyancy is set at 0 meters from the centre of the dredge (half the waterline length). Due to the lack of information and time available this value for the buoyancy is chosen. The input of the real buoyancy value increases the accuracy of the power that is needed to propel the dredge.
The appendages are roughly estimated according to the Holtrop and Mennen method. values are given to certain types of appendages. It is impossible to determine the exact magnitude of resistance the appendages add. For more accuracy, CFD or model testing should be performed.
The power required by the pumps are calculated simplified. More precise numerical calculations are available but not used within this model. The final offset between the model and the daily data is also dependent on the variation of required pump power.

3.3.2 Results of the Emission Model

The offset of the emissions model with the daily data is shown in Table 5 below. The jobs are shown on the left, followed by the results of the daily data. On the right side the results of the emission model are shown with the offset between the model and the daily data.

Job	Daily Data		Emission Model		Offset
Cape May	11.24	L/min	11.29	L/min	+ 0.4%
Arcadian Shore	11.64	L/min	11.23	L/min	- 3.7%
Myrtle Beach	11.30	L/min	11.27	L/min	- 0.3%
Delaware Beach	10.88	L/min	10.46	L/min	- 4.0%

Table 5: Results Daily Data versus Emission Model

Four most recent completed beach nourishments jobs are chosen. The daily data is registered by site engineers present on the job. The data varies from the amount of fuel used per day to the down time of the dredge. The field engineers send the data to the office employees. All necessary data should be present for the emission model within the daily data. To present an as accurate as possible verification, the average of the daily data is taken for all input. The same setup within the model is used to verify the results. Only the input stated in Chapter 3.2.1 was variating depending on the job. The exact input is described below.

Cape May Beach

Cape May Beach is the first job to be compared with the emission model.
Table 17 in Appendix 7.1.17 shows the input values of the model, based on the daily data of the Dodge Island for Cape May Beach. The public beach of Cape May is found in the most southern point of New Jersey. The nourishment job took place in September 2019. No situations that could influence the results were noticed.

Arcadian Shore

The Arcadian Shore is found in South Carolina, the job took place just before the job of Cape May Beach in 2019. The input is shown in Table 18 in Appendix 7.1.18. The soil of this job was less dense than expected. Not only the jets and the teeth excavated the soil, but the suction force as well, this causes a decrease in loading time. This contributed to the offset between the daily data and the results of the model.

Myrtle Beach

Myrtle Beach lies just a few miles south of Arcadian Shore. The job of Myrtle Beach was completed at the end of 2018. Table 19 in Appendix 7.1.19 shows the input of the job. The fuel consumption was very scattered with some unrecorded days. An approximation was made when the dredge showed activity with a duration between 22 and 24 hours.

Rehoboth Beach

On the east coast in the State Delaware, there is Dewey and Rehoboth beach. The Dodge and Padre Island did a beach nourishment job which took place in the autumn and winter of 2019. In Table 20 in Appendix 7.1.20 the input of the Rehoboth beach job is shown.

The four most recent jobs finished by the Dodge Island show that the emission model stays within an offset range of -4% to + 1%. A constant offset within the results is visible which indicates a stable emission model. The Dodge Island is equipped with old engines and the dredge itself is in business for 40 years. To take the age of the dredge into account together with inefficiencies of the propeller, the total resistance of the dredge is increased by 10%. Inefficiencies of the propeller are damage of the blades by cavitation or contact with objects. Due to the age of the dredge the hull can be damaged, or more easily be covered in biofouling. To take the age of the engines into account the specific fuel consumption is also increased by 10%. The fuel consumption depends on the running hours of the engine. One of the reasons is that the rotating parts are subdue to wear. Over time, the piston is covered with the residue of burned diesel which decreases the cylinder volume slightly. More fuel is needed to generate the same amount power without the residue. Residue of oil and diesel can also attach to the insides of the tubes, this means more power is needed to deliver the same volume of fluid. More factors negatively influence the fuel consumption of the engine with a significant amount of running hours.
Looking at the offset of the emission model and the four operation, the model is accurate within a range of 4%. This is achieved by including coefficient of realistic magnitude. With further research and expansion of the model, the accuracy can increase.

4

METHODS AND THEIR VIABILITY TO REDUCE EMISSIONS

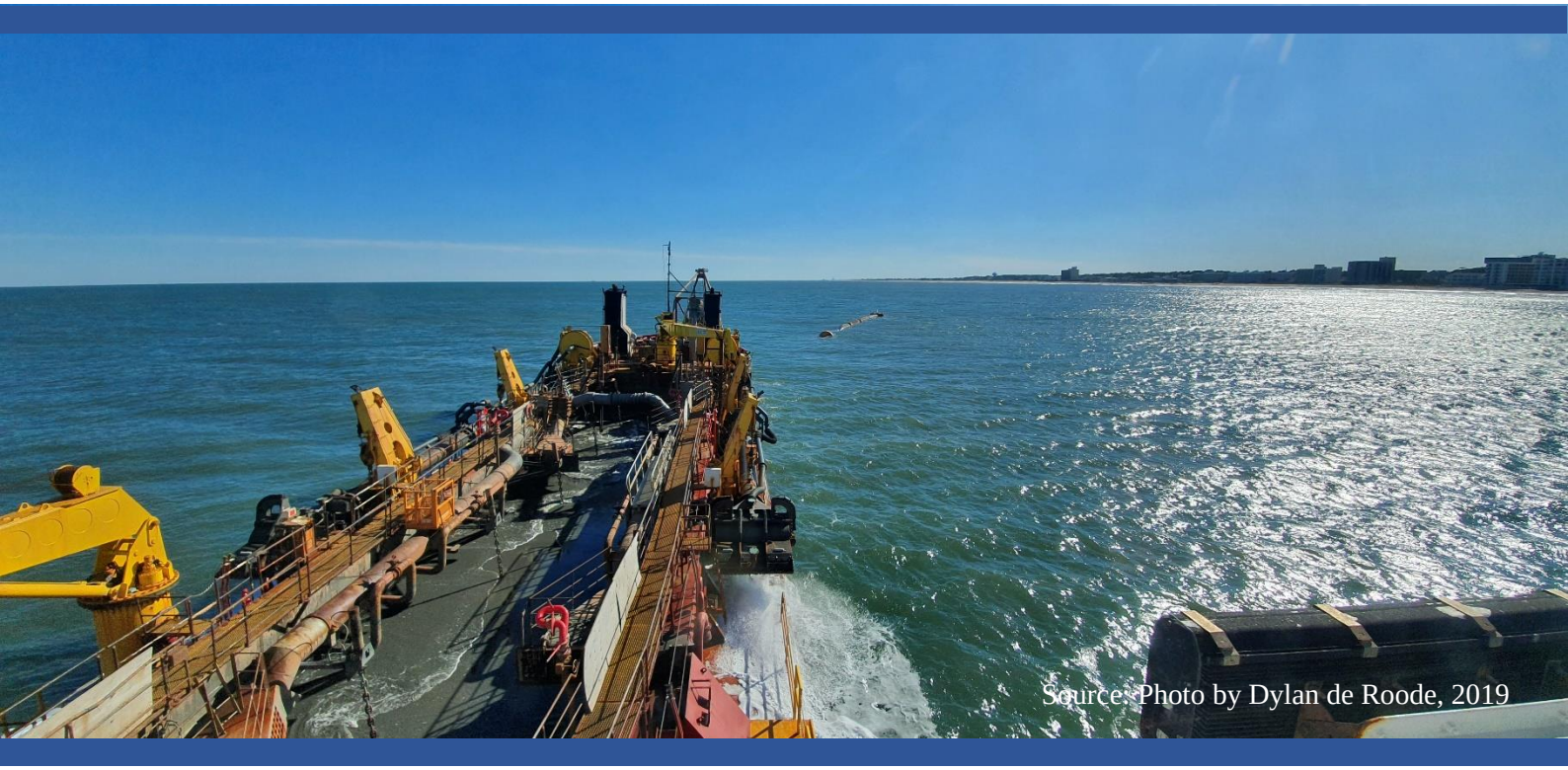

Source: Photo by Dylan de Roode, 2019

4. Methods and their Viability to Reduce Emissions

This chapter covers multiple methods to reduce the emissions of dredges during operation. The design philosophy of the company and the future outlook of the emission restriction determine the viability of the methods. These conditions of viability are presented in the first sub chapter. The second sub chapter explains the viable available methods to reduce the emissions.

4.1 Conditions of Viability

To conclude the design philosophies (see Chapter 2.4.3) of the Great Lakes Dredge & Dock Company, the company has to take into account multiple external and internal factors. These factors narrow down the freedom of designing new dredges. With those factors, conditions of viability of methods to reduce the emissions are formed. Some conditions are strict and measurable, others are more open for interpretation and are more subjective. The conditions are defined within this sub chapter.
The following conditions for the reduction methods are defined according to the design philosophy of GLDD and the scope of this research:

1. Methods must be in line with the expected emission reductions
2. The focus of the type of job is beach nourishments
3. All types of costs are neglected
4. The methods are valid for existing and new dredges
5. Mechanical, hybrid or electrical power arrangement are possible
6. The methods must be reasonable to be executed

4.2 Methods to Reduce the Emissions

The amount of burned fuel and type of fuel by a combustion engine is related to the emissions emitted. To decrease the emissions, one solution is to reduce the fuel consumption. Within the model, multiple solutions to decrease the fuel consumptions are found and backed up with the relevant equations. This sub chapter covers five methods to reduce the emissions, the first sub chapter compares different power arrangements. The second explains the advantages of different propellers. The third sub chapter covers the optimal trailing speed while loading. The scrubber is explained in the fourth sub chapter. In the last sub chapter, the reduction method to shut off the engines is discussed.

4.2.1 Power Arrangements

Many power arrangements are available and deciphering which arrangement is most efficient for a particular dredge requires specific research pertaining to that dredge. For each dredge a specific case study has to be executed in order to confirm the most efficient power arrangement. Within this case study, three different power arrangement that are used in future dredges are approached. The advantages and disadvantages of those arrangements are presented in Chapter 2.1.3.5. The following sub chapters describe a case study where the different power arrangements are compared in terms of emissions. To narrow down the results the following scope is defined:

- This case study is fully focussed on the amount of CO_2 emitted
- The following parameters are not taken into account:
    - Costs
    - Additional engine room space
    - Retrofit possibilities

The Dodge Island is taken as basis for the calculations. All the specifications of the dredge stay the same except for the power arrangement. The different power arrangements are compared for the phases loading, sailing empty, sailing loaded and discharging. To visualise what power arrangement could be less pollutant, three scenarios are formed. The scenarios differ in loading/discharge and sailing time relatively. Scenario one simulates very short sailing distance where 80% of the time is spent on loading

and discharging. Just 20% of the time is spent on sailing (empty and loaded). Scenario two the time is equally divided, 50% of the time the dredge sails and 50% the dredge loads and discharges. Scenario three simulates that 20% of the time is loading and discharging and 80% is sailing. See also Table 6 for the distribution of the time per phase.

	loading	**transit loaded**	**transit empty**	**discharge**
Scenario 1	40%	10%	10%	40%
Scenario 2	25%	25%	25%	25%
Scenario 3	10%	40%	40%	10%

Table 6: Distribution of Time per Phase per Scenario

Not all energy consumers are active during each phase, the table below shows the whether or not in which phase a consumer is active.

	loading	**transit loaded**	**transit empty**	**discharge**
propulsor	Active	Active	Active	Not Active
jet pumps	Active	Not Active	Not Active	Active
dredge pumps	Active	Not Active	Not Active	Active
bowthruster	Active	Not Active	Not Active	Active
auxiliary	Active	Active	Active	Active

Table 7: Activity of Energy Consumers per Phase

The required amount of power in kilowatt is calculated by taking 80% of the maximum available power (power required) onboard the Dodge Island. The maximum available power according to the specific engines are shown in Table 8. The 80% load counts for the propulsor, jet pumps and dredge pumps. As the bowthruster is not used continuously during the phases where it is needed, only 20% of its maximum power is taken. The simultaneously factor is hereby taken into account. The required electrical auxiliary power is taken as the available power as it is constant during each phase. The (prime) movers have to generate the power listed under 'total required power'. Table 9 shows the details that determine the total required power.

	Engine	**Power [kW]**
M.E. small	EMD L12-645-E7	1770
M.E. large	CAT 3612	3714
D.E.	CAT 3512	1100
J.E.	CAT D379	410
B.T.	CAT D379	410

Table 8: Engine Power

Energy consumers	**Available power [kW]**	**Power required [kW]**	**Nr. of Engines**	**Total required power [kW]**
Propulsor	1770	1416	2	2832
Jet pumps	410	328	2	656
Dredge pumps	1100	880	2	1760
Bowthruster	410	82	1	82
Auxiliary	400	400	1	400

Table 9: Required Power per Energy Consumer

All engines have a specific fuel consumption. As the total required power is 80% of the maximum deliverable power, the sfc of the engines are taken at a load of 80%.

4.2.1.1 Mechanical

Two types of mechanical power arrangements are included. The first one is the direct drive where all the energy consumers are directly driven by one energy producer. The second one is the combined drive, where the propulsors and the dredge pumps are driven by each one engine.

Direct Drive

The conventional power arrangement is the mechanical power arrangement. A mechanical power arrangement is a relatively to the other arrangements the simplest arrangement to realise. Each energy consumer is provided by a prime mover. Figure 49 in Appendix 7.1.2 shows the mechanical power arrangement of the Dodge Island. Within this arrangement the main engines are the EMD L12-645-E7 (M.E. small). Table 9 showed the total required power, the total break power of the engines is calculated with the efficiencies of the drive train. The gearbox efficiency is taken as 96%, the shaft efficiency is taken as 99% and the relative rotation efficiency as 98%. The efficiency of the generator to create electrical energy is 97%. Assumed is that all engines have an efficiency of 37%, this means that 37% of the potential energy from the used fuel is converted into mechanical energy available. The efficiencies included, Table 10 shows the required engine power of each energy consumer per phase.

Power [kW]	loading	transit loaded	transit empty	discharge
propulsor	3041	3041	3041	0
jet pumps	683	0	0	683
dredge pumps	1833	0	0	1833
bowthruster	85	0	0	85
auxiliary	419	419	419	419

Table 10: Required Break Engine Power per Phase per Consumer

To be able to calculate the CO_2 emission in kilograms, the engine efficiency, the specific fuel consumption per engine, the running time and CO_2 content within the fuel have to be known. Table 11 shows the specific fuel consumption. The engine efficiencies and the running time are already known and the content of CO_2 in ULSD is 3.114 kg/kg.

	Value	Unit	Engine type
sfc Main Engine (small)	0.214	kg/kWh	EMD L12-645-E7
sfc Main Engine (large) at 780 rpm	0.192	kg/kWh	Caterpillar 3612
sfc Main Engine (large) at 675 rpm	0.199	kg/kWh	Caterpillar 3612
sfc Main Engine (large) at 475 rpm	0.212	kg/kWh	Caterpillar 3612
sfc Dredge Engine	0.235	kg/kWh	Caterpillar 3512
sfc Auxiliary Engine	0.243	kg/kWh	Caterpillar D398
sfc Jet Engine	0.243	kg/kWh	Caterpillar D379
sfc Bowthruster Engine	0.243	kg/kWh	Caterpillar D379

Table 11: SFC and Engine Type per Engine

The CO_2 emissions are calculated as follows:

$$\left(\frac{\%\ running\ time * 24\ [h] * required\ power\ [kW] * s.f.c.[kg/kWh]}{engine\ efficiency}\right) * per\ [kg/kg] \quad (206)$$

For each scenario, energy consumer and phase, the CO_2 emissions are determined. The total emitted emission of each power arrangement is then compared. In Chapter 4.2.6.1 the results are shown and discussed.

Combined Drive

The same calculation method for the combined drive is true as for the direct drive. The dredge pump and the propulsor are driven by one engine, which is the only difference with a direct drive. Figure 62 in Appendix 7.2.1 shows the power arrangement of the combined drive. In the loading phase, both the dredge pumps and the propulsor consume energy from the main engine. Within this arrangement the Caterpillar 3612 is used as this engine can generate enough power to provide both consumers.

4.2.1.2 Hybrid

A hybrid power arrangement consists of a combination of electrical and mechanical driven energy consumers. Two hybrid configurations are used for the case study, they can also be called diesel-electric power arrangements. It is chosen that one of the two largest engines are each mechanically driven as this creates the most impact on energy usage. In the first hybrid arrangement (hybrid 1), the dredge pump is mechanically driven by a combustion engine. All other energy consumers are electrically driven. An electrical drive train brings other efficiencies than a mechanical drive train. Also, more components are required to power the pumps and propellers. To provide for the total required power, three main engines are to be installed within this hybrid arrangement. The main engines provide the required mechanical energy. This type of energy is converted to electrical energy by alternators. The electrical energy is then transported to the main switchboard where the energy is being distributed. Before the electrical energy is used by the energy consumers, it runs through a frequency converter. The electrical motor receives the correct frequency and can drive the pumps and propulsor. The power arrangement is visualised in Figure 63 in Appendix 7.2.2.

The efficiencies of the components to convert mechanical energy into useful electrical energy are shown in Table 12 below.

Component	Efficiency
Alternator	97,0%
Main Switchboard	99,8%
Frequency Converter	98,5%
Electric Propulsion motor	96,0%

Table 12: Efficiencies Electrical Components [52]

In the second hybrid arrangement (hybrid 2), the propulsor is mechanically driven by a combustion engine. The same efficiencies are used as shown in Table 12 for all pumps that use electrical energy. The drive train calculations for the propulsors are equal to the mechanical power arrangement calculations. Within this power arrangement two main engines are required to provide all the energy besides the energy required by the propulsors. Figure 64 in Appendix 7.2.3 shows the hybrid power arrangement.

4.2.1.3 Electrical

The fully electrical power arrangement is powered by four main engines. The switchboard divides the electrical energy to all the energy users as is shown in Figure 65 in Appendix 7.2.4. The used efficiencies are shown in Table 12.

4.2.2 Propulsor Type

Great loss is found in the efficiency of the propeller in loading condition. At trailing speeds of 1 knot, a fixed pitch propeller efficiency is just 11%. This efficiency is according to the results of the calculations of the model with the Dodge Island with a K4-70 propeller with a 19A nozzle. The difficulty of choosing the best propeller is the variating rotational speed of the propeller and the related vessel speed. In loading condition, the vessel speed is very low due to the additional resistance of excavating. Then, there are the two sailing conditions of which one of them is sailing fully loaded and the other one is sailing empty. A trade-off at the designing stage for the type of propeller has to be made where the most efficient propeller

must be chosen. The trade-off consists of predicting the amount of time the dredge executes the three phases in order to find the optimal efficiency for a certain type of propeller. These days, most TSHDs are equipped with a controllable pitch propeller. Because of the changeable pitch, the overall propeller efficiency increases. Therefore, the ratio of fuel consumption versus the dredged soil decreases as result of a better overall efficiency. Some other advantages of using a CPP is the better acceleration as the pitch of the propeller can gradually be adjusted. For every load and speed, the most optimal pitch is used. The rotational speed of the engines can also be influenced as the pitch of the propeller is adjusted. This enables the engines to run at a more efficient speed.

4.2.3 Loading at Optimal Trailing Speed

The fuel consumption is optimised by executing the trade-off between the trailing speed of the dredge and a certain cutting depth. As the optimal trailing speeds of the fixed and floated visor differ, this sub chapter is split up into two parts, optimum trailing speed for fixed and for floating visors. The results are calculated per load of 2754 m^3 for a fixed and floating visor.

Fixed Visor Optimal Trailing Speed

The optimal trailing speed for the fixed visor is highly dependent on the limit of the jet penetration. This limit is set manually within the model. At the transition where the jet penetration decreases below the limit and thus the cutting forces of the teeth increase, the optimal trailing speed is found. The most common visor angle of the Dodge Island of 40 degrees has got a penetration depth of 0.39 m. The limit of the jet penetration was set at 0.30 m, where it was constant until a trailing speed of 0.7 m/s was reached. Theoretically, until the speed of 0.7 m/s, the jets have enough penetration force to liquify all the saturated sand before the soil ends up in the suction pipe. Until that speed, the only variable that influences the production of the draghead is the trailing speed. With speeds greater than 0.7 m/s, the jet penetration decreased which increases the cutting force and thus the trailing force.
Three graphs are generated to find the optimal trailing speed. Optimal trailing speeds are shown in terms of fuel consumption and production. Figure 66 in Appendix 7.2.5 shows the required engine power to propel the dredge versus the trailing speed. For the fixed visor it is clear where the jet penetration decreases. The figure shows the increase of required power at 0.7 m/s due to the increased cutting forces. Both speed and teeth penetration depth increase.
The production of the visor types and the jets versus the trailing speed are shown in Figure 67 in Appendix 7.2.6. The jets have a good production rate (m^3/s) and the production versus the trailing speed is high until the jet penetration limit is reached. This is shown in Figure 68 in Appendix 7.2.7, where the graph peaks at a speed of 0.7 m/s. The visor is fixed which means the cutting forces increase due to the increasing penetration depth and the trailing speed. The last graph, Figure 69: Production per Amount of Fuel versus Trailing Speed in Appendix 7.2.8, shows the production per kilogram fuel used versus the trailing speed per load. The optimum lies again at 0.7 m/s, after that speed the production per kilogram of fuel slowly decreases.

Floating Visor Optimal Trailing Speed

If the angle of the visor is not fixed, the weight of the visor determines the cutting depth. The penetration of the jets clears the way for the floating visor to sink into the ocean floor. With an increasing speed the penetration depth of the floating visor becomes less. This is due to the angle and the type of the teeth, but also the weight of the visor and the soil characteristics.
The power requirement of the floating visor per speed increases less with an increasing speed. The forces on the visor are independent to the jets. The power requirement for the floating visor is shown in Figure 66. The production of the jets differs from the production of the teeth. The decrease of production versus the trailing speed shown in Figure 68 is because the jet penetration becomes less than 0.3 m. The production of the floating visor per amount of used fuel increases strongly until the speed of 0.7 m/s is reached, then a strong decrease is visible. The decrease is caused by the decreasing production rate of the jets.

4.2.4 Scrubber

As mentioned, a new limit on SOx pollution has been set for the 1st of January 2020. Many shipowners choose to install a scrubber to reduce the SOx content and comply with the restrictions of the IMO. To comply with the sulfur cap, ultra low sulfur diesel can be bought. For the long term, a scrubber is a better option as the capital expenditure provides returns in fuel cost savings. ULSD is more expensive than MDO, with a scrubber installed, MDO can be used a primary fuel.

Marine scrubbers are split up into two main types, wet scrubbers and dry scrubbers [53]. The main purpose of scrubbers is to reduce the release of particular matter and SOx from the exhaust gasses. Exhaust gasses produce SOx in the following form [54]:

$$S + O_2 \rightarrow SO_2 \ (\approx 95\%) \tag{207}$$

$$SO_2 + \frac{1}{2}O_2 \rightarrow SO_3 \ (\approx 5\%) \tag{208}$$

Within the scrubber, the SOx react with either sea water or fresh water with additives and the following chemical reaction occurs:

$$SO_2 + H_2O \rightarrow H_2SO_3 \tag{209}$$

$$SO_3 + H_2O \rightarrow H_2SO_4 \tag{210}$$

Dry scrubbers use a solid lime as the alkaline scrubbing material. When the exhaust gasses run through the scrubber, the SOx is removed. The caustic lime ($Ca(OH)_2$) within the scrubber reacts with the SO_2:

$$SO_2 + Ca(OH)_2 \rightarrow CaSO_3 + H_2O \tag{211}$$

The calcium sulfite then reacts with the air, forming gypsum:

$$CaSO_3 + \frac{1}{2}O_2 \rightarrow CaSO_4 \tag{212}$$

The caustic lime also reacts with the SO_3:

$$SO_3 + Ca(OH)_2 \rightarrow CaSO_4 + H_2O \tag{213}$$

The end product then reacts with water forming the following molecule:

$$CaSO_4 * 2H_2O \tag{214}$$

Dry scrubbers in general require a lot of storage space for the scrubbing material. Once the material loses its purpose, new material must be present to continue cleaning the exhaust gasses. The storage space depends on the duration of the travel and availability of the scrubbing material in ports.

Wet scrubbers are split up into three main categories, open loop, hybrid and closed loop scrubbers. What defines a wet scrubber is the usage of alkaline in water.

Open loop scrubbers use sea water which contains alkaline and is used to remove the PM, SOx and NOx content in the exhaust gasses. Via a venturi tube, the exhaust gasses suck up the sea water with the created low pressure. The mix enters the scrubber where chemical reactions take place. Scrubbing liquid gathers at the bottom of the scrubber and flows to the water treatment system. Exhaust gas with reduced emissions leaves the scrubber at the gas outlet. One advantage of an open loop scrubber is the simplicity and the effectiveness. In comparison with the closed loop scrubbers, less space is required for the installation and operation of the system. Even so, this type of scrubber is less popular than closed loop

scrubbers. As mentioned, in some areas and ports this system is prohibited. Also, the content of alkaline in the used sea water must be sufficient. Sea water with a high ambient temperature or brackish water do not contain a sufficient amount of alkaline for the system to work optimal.
Closed loop scrubbers use either recirculating sea water or fresh water with chemical additives. Useful additives to remove the PM and SOx are caustic soda (NaOH) and limestone (CaCO3) [53]. In comparison with an open loop scrubber, the closed loop requires a more extensive system. As the scrubbing liquid leaves the scrubber, it flows to the process tank where fresh water is added. Any chemical addition is added before the water flows through a cooler. After reaching lower temperatures, the water enters again the scrubber. A wash water treatment plant is introduced to process the bleed off from the process tank. Before the wash water is dumped it is to be treated. A sludge tank stores the chemicals that are prohibited from being dumped and the residue of the water is dumped into the sea. The biggest downside of a closed loop system is the required space. If enough space is available, this system reduces emissions significantly and is used worldwide. Figure 47 shows the closed loop scrubber (left) and the open loop scrubber (right).
Hybrid systems are a combination of open and closed loop scrubbers. As in some areas and ports, open loop scrubbers are prohibited, a hybrid system can switch to a closed loop system to avoid any violation. The primary goal of a scrubber is to remove the toxic SOx content of the exhaust gasses.

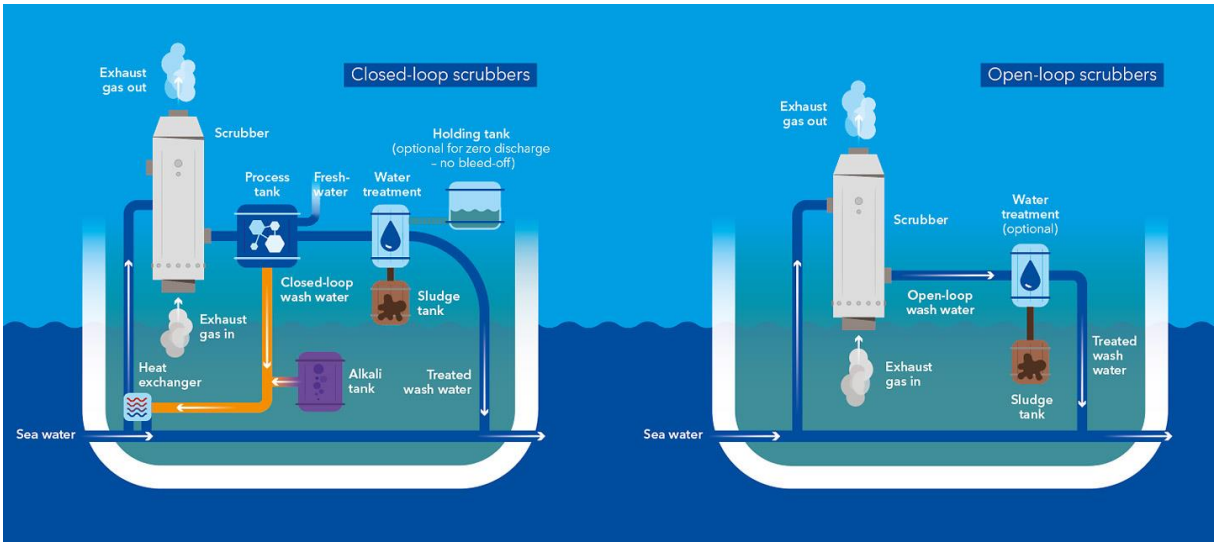

Figure 47: Open Loop and Closed Loop Scrubber Systems

Source: https://www.dnvgl.com/Images/MF_Industry_067_Closed-loop_open_loop_scrubbers_tcm71-130965.jpg

4.2.5 Engine Shut Off

Depending on the power arrangement, the main engines during the operation are normally kept running. This consumes an unnecessary amount of fuel as the generated energy is not used. The combustion process is very inefficient as there is no load on the engines.
The reason the engines are not shut off while not in use for a longer period of time is the increased wear on the engines. This extra wear on the internal engine components are caused by the decrease oil temperature. When the engine is turned off, the oil slowly cools down as well as the internal engine components. An engine is most efficient at a specific operational temperature. Running an engine at lower temperatures than the operational temperature causes increased wear and less efficient combustion cycles.
One solution to the increased wear problem is to keep the temperature of the oil and internal engine components steady with the oil pump and oil heater running. Warm oil runs through the engine and keeps the components at the operational temperature. The trade-off that has to be made here is the required energy to keep the oil running through the engine and to keep it at a specific temperature versus

the energy required to keep the engine at idle speed. Another variable to be researched is the increased wear to the engine which is difficult to determine.

4.2.6 Results of the Emission Reduction Methods

This sub chapter presents the results of the five emission reduction methods.

4.2.6.1 Power Arrangement

The results show that in all three scenarios, the mechanical power arrangement with a combined drive emits less CO_2 in comparison with the other power arrangements. The two large main engines are more fuel economic than the smaller engines which gives the combined drive a big advantage. As the combined drive is a mechanical power arrangement, there are less components to transfer the energy to the users. This gives an advantage to the mechanical power arrangements in terms of efficiency. Furthermore, the direct drive become less pollutant than the two types of hybrid power arrangements when the sailing time increases.

The results also show that the hybrid configuration with the mechanically driven propulsors is second less pollutant in all scenarios. The drive train from the main engines to the propulsors are more efficient mechanically driven than electrically driven. An electrical drive brings more inefficiencies as there are more components required to transfer the energy.

For all three scenarios, the difference between the mechanical (DD), electrical and hybrid arrangement is maximum 3 tonnes of CO_2. Within this hybrid power arrangement, the dredge pumps are mechanically driven. The electrical power arrangement emits most CO_2 in all scenarios compared to all other power arrangements. This is due the loss in efficiency that is brought by the components to convert mechanical energy into useful electrical energy. The mechanical power arrangement (DD) becomes less pollutant than the hybrid in scenario 2 and 3 where the sailing time increases. The hybrid in these scenarios loses its advantage of mechanically driven dredge pumps as loading and discharge times decrease.

The most important factors of choosing the most efficient power arrangement for a dredge is the fuel consumption of the engines. Within this case study, the fuel consumption of the individual engines has great influence to the results. Figure 48 shows the emitted CO_2 in tonnes per scenario and per power arrangement.

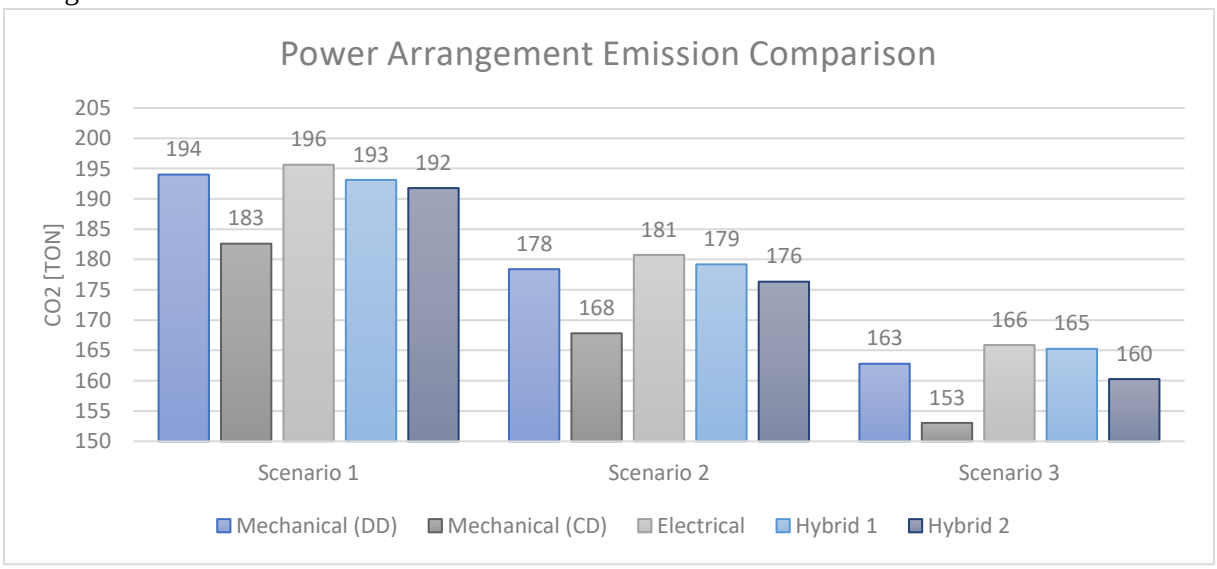

Figure 48: Power Arrangement Emission Comparison

4.2.6.2 Propeller Type

As the efficiency per volume of dredged soil increases, the total emission of CO_2 and SOx also decreases per operation. The NOx emissions are dependent on the rotational speed and the specific fuel consumption of the engine. When the rotational speed is influenced by a CPP, the NOx emissions can

also be reduced by the use of a CPP. The price and additional maintenance for a CPP is the downside of the system in comparison with a FPP. The period to earn back the investment depends on the type and price of the CPP.

4.2.6.3 Loading at Optimal Trailing Speed

According to the graph that shows the production per kilogram fuel used, the optimal speed for the fixed and floating visor is 0.7 m/s (Figure 69). The optimal speed is highly sensitive to the manual input of the jet penetration limit.

4.2.6.4 Scrubber

TSHDs are mainly used for beach nourishments, which take place within the ECAs. A long-term solution to comply to the stringent SOx regulations is to install a scrubber. For dredges operating along the coasts where the temperatures of the water and the content of alkaline vary, a closed loop or dry scrubber would be the best option. The hybrid solution is too extensive as an open loop system is not effective in the dredging areas. An open loop system would be too inefficient due to the variation of water temperature and in some ports this system is prohibited. Depending on the alkalinity of the sea water for open loop scrubbers, the removal rate of SOx is more than 96%. Up to 60% of the particular matter is removed as well [54].

4.2.6.5 Engine Shut Off

For one of the main engines of the Dodge Island this gives the following. At idling speed (350 rpm) the engine can deliver 228 kW at 100% throttle. The least amount of throttle that is given is 16%, which gives an available power of 36.5 kW and a fuel consumption of 8.7 kg/h per engine. For the operation Myrtle beach in the scenario where the two main engines of the Dodge Island were turned off during the connecting, disconnecting and discharge phase, the fuel saving would have been 0.55% which results in 0.55% less CO_2 emission.

5

CONCLUSIONS AND RECOMMENDATIONS

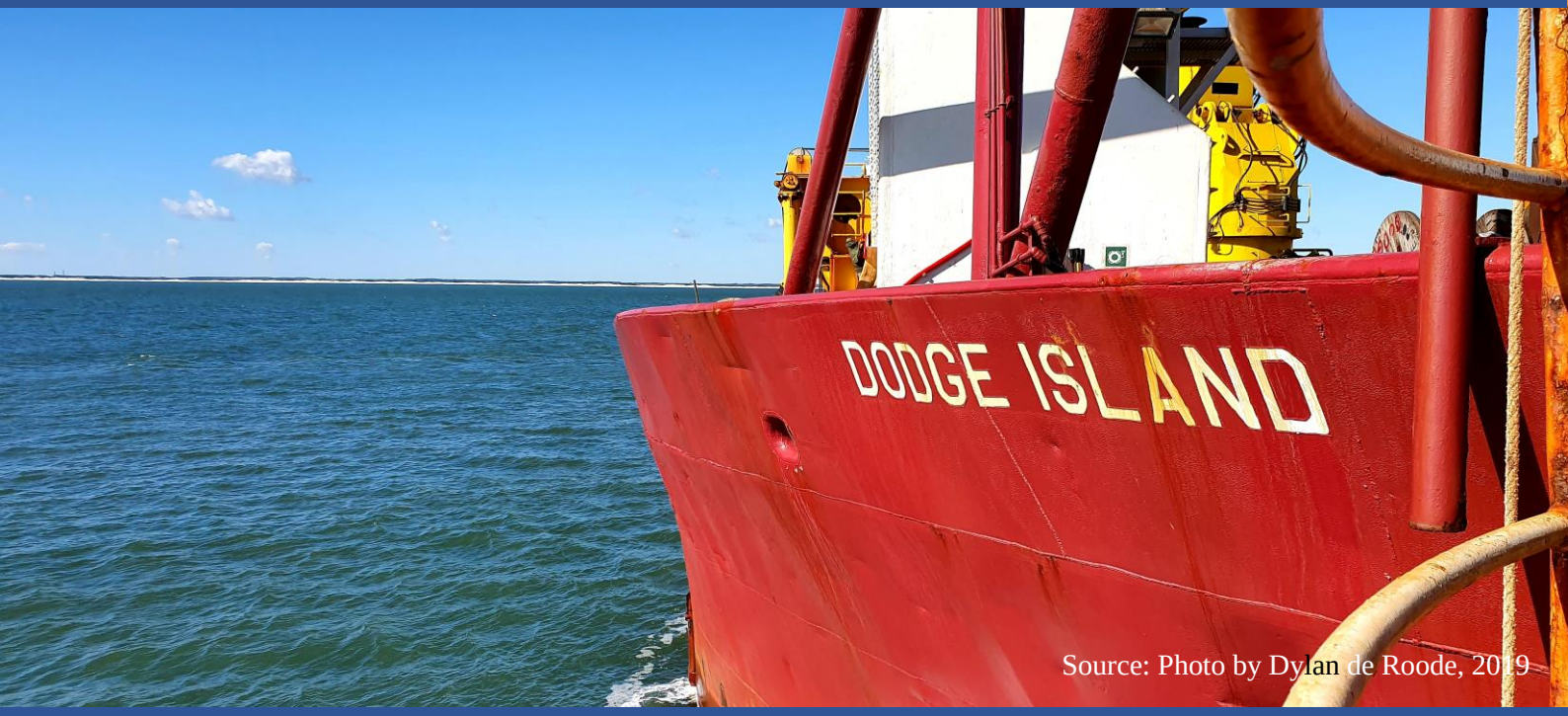

Source: Photo by Dylan de Roode, 2019

5. Conclusion and Recommendations

The first sub chapter covers the conclusion of the research. The second sub chapter discusses recommendations for future purposes. Recommendations are given for further research for the reduction methods and the emission model.

5.1 Conclusion

The purpose of this research is to provide an emission model and present methods to reduce the emissions of trailing suction hopper dredges during operation. The model is capable of determining the total energy requirement and emission profile for TSHDs for individual jobs. The used power arrangement is mechanical with a direct drive. The discharge method can vary between discharge via a pipeline or splitting the hull. Different TSHDs can be implemented in the database which makes the model independent to one specific TSHD. The type of visor can vary between a floating and a fixed visor. The model gives several different outputs. The main outputs are the amount of the emissions (CO_2, SOx and NOx), the amount of fuel used and the cost of fuel, all per dredged m^3.

Several viable methods to reduce the emissions in accordance with the design philosophy of Great Lakes Dredge and Dock are researched. The design philosophy is formed by internal and external factors. External factors are the availability of knowledge within shipyards to build a modern dredge, the expectations of the market, the available technology and the height of the building costs. Internal factors are preferably interchangeable parts and the determination of the focus of the market. The philosophy creates viable methods to reduce the emissions of TSHDs.

The first method consists of determining which type of power arrangement is most emission friendly. Three types of power arrangements are researched, mechanical, electrical and hybrid power arrangements. It is seen that the results are sensitive to multiple factors which can change the outcome of the research. The mechanical power arrangement with a combined drive brought the least emission pollution. The second reduction method takes into account the propeller type. To increase the efficiency of the propeller in all three phases, controllable pitch propellers form the solution. Besides a multitude of advantages, a controllable pitch propeller reduces the fuel consumption and emissions. The optimisation of the excavation depth and the trailing speed is the third method to reduce the fuel consumption and emissions. The optimisation was executed for a floating and fixed visor. It was clear that the jet penetration depth is the leading factor to determine the optimal trailing speed. The fourth method to reduce the emissions is the scrubber. The main forms of a marine scrubber are the dry, open loop, closed loop and the hybrid scrubber. For dredges operating at the coast, a dry or a closed loop scrubber would be most efficient in terms of filtering the emissions of the exhaust gasses. Engines running at idle speed are inefficient and the generated power is not used. The fifth method to reduce the emissions is to shut off the engines when not in use for a long time. A disadvantage of shutting off the engines is the increased wear of the engines cause by the reduced temperature.

The basis is made for a model with the capability of predicting the fuel consumption and the emissions for multiple TSHDs with each their unique specifications. By also using the model to optimise dredging characteristics such as trailing speed and penetration depth, fuel consumption and the emissions can be reduced.

5.2 Recommendations

This sub chapter is split up into two parts. The first part covers recommendations to improve and extend the current model. The second part covers recommendations for further research on the reduction methods.

5.2.1 Recommendations for Further Research on the Emission Model

The emission model is useful for multiple TSHDs. With the current model, only TSHDs with a direct drive are used as an input. To cover a wider variation of TSHDs, several different power arrangements can be implemented. Furthermore, the model is based on the Tame Dragon Draghead. Multiple types of draghead can be implemented for further research.

It was assumed that the distance of the centre of buoyancy from ½ L_{pp} of the dredges was zero. The centre of buoyancy can be included for future calculations. The displacement of the dredges during loading was taken as fully loaded to simplify the calculations and the little effect for the required propulsion power. To improve the model, the variating displacement can be taken into account. In the same phase, the settlement time of the soil is neglected. Assumed is a settlement time of zero where the soil is settled once it ends up in the hopper. The settlement time can be included to improve the accuracy of the loading time.

The pump power calculations within the emission model covers the basic of required pumping power. More extensive calculations increase the accuracy of the pump power and the loading and discharge time. Spillage of the draghead, jets and the pumps can also be introduced in the model. When the dredge is loading and trails the draghead along the ocean floor, it is assumed that the seabed is flat. In practise this is never the case and therefore additional resistance can be introduced in within the model. To increase the accuracy of the power usage, the electrical load balance should be measured for each dredge individually. The current model contains the power usage for the Dodge Island. The current method to determine the resistance of the hull is based on the method of Holtrop and Mennen. For more accurate results, testing with models or CFD calculations should be made to compute the total hull resistance.

At the moment, the model provides multiple values next to the results. For the sailing phases, the model shows the required fuel consumption per vessel velocity. The extra fuel cost can be calculated with an increase of velocity. This is related to the emissions and required engine power. The type of visor can be chosen according to the desired loading speed and the relating optimal production. When costs of the entire job are taken into account, trade-offs can be made between the total operation cost and the speed of the dredge.

5.2.2 Recommendations for Further Research on the Reduction Methods

The possible reduction methods are narrowed down by the design philosophy of GLDD to make them useful for the company. For further research to reduce the emissions for TSHDs, methods that do not comply with the design philosophy of GLDD can be researched. It is recommended that the methods are more investigated per individual dredge. More accurate results are achieved when the reduction methods can be determined for a certain dredge. More variables can be taken into account, for example the costs and the available space on board.

For future research regarding the optimal trailing speed, a comparison should be made between the costs of the time that is lost due to loading at certain phase versus the fuel savings and increased production. The jet penetration limit which can be set manually is the biggest factor for the shown results. Further research should be done to determine the limit in more detail.

6

REFERENCES

Source: Photo by Dylan de Roode, 2019

6. References

[1] N. Statt, “Norway will install the world’s first wireless electric car charging stations for Oslo taxis,” The Verge, 21 3 2019. [Online]. Available: https://www.theverge.com/2019/3/21/18276541/norway-oslo-wireless-charging-electric-taxis-car-zero-emissions-induction. [Accessed 23 12 2019].

[2] IMO, “Green House Gas Emissions,” IMO, 2019. [Online]. Available: http://www.imo.org/en/OurWork/Environment/PollutionPrevention/AirPollution/Pages/GHG-Emissions.aspx. [Accessed 13 June 2019].

[3] IADC, “Facts about trailing suction hopper dredgers,” *An information update from the IADC*, p. 4, 1 2014.

[4] E. D. Association, “About dredging; Mechanical dredger,” [Online]. Available: https://www.european-dredging.eu/Mechanical_dredger. [Accessed 4 10 2019].

[5] E. D. Association, “About dredging; Other types of dredger,” [Online]. Available: https://www.european-dredging.eu/Other_types_of_dredger. [Accessed 4 19 2019].

[6] Wikipedia, “Dredging,” [Online]. Available: https://en.wikipedia.org/wiki/Dredging. [Accessed 4 10 2019].

[7] F. C. Scheffauer, The Hopper Dredge, Washington, 1954.

[8] G. v. d. Schrieck, Dredging Technology, Aerdenhout: GLM van der Schrieck BV, 2013.

[9] Great Lakes Dredge and Dock, “TSHD Standards,” Chicago, 2014.

[10] G. data, “Geotechdata geotest standard penetration test,” Geotech data, 07 02 2016. [Online]. Available: http://www.geotechdata.info/geotest/standard-penetration-test.html. [Accessed 28 01 2020].

[11] S. Miedema, OE4607 Introduction Dredging Engineering, Delft, 2015.

[12] dictionary.com, “Dictionary,” [Online]. Available: https://www.dictionary.com/browse/permeability?s=t. [Accessed 28 01 2020].

[13] M. Webster, “Merriam Webster greenhouse gas,” 2019. [Online]. Available: https://www.merriam-webster.com/dictionary/greenhouse%20gas. [Accessed 19 12 2019].

[14] E. observatory, “Effects of changing the carbon cycle,” earh observatory, 16 06 2011. [Online]. Available: https://earthobservatory.nasa.gov/features/CarbonCycle/page5.php. [Accessed 31 12 2019].

[15] D. Lappi, “The big picture: 65 million years of temperature swings,” JoNova, 02 2010. [Online]. Available: http://joannenova.com.au/2010/02/the-big-picture-65-million-years-of-temperature-swings/. [Accessed 19 12 2019].

[16] IPCC, “Climate Change 2014 Synthesis Report,” IPCC, 2014.

[17] L. Rebecca, “Climate change: atmospheric carbon dioxide,” Climate.gov, 19 09 2019. [Online]. Available: https://www.climate.gov/news-features/understanding-climate/climate-change-atmospheric-carbon-dioxide. [Accessed 31 12 2019].

[18] Nasa, “The Effects of Climate Change,” NASA, [Online]. Available: https://climate.nasa.gov/effects/. [Accessed 28 01 2020].

[19] K. Pierr-Louis, “Ocean warming is accelerating faster than thought, new research finds,” The new york times, 11 01 2019. [Online]. Available: https://www.nytimes.com/2019/01/10/climate/ocean-warming-climate-change.html. [Accessed 28 01 2020].

[20] EBSCO, “EBSCO Publishing Service Selection Page,” EBSCO, 21 04 2016. [Online]. Available: http://web.a.ebscohost.com/ehost/pdfviewer/pdfviewer?sid=5fce181f-216b-4c6e-b9c9-7f5308d1d36f%2540sessionmgr4004&vid=1&hid=4207. [Accessed 28 01 2020].

[21] A. K. Ibrahim Aslan, “The pollutant emissions from diesel-engine vehicles and exhaust aftertreatment systems,” *Clean technologies and environmental policy,* vol. 17, no. 1, p. 12, January 2015.

[22] Anish, “what is nitrogen oxides or nox air pollution from ships,” marine insight, 3 12 2019. [Online]. Available: https://www.marineinsight.com/maritime-law/what-is-nitrogen-oxides-or-nox-air-pollution-from-ships/. [Accessed 31 12 2019].

[23] F. Beaudry, “How does nitrogen oxide pollution affect the environment?,” ThoughtCo, 07 11 2019. [Online]. Available: https://www.thoughtco.com/what-is-nitrogen-oxide-pollution-1204135. [Accessed 31 12 2019].

[24] E. P. Agency, “U.S. Greenhouse Gas Emissions and Sinks,” 2019.

[25] IMO, “Introduction to IMO,” IMO, 2019. [Online]. Available: http://www.imo.org/en/About/Pages/Default.aspx. [Accessed 13 June 2019].

[26] IMO, “Structure of IMO,” IMO, 2019. [Online]. Available: http://www.imo.org/en/About/Pages/Structure.aspx. [Accessed 13 June 2019].

[27] E. Commission, “Transport emissions,” 2019. [Online]. Available: https://ec.europa.eu/clima/policies/transport/shipping_en. [Accessed 19 12 2019].

[28] MARPOL, “Third IMO Greenhouse Gas Study 2014,” 2015.

[29] M. IMO, “Sulphur oxides sox,” IMO, 2019. [Online]. Available: https://www.marpol-annex-vi.com/emissions/sulphur-oxides-sox/. [Accessed 18 01 2020].

[30] D. Energy, “Sulfur Dioxide Scrubbers,” Duke Energy, [Online]. Available: https://www.duke-energy.com/our-company/environment/air-quality/sulfur-dioxide-scrubbers. [Accessed 12 02 2020].

[31] EPA, “The act to prevent pollution from ships (APPS) enforcement case resolutions,” 15 februari 2019. [Online]. Available: https://www.epa.gov/enforcement/act-prevent-pollution-ships-apps-enforcement-case-resolutions. [Accessed 23 july 2019].

[32] W. Blowers, “Act to Prevent Pollution from Ships,” [Online]. Available: https://www.whistleblowers.org/act-to-prevent-pollution-from-shipsmarpol/. [Accessed 26 12 2019].

[33] EPA, “Enforcement of MARPOL Annex VI - Memorandum of Understanding,” 27 06 2011. [Online]. Available: https://www.epa.gov/sites/production/files/documents/annexvi-mou062711.pdf. [Accessed 12 26 2019].

[34] GLDD, “GLDD Timeline,” GLDD, 2018. [Online]. Available: https://www.gldd.com/gldd-timeline/. [Accessed 20 12 2019].

[35] P. Moazzen, “Top 10 Dredging and Reclamation companies in the world,” Linkedin, 26 08 2014. [Online]. Available: https://www.linkedin.com/pulse/20140826103053-63488664-top-10-dredging-companies-in-the-world. [Accessed 20 12 2019].

[36] GLDD, “GLDD History,” GLDD, 2019. [Online]. Available: gldd.com/gldd-history/. [Accessed 01 02 2020].

[37] Great Lakes Dredge and Dock, “Annual Report 2018,” Oak Brook, 2018.

[38] T. U. A. C. o. Engineers, “Missions,” USACE, [Online]. Available: https://www.usace.army.mil/Missions/. [Accessed 27 12 2019].

[39] J. H. a. G. Mennen, “An approximate power prediction method,” 1982.

[40] G. t. Meulen, “Draghead Analysis,” Delft, 2018.

[41] S. A. Miedema, “The delft sand, rock and clay cutting model,” IOS Press, Delft, 2015.

[42] S. Miedema, “Production estimation of water jets in drag heads,” Delft.

[43] H. K. Woud and D. Stapersma, Design of propulsion and electric power generation systems, IMarEST, 2002.

[44] M. Milnes, “The mathematics of pumping water,” AECOM, -.

[45] H. O. Kristensen, Prediction of Resistance and Propulsion Power of Ships, Denmark, 2013.

[46] Tom Benson; Nasa, “Reynolds number,” 2014.

[47] C. v. Rhee, “De invloed van ee nwaterstraal op en zandpakket,” Delft, 1986.

[48] C. v. Rhee, “Orienterende jetproeven op 190 mum zand met middelvaste pakking,” 1987A.

[49] C. v. Rhee, “Orienterende jetproeven op 190 mum zand met vaste en zeer losse pakking,” Delft.

[50] ankur2061, “cheresources,” cheresources.com, 15 03 2013. [Online]. Available: https://www.cheresources.com/invision/blog/4/entry-340-calculating-physical-properties-of-slurries/. [Accessed 18 01 2020].

[51] P. flow, “pipe roughness,” [Online]. Available: https://www.pipeflow.com/pipe-pressure-drop-calculations/pipe-roughness. [Accessed 18 01 2020].

[52] MAN, “Diesel-Electric Drives,” MAN.

[53] S. Sethi, “A guide to scrubber system on ship,” Marine insight, 17 03 2020. [Online]. Available: https://www.marineinsight.com/tech/scrubber-system-on-ship/. [Accessed 26 03 2020].

[54] ABS, “ABS advisory on exhaust gas scrubber systems,” ABS, Shutterstock, 2017.

[55] D. Today, “Dredging Vessel Directory,” 2019.

[56] D. Stapersma, “Main Propulsion Arrangement and Power Generation Concepts,” Delft.

[57] NASA, “GISS Surface Temperature Analysis (v4),” NASA, 2019. [Online]. Available: https://data.giss.nasa.gov/gistemp/graphs_v4/. [Accessed 19 12 2019].

[58] D. GL, “Different Ways to Meet NOx Tier III Standard,” 04 12 2019. [Online]. Available: https://www.marineinsight.com/tech/different-ways-meet-nox-tier-iii-standards/. [Accessed 26 12 2019].

[59] AirClim, “Air pollution from ships,” 12 04 2019. [Online]. Available: https://www.airclim.org/air-pollution-ships. [Accessed 12 26 2019].

[60] F. N. S. M. Zhi Liu, *Optimized design method for TSHD's swell compensator basing on modeling and simulation,* 2009.

[61] L. Rebecca, “Climate change: atmospheric carbon dioxide IMAGE: CO2 during ice ages and warm periods for the past 800,000 years,” Climate.gov, 19 09 2019. [Online]. Available: https://www.climate.gov/sites/default/files/paleo_CO2_2018_1500.gif. [Accessed 31 12 2019].

[62] M. w. R. m. S. k. J. hendriksen, “Engineering analysis of turtle exclusion device,” in *Dredging Summit and Expo 2015*, Texas, 2015.

[63] H. K. D. Stapersma, “Practical emission research for a navy,” Royal Netherlands Naval College, Den Helder, 1998.

7

APPENDIX

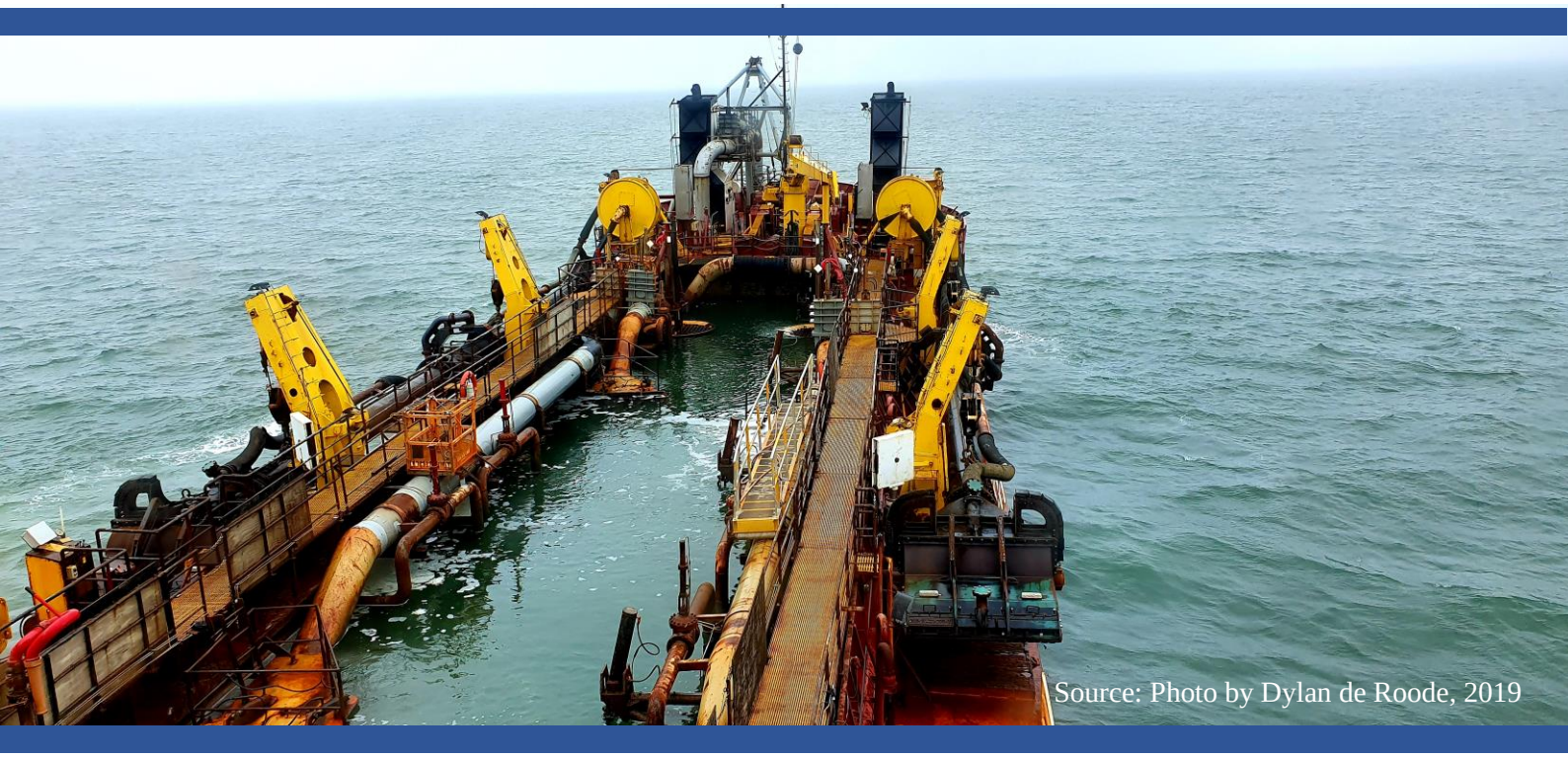

Source: Photo by Dylan de Roode, 2019

7. Appendix

7.1 Chapter 3: Emission Model: TSHD in Operation

This sub chapter shows the figures, equations and tables of chapter 3.

7.1.1 Specifications of the Dodge Island

Length waterline [m]	82.04	Bow Thruster	yes
Breadth [m]	15.85	Immersed Transom	no
Draft Loaded [m]	6.05	Combined Engine prop. & pump	no
Draft Empty [m]	4.34	Power Arrangement	Direct
Depth [m]	6.63	Bow Thruster [kW]	410
Hopper size [m^3]	2754	Number	1
number of propellers [-]	2	sfc [g/kWh]	243
Gearbox reduction Transit [-]	3.407	Jet [kW]	410
Gearbox reduction Loading [-]	3.407	Number	2
Midship coefficient [-]	0.99	sfc [g/kWh]	243
Wet ship incl. fuel and water [ton]	3164	Pump power [kW]	1104
Displacement Loaded [ton]	6985	Number	2
Displacement Empty [ton]	3630	sfc [g/kWh]	216
Pitch Prop [m]	2.2921	Generator [kW]	500
Diameter Prop [m]	2.4384	Number	1
Bulbous Bow	no	sfc [g/kWh]	216

Table 13: Specifications of the Dodge Island

7.1.2 Direct Power Arrangement of the Dodge Island

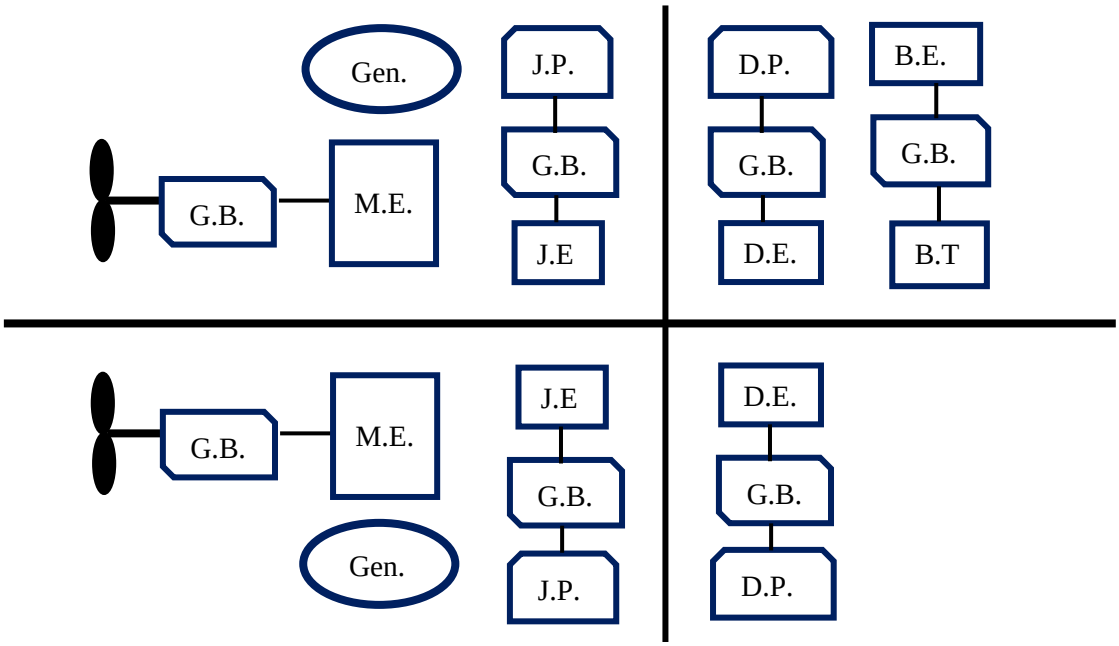

Figure 49: Power Arrangement Dodge Island

Legend:

J.P.	Jet Pump	D.E.	Dredge Engine	Gen.	Generator
G.B.	Gearbox	J.E.	Jet Engine	B.T.	Bowthruster
M.E.	Main Engine	D.P.	Dredge Pump	B.E.	Bowthruster Engine

7.1.3 Froude number versus the Total Resistance of the Dodge Island

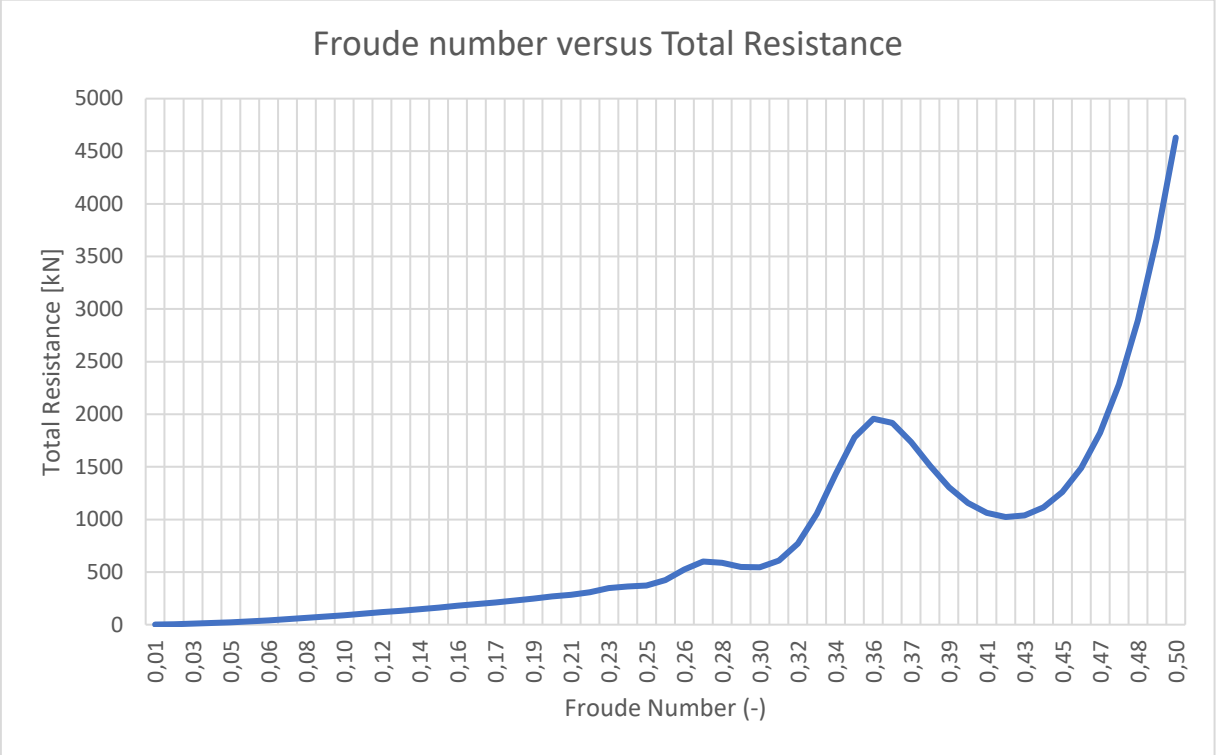

Figure 50: Froude number versus Total Resistance for the Dodge Island at Full Load

7.1.4 Approximate 1+k2 values for vessels

Approximate $1+k_2$ values	
Rudder behind skeg	1.5 - 2.0
Rudder behind stern	1.3 – 1.5
Twin-screw balance rudders	2.8
Shaft brackets	3.0
Skeg	1.5 – 2.0
Strut bossings	3.0
Hull bossings	2.0
Shafts	2.0 – 4.0
Stabilizer fins	2.8
Dome	2.7
Bilge keels	1.4

Table 14: Approximate $1+k_2$ values

7.1.5 Specifications of the Suction Pipes

Weights	Name	Mass (kg)	Volume (m^3)	Submerged force (N)
arm piece assembly 1	Fa	200	0.016	1945
arm piece assembly 2	Fb	200	0.016	1945
upper part pipe	Fc	1396	0.179	13513
arm piece assembly 3	Fd	200	0.016	1945
turning gland assembly	Fe	200	0.016	1945
Lower part pipe	Ff	1261	0.162	12207
Draghead	Fg	8872	1.140	85866
Visor	Fv	3828	0.490	37050
TED	Fted	982	0.212	9416

Table 15: Specifications Suction Pipes

7.1.6 Force Overview of the Static Situation with Vertical Soil Force

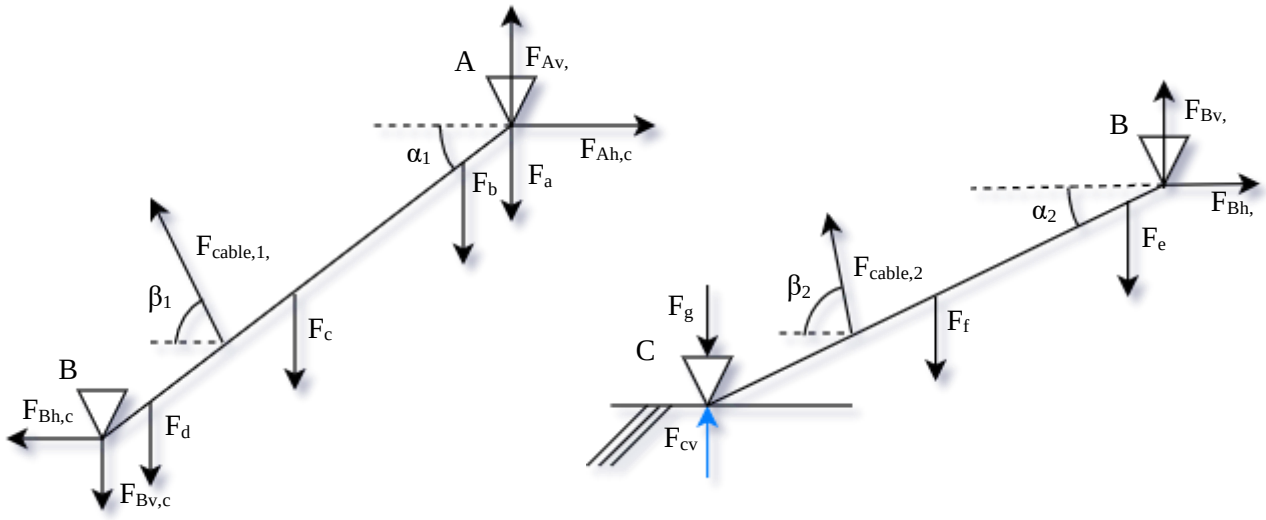

Figure 51: Force Overview Static Situation with Vertical Soil Force for Upper (left) and Lower (right) Suction Pipe

7.1.7 Force Overview of the Static Situation with Compensated Vertical Soil Reaction Force and Increasing Velocity

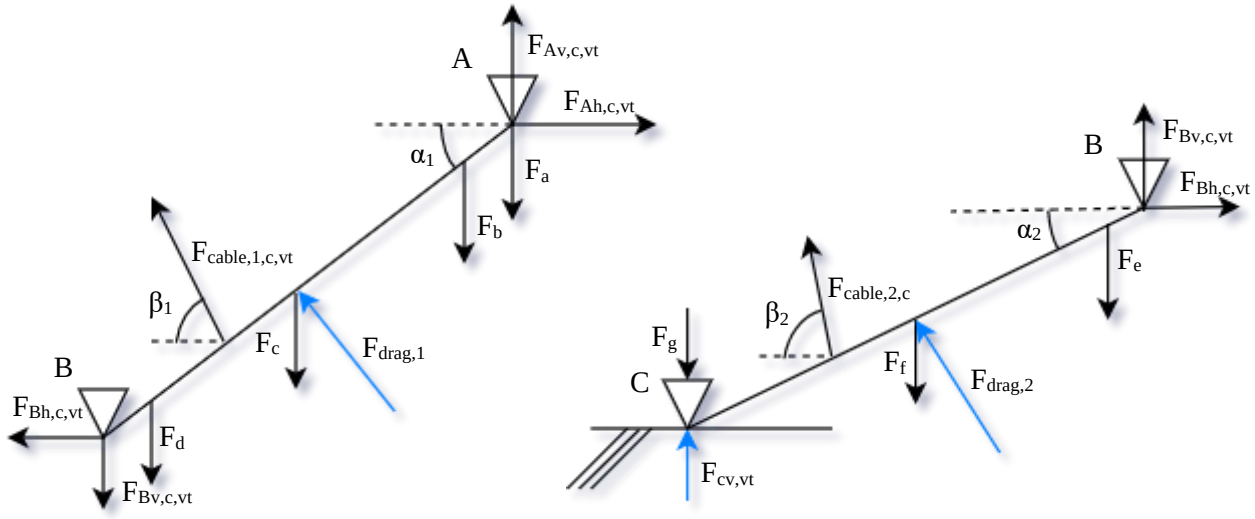

Figure 52: Force Overview Static Situation with Compensated Vertical Soil Reaction Force and Increasing Velocity for Upper (left) and Lower (right) Suction Pipe

7.1.8 Force Overview of the Static Situation with Compensated Soil Excavation Forces and Increasing Velocity

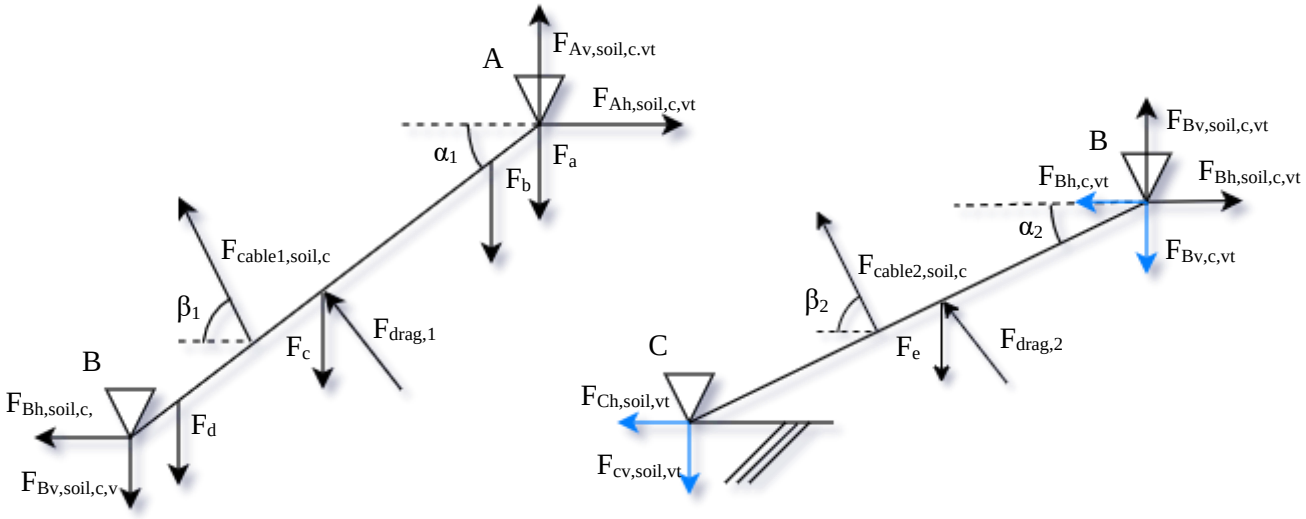

Figure 53: Force Overview Static Situation with Compensated Soil Excavation Forces and Increasing Velocity for Upper (left) and Lower (right) Suction Pipe

7.1.9 Variables for the Shear Plane and the Total Resistance of the Flow Lines

$$s_1 = (L_{max} - L) * \left(\frac{\pi}{2} + \theta_1\right) + \frac{h_b}{\sin(\alpha)} \tag{215}$$

With:

$$\theta_1 = \frac{\pi}{2} - (\alpha + \beta) \tag{216}$$

And:

$$s_2 = 0.8 * L * \theta_2 \tag{217}$$

With:

$$\theta_2 = \alpha + \beta \tag{218}$$

And:

$$s_3 = 0.8 * L * \theta_3 \tag{219}$$

With:

$$\theta_3 = \pi - \beta \tag{220}$$

And:

$$s_4 = (L_{max} - L) * \theta_4 + 0.9 * h_i * \left(\frac{h_i}{h_b}\right)^{0.5} * (1.85 * \alpha)^2 * \left(\frac{k_i}{k_{max}}\right)^{0.4} \tag{221}$$

With:

$$\theta_4 = \pi + \beta \tag{222}$$

The total resistance of the flow lines is calculated as follows:

$$\frac{1}{R_t} = \frac{1}{R_1} + \frac{1}{R_2} + \frac{1}{R_3} + \frac{1}{R_4} \tag{223}$$

With:

$$R_1 = \frac{s_1}{k_{max}} \tag{224}$$

$$R_2 = \frac{s_2}{k_{max}} \tag{225}$$

$$R_3 = \frac{s_3}{k_i} \tag{226}$$

$$R_4 = \frac{s_4}{k_i} \tag{227}$$

7.1.10 Variables for the Blade and the Total Resistance of the Flow Lines

$$s_1 = \frac{h_b}{\sin(\alpha)} \tag{228}$$

And:

$$s_2 = 0.8 * L_{max} * \theta_2 \tag{229}$$

With:

$$\theta_2 = \alpha + \beta \tag{230}$$

And:

$$s_3 = 0.8 * L_{max} * \theta_3 \tag{231}$$

With:

$$\theta_3 = \pi - \beta \tag{232}$$

And:

$$s_4 = 0.9 * h_i * \left(\frac{h_i}{h_b}\right)^{0.5} * (1.85 * \alpha)^2 * \left(\frac{k_i}{k_{max}}\right)^{0.4} \tag{233}$$

The total resistance can now be determined:

$$\frac{1}{R_{t,i}} = \frac{1}{R_{1,i}} + \frac{1}{R'_2} \tag{234}$$

With:

$$R_{1,i} = \frac{s_{1,i}}{k_{max}} * \left(1 - \frac{i}{N}\right) \tag{235}$$

And:

$$R_2 = \frac{s_2}{k_{max}} \tag{236}$$

7.1.11 Combined Power and Torque Curve for Loading Condition

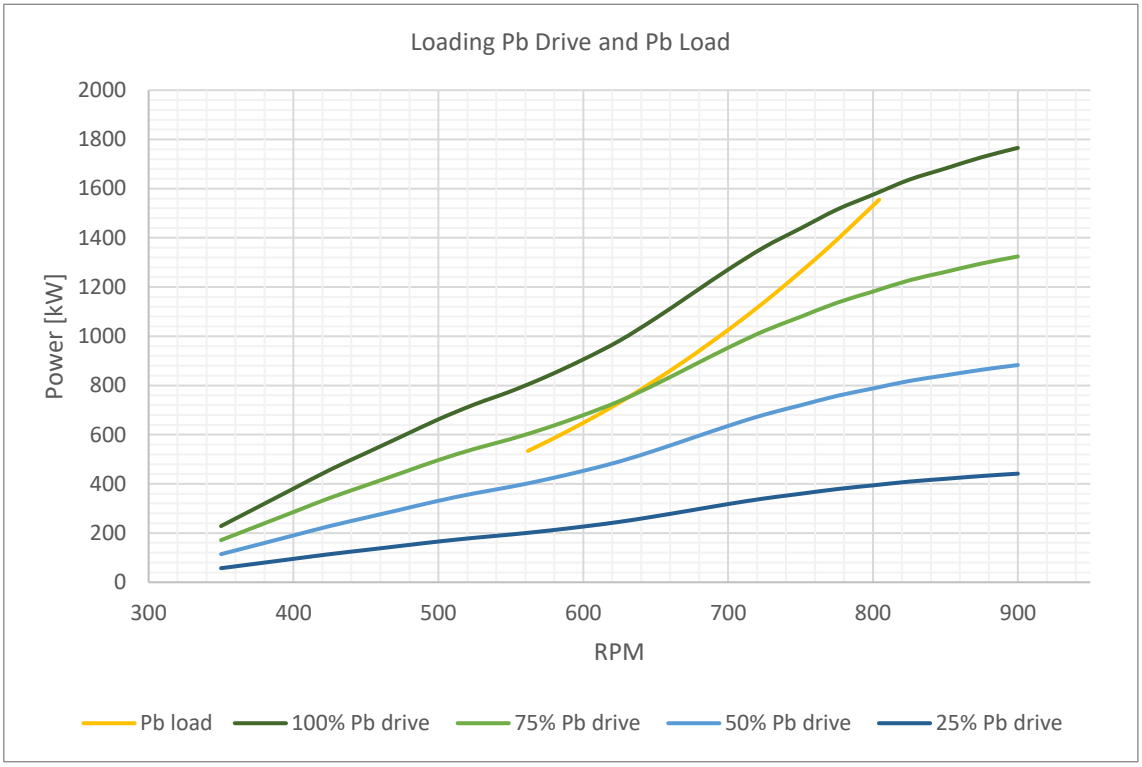

Figure 54: Combined Power Curve Drive and Load for Loading

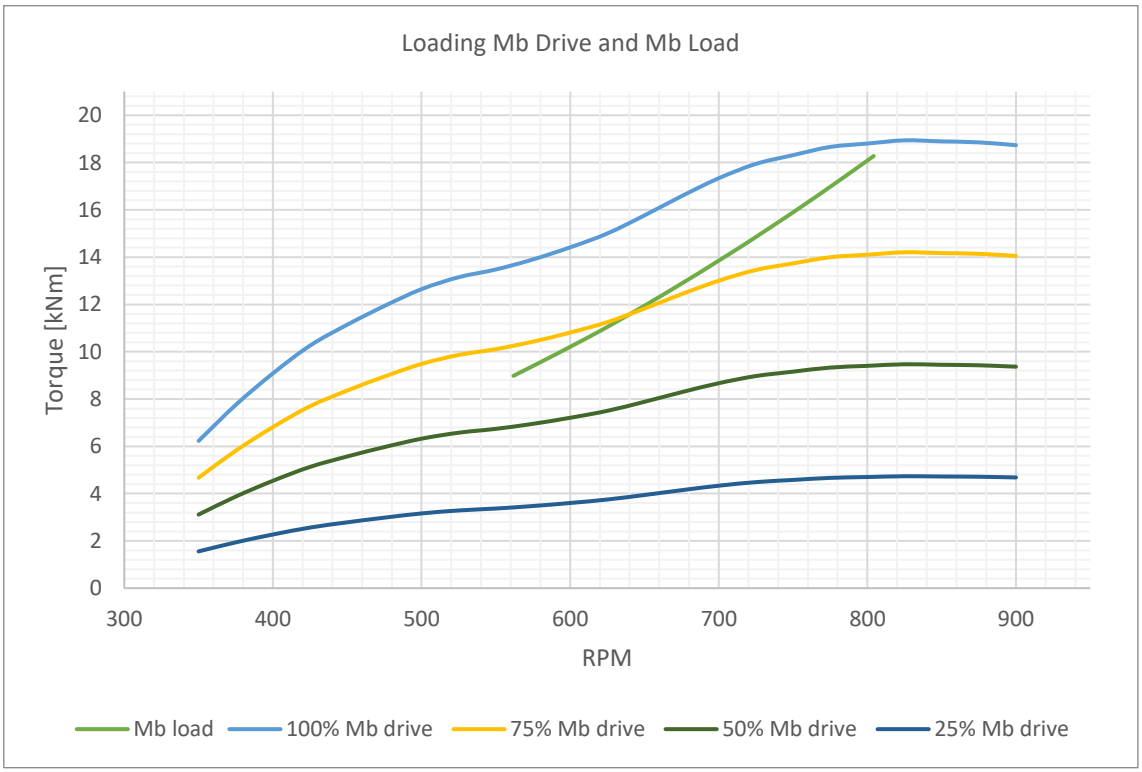

Figure 55: Combined Torque Curve Drive and Load for Loading

7.1.12 Combined Power and Torque Curve for Loaded Condition

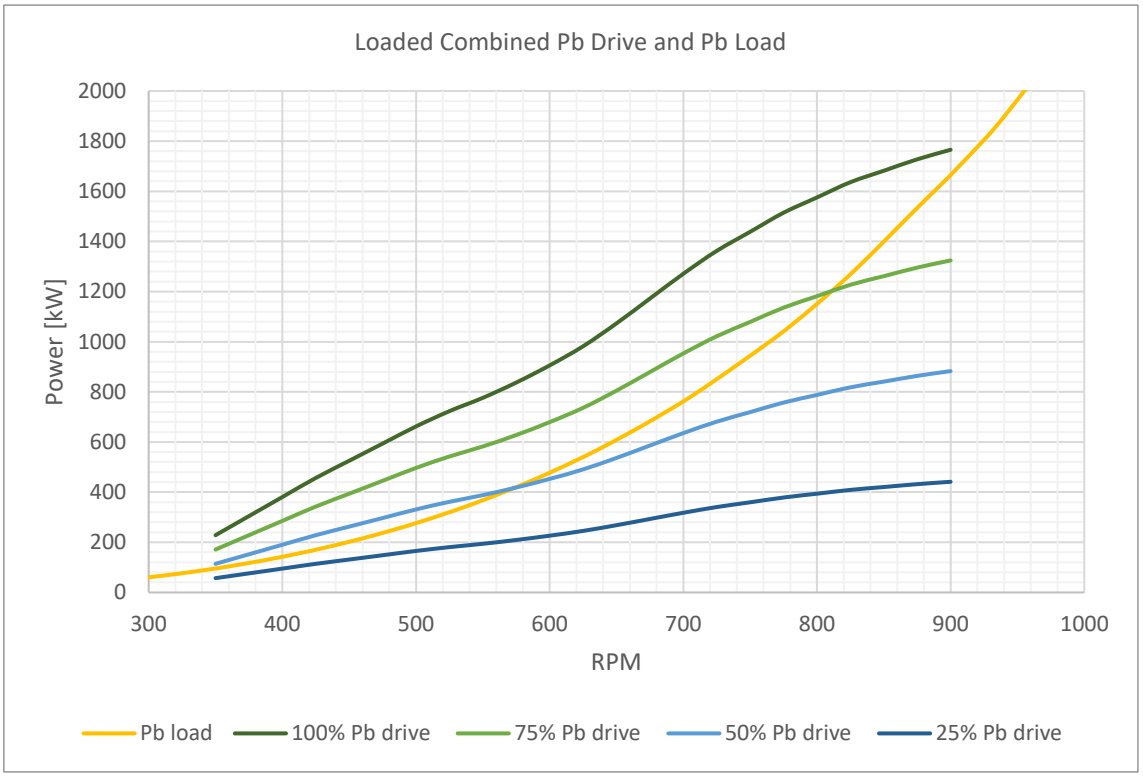

Figure 56: Combined Power Curve Drive and Load for Loaded

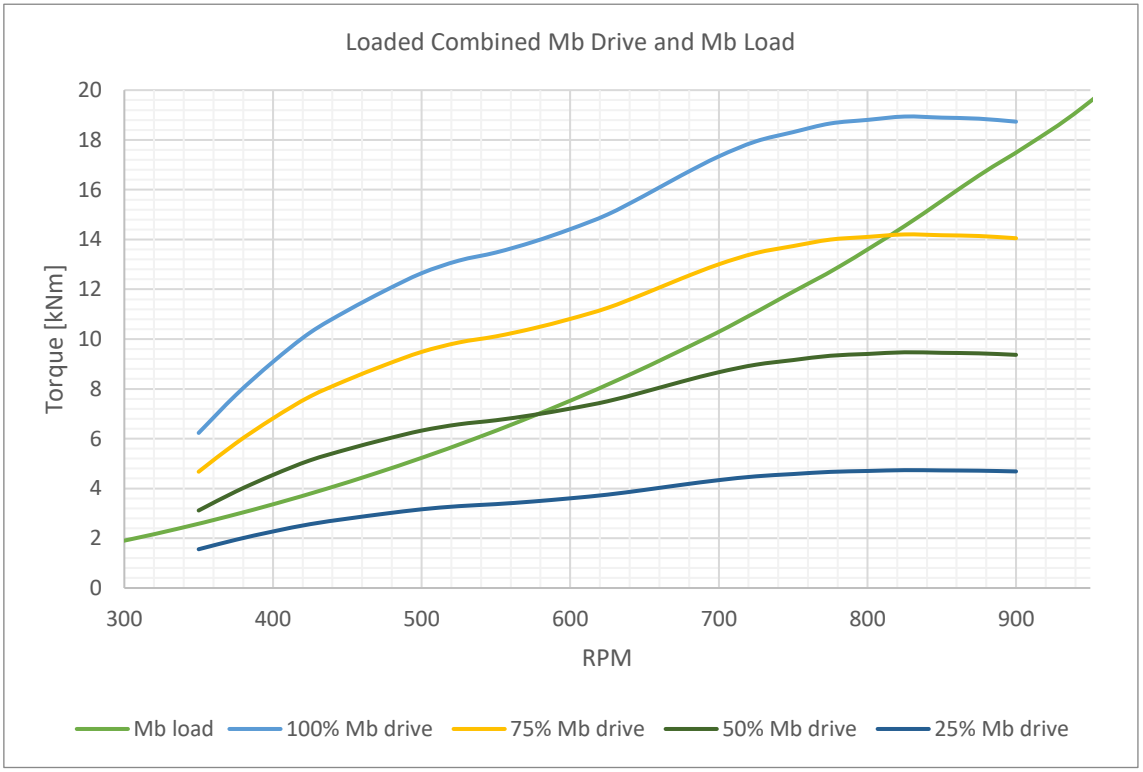

Figure 57: Combined Torque Curve Drive and Load for Loaded

7.1.13 Combined Power and Torque Curve for Empty Condition

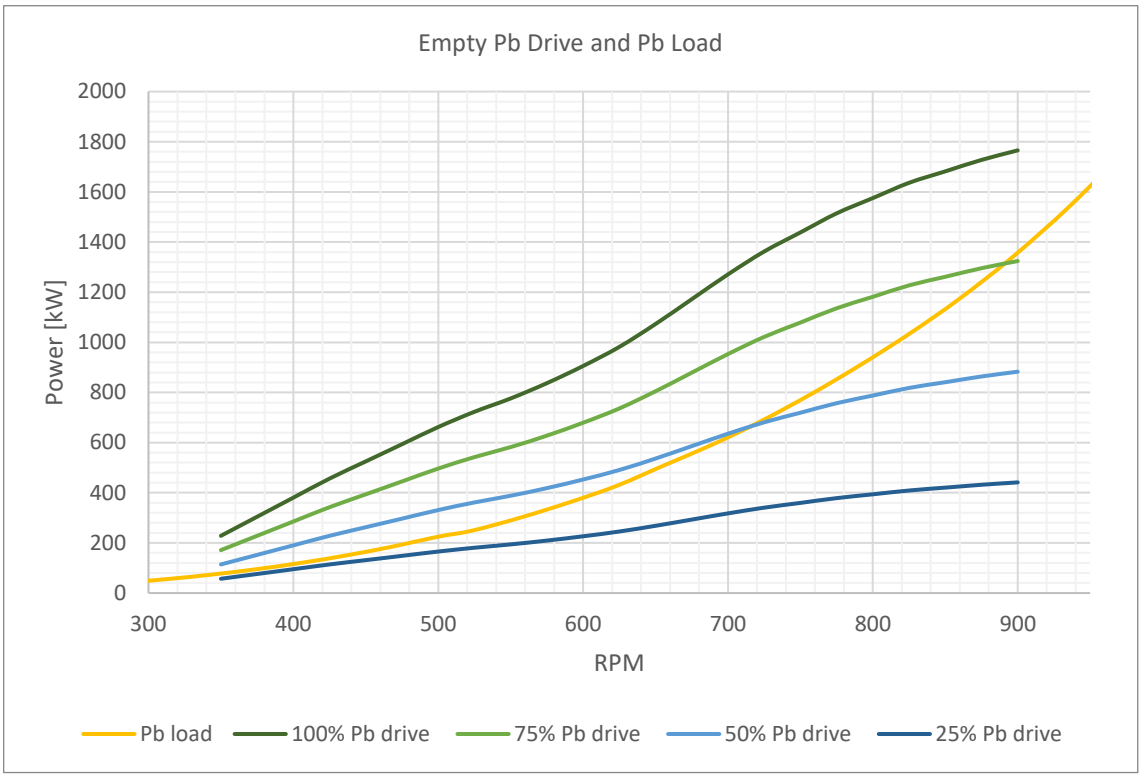

Figure 58: Combined Power Curve Drive and Load for Empty

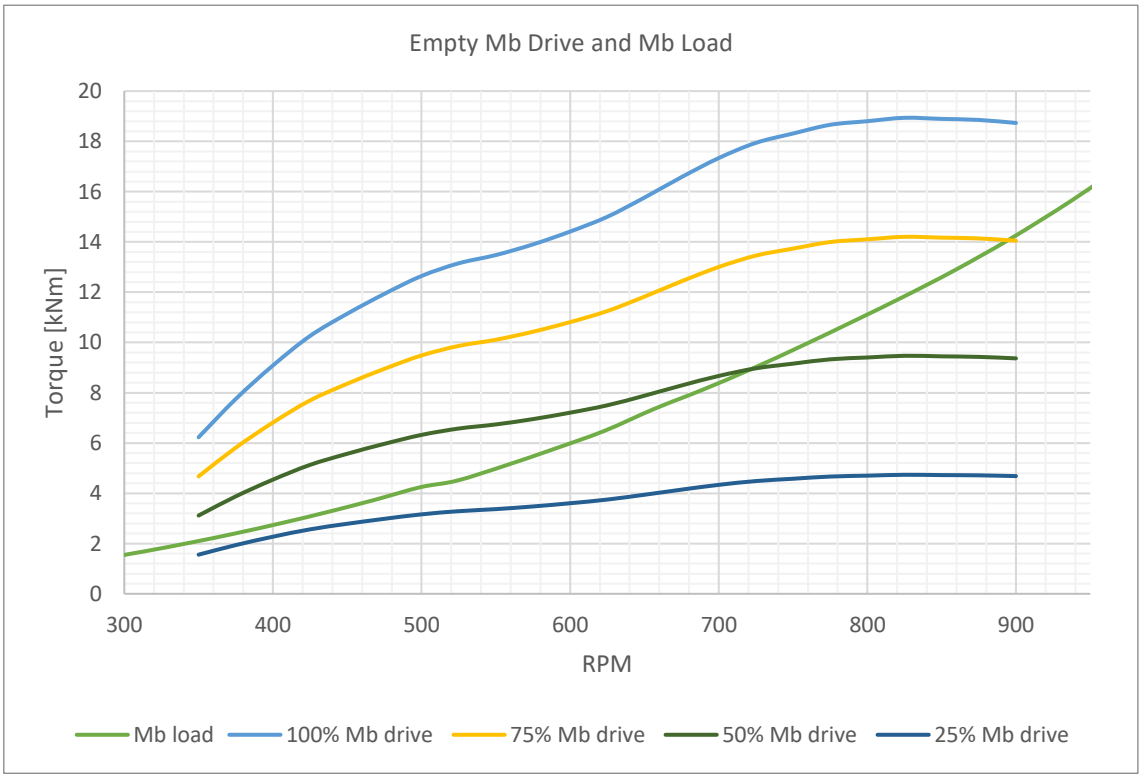

Figure 59: Combined Torque Curve Drive and Load for Empty

7.1.14 Calculation Sheet for the Generators and Dredge Engines

DODGE ISLAND

Specifications							Fuel Consumption					Costs			Emissions							
			Total power	Time of phase	phase time per day		Power per day	fuel consumption (m	fuel consumption (m	volume fuel consump	volume fuel per day	Costs fuel	Costs fuel	Cost fuel	emission flow CO2 (m	emission flow SOx (m	emission flow NOx (m	emission flow HC (m	emission flow CO (m	CO2 emission	CO2 emission
		Phase	kW	min	h		kWh/day	g/min	ton/h	m3/h	L/day	$/h	$/phase	$/day	kg/h	g/h	g/h	g/h	g/h	kg/phase	kg/day
Generator		**Totals**	**2087**	**183**	**24**						**2693**		**$ 185**	**$ 1.457**						**902**	**7093**
Caterpillar D398		Loading	**396**	**57**	**7,5**		2981	1743	0,105	0,124	**930**	$ 67	$ 64	**$ 503**	325,7	418	7321	235	1360	312	**2450**
engine efficiency	ηe	Transit Loaded	**345**	**28**	**3,7**		1286	1517	0,091	0,108	**401**	$ 58	$ 28	**$ 217**	283,5	364	6373	205	1184	134	**1057**
specific fuel consumption	sfc	Connecting	**328**	**9**	**1,2**		387	1443	0,087	0,102	**121**	$ 55	$ 8	**$ 65**	270	346	6059	195	1125	40	**318**
heating value MDO	hL	Discharge	**345**	**57**	**7,4**		2565	1518	0,091	0,108	**801**	$ 58	$ 55	**$ 433**	284	364	6377	205	1184	268	**2109**
Price MDO	$MDO	Disconnecting	**328**	**7**	**0,9**		301	1443	0,087	0,102	**94**	$ 55	$ 6	**$ 51**	270	346	6059	195	1125	31	**247**
Density MDO	ρMDO	Transit Empty	**345**	**25**	**3,2**		1109	1517	0,091	0,108	**346**	$ 58	$ 24	**$ 187**	284	364	6373	205	1184	116	**912**
Dredge Engines		**Totals**	**3336**	**183**	**24,0**						**6605**		**$ 454**	**$ 3.573**						**2212**	**17401**
Caterpillar 3512		Loading	**1388**	**57**	**7,5**		10445	5498	0,330	0,390	**2934**	$ 211	$ 202	**$ 1.587**	1027	1319	23090	742	4289	982	**7728**
engine efficiency	ηe	Transit Loaded	**0**	**28**	**3,7**		0	0	0,000	0,000	**0**	$ -	$ -	**$ -**	0	0	0	0	0	0	**0**
specific fuel consumption	sfc	Connecting	**110**	**9**	**1,2**		130	437	0,026	0,031	**37**	$ 17	$ 3	**$ 20**	82	105	1836	59	341	12	**96**
heating value MDO	hL	Discharge	**1727**	**57**	**7,4**		12842	6840	0,410	0,485	**3607**	$ 262	$ 248	**$ 1.951**	1278	1642	28727	923	5336	1208	**9501**
Price MDO	$MDO	Disconnecting	**110**	**7**	**0,9**		101	437	0,026	0,031	**28**	$ 17	$ 2	**$ 15**	82	105	1836	59	341	10	**75**
Density MDO	ρMDO	Transit Empty	**0**	**25**	**3,2**		0	0	0,000	0,000	**0**	$ -	$ -	**$ -**	0	0	0	0	0	0	**0**

Figure 60: Fuel Consumption and Emission Calculation Sheet for the Generators and Dredge Engines

7.1.15 Fitting Items and Their K-values

Fitting Items	K-value
pipe entrance	0.05
90° bend	0.75
45° bend	0.30
butterfly valve	0.30
non return valve	1.00
bellmouth outlet	0.20

Table 16: Fitting K-values

7.1.16 Representation of the ELB within the Emission Model

DODGE ISLAND

			Operation tim: 183			Loading 57			Transit Lo 28			Connectir 9			Discharge 57			Disconnec 7			Transit En 25			Season	Day (6am-6 720			Night (6pr 720		
			Installed Power	Measured Amps	Measured Power	Load factor	sim.factor	averageabsorbed power	Load factor	sim.factor	averageabsorbed power	Load factor	sim.factor	averageabsorbed power	Load factor	sim.factor	averageabsorbed power	Load factor	sim.factor	averageabsorbed power	Load factor	sim.factor	averageabsorbed power	Summer/Winter/Both	Load factor	sim.factor	averageabsorbed power	Load factor	sim.factor	averageabsorbed power
Systems / Components	**Item nr.**	**Description**	[kW]	[A]	[kW]			[kW]			[kW]			[kW]			[kW]			[kW]			[kW]				[kW]			[kW]
	36	Ice flaker	1,09		0,00	0,00	0,0	0,00	0,00	0,0	0,00	0,00	0,0	0,00	0,00	0,0	0,00	0,00	0,0	0,00	0,00	0,0	0,00	B	0,9	1,0	0,98	0,9	1,0	0,98
	37	Oven	23,10		0,00	0,00	0,0	0,00	0,00	0,0	0,00	0,00	0,0	0,00	0,00	0,0	0,00	0,00	0,0	0,00	0,00	0,0	0,00	B	0,5	0,4	4,62	0,5	0,6	6,93
	38	Refridge	6,96		0,00	0,00	0,0	0,00	0,00	0,0	0,00	0,00	0,0	0,00	0,00	0,0	0,00	0,00	0,0	0,00	0,00	0,0	0,00	B	0,3	1,0	2,09	0,9	1,0	6,26
	39	Water fountain	0,37		0,00	0,00	0,0	0,00	0,00	0,0	0,00	0,00	0,0	0,00	0,00	0,0	0,00	0,00	0,0	0,00	0,00	0,0	0,00	B	0,5	0,1	0,02	0,5	0,1	0,02
Gland Seal	**40**	Gland seal pump port	29,83	20,80	13,82	0,46	1,0	13,72	0,40	1,0	11,93	0,10	1,0	2,98	0,10	1,0	2,98	0,10	1,0	2,98	0,40	1,0	11,93	B						
	41	Gland seal pump starboard	29,83	20,80	13,82	0,46	1,0	13,72	0,40	1,0	11,93	0,10	1,0	2,98	0,10	1,0	2,98	0,10	1,0	2,98	0,40	1,0	11,93	B						
	42	Gland seal pump hp	29,83	38,00	25,24	0,85	1,0	25,35	0,20	1,0	5,97	0,20	1,0	5,97	0,80	1,0	23,86	0,20	1,0	5,97	0,20	1,0	5,97	B						
	43	Gland seal pump lp	11,03	0,00	0,00	0,00	1,0	0,00	0,00	1,0	0,00	0,00	1,0	0,00	0,00	1,0	0,00	0,00	1,0	0,00	0,00	1,0	0,00	B						
HVAC	**44**	Air conditioning	36,78	32,00	21,26	0,70	0,0	0,00	0,70	0,0	0,00	0,70	0,0	0,00	0,70	0,0	0,00	0,70	0,0	0,00	0,70	0,0	0,00	S	0,72	0,8	21,18	0,5	0,8	14,71
	45	Heater engine room	30,00	0,00	0,00	0,00	0,0	0,00	0,00	0,0	0,00	0,00	0,0	0,00	0,00	0,0	0,00	0,00	0,0	0,00	0,00	0,0	0,00	W						
	46	Heater head	1,50	0,00	0,00	0,00	0,0	0,00	0,00	0,0	0,00	0,00	0,0	0,00	0,00	0,0	0,00	0,00	0,0	0,00	0,00	0,0	0,00	W						
	47	Heater pump room	5,00	0,00	0,00	0,00	0,0	0,00	0,00	0,0	0,00	0,00	0,0	0,00	0,00	0,0	0,00	0,00	0,0	0,00	0,00	0,0	0,00	W						
	48	Heating boiler	0,26		0,00	1,00	1,0	0,26	1,00	1,0	0,26	1,00	1,0	0,26	1,00	1,0	0,26	1,00	1,0	0,26	1,00	1,0	0,26	B						
	49	Ventilation blower bt	1,10	1,80	1,20	1,00	0,0	0,00	1,00	0,0	0,00	1,00	0,0	0,00	1,00	0,0	0,00	1,00	0,0	0,00	1,00	0,0	0,00	S						
	50	Ventilation engine room	39,69	23,30	15,48	0,40	0,0	0,00	0,40	0,0	0,00	0,40	0,0	0,00	0,40	0,0	0,00	0,40	0,0	0,00	0,40	0,0	0,00	S	0,4	1,0	15,88	0,4	1,0	15,88
	51	Ventilation pump room	39,69	13,00	8,64	0,20	0,0	0,00	0,20	0,0	0,00	0,20	0,0	0,00	0,20	0,0	0,00	0,20	0,0	0,00	0,20	0,0	0,00	S	0,2	1,0	7,94	0,2	1,0	7,94
	52	Ventilation quarters	39,69	12,80	8,50	0,20	0,0	0,00	0,20	0,0	0,00	0,20	0,0	0,00	0,20	0,0	0,00	0,20	0,0	0,00	0,20	0,0	0,00	S	0,2	1,0	7,94	0,2	1,0	7,94
Hydraulic Service System	53	Hydraulic s.s. port 1	22,07	14,00	9,30	0,52	0,8	9,18	1,00	0,0	0,00	1,00	0,0	0,00	1,00	0,0	0,00	1,00	0,0	0,00	1,00	0,0	0,00	B						
	54	Hydraulic s.s. port 2	22,07	14,00	9,30	0,52	0,8	9,18	1,00	0,0	0,00	1,00	0,0	0,00	1,00	0,0	0,00	1,00	0,0	0,00	1,00	0,0	0,00	B						

Figure 61: Part of the ELB within the Emission Model

7.1.17 Cape May Beach

Job Name	Job #	Date
Cape May Beach	15829	
Job Specifications		
Amount to be Dredged	296651	m3
Density Soil	1.95	ton/m3
Dredging Depth	10.0	m
Water Depth Sailing	10.0	m
Minimum Water Depth Sailing	7.0	m
Distance with min. Water Depth	1000.0	m
Water Density	1.025	ton/m3
Number of Blows	15	blows/foot
Fixed Visor Min Angle	40	deg
Fixed Visor Max Angle	50	deg
Sailing Distance One Way	5219	m
Discharge		
Length Discharge Pipe	1739	m
Line Speed Discharging	4.21	m/s
Diameter Discharge Pipe	0.762	m
Discharge Mixture Density	1.243	ton/m3
Speed Sailing		
Speed Loading Average	1.07	knots
Speed Transit Loaded Max	10.00	knots
Speed Transit Empty	10.50	knots
Acceleration		
Acceleration Loaded	80	kn/h
Deceleration Loaded	-67.5	kn/h
Acceleration Empty	145	kn/h
Deceleration Empty	-120	kn/h
Fuel Specifics		
ULSD Heating Value	45640	kJ/kg
ULSD Price	541	$/m3
ULSD Density	0.846	ton/m3
Soil Specifics		
d10	0.1	mm

Table 17: Input for Cape May Beach

7.1.18 Arcadian Shore

Job Name	Job #	Date
Arcadian Shore	72652	
Job Specifications		
Amount to be Dredged	341043	m3
Density Soil	1.95	ton/m3
Dredging Depth	9.1	m
Water Depth Sailing	9.1	m
Minimum Water Depth Sailing	7.0	m
Distance with min. Water Depth	1000.0	m
Water Density	1.025	ton/m3
Number of Blows	15	blows/foot
Fixed Visor Min Angle	40	deg
Fixed Visor Max Angle	50	deg
Sailing Distance One Way	3704	m
Discharge		
Length Discharge Pipe	1096	m
Line Speed Discharging	4.59	m/s
Diameter Discharge Pipe	0.762	m
Discharge Mixture Density	1.260	ton/m3
Speed Sailing		
Speed Loading Average	0.64	knots
Speed Transit Loaded Max	9.14	knots
Speed Transit Empty	9.34	knots
Acceleration		
Acceleration Loaded	53	kn/h
Deceleration Loaded	-80	kn/h
Acceleration Empty	69	kn/h
Deceleration Empty	-145	kn/h
Fuel Specifics		
ULSD Heating Value	45640	kJ/kg
ULSD Price	541	$/m3
ULSD Density	0.846	ton/m3
Soil Specifics		
d10	0.1	mm

Table 18: Input for Arcadian Shore

7.1.19 Myrtle Beach

Job Name	Job #	Date
Myrtle Beach	72623	
Job Specifications		
Amount to be Dredged	1187734	m3
Density Soil	1.95	ton/m3
Dredging Depth	7.9	m
Water Depth Sailing	7.9	m
Minimum Water Depth Sailing	7.0	m
Distance with min. Water Depth	1000.0	m
Water Density	1.025	ton/m3
Number of Blows	15	blows/foot
Fixed Visor Min Angle	40	deg
Fixed Visor Max Angle	50	deg
Sailing Distance One Way	6112	m
Discharge		
Length Discharge Pipe	1600	m
Line Speed Discharging	4.25	m/s
Diameter Discharge Pipe	0.762	m
Discharge Mixture Density	1.240	ton/m3
Speed Sailing		
Speed Loading Average	0.73	knots
Speed Transit Loaded Max	9.59	knots
Speed Transit Empty	10.40	knots
Acceleration		
Acceleration Loaded	58	kn/h
Deceleration Loaded	-46	kn/h
Acceleration Empty	74	kn/h
Deceleration Empty	-85	kn/h
Fuel Specifics		
ULSD Heating Value	45640	kJ/kg
ULSD Price	541	$/m3
ULSD Density	0.846	ton/m3
Soil Specifics		
d10	0.1	mm

Table 19: Input for Myrtle Beach

7.1.20 Rehoboth Beach

Job Name	Job #	
Rehoboth Beach	15720	
Job Specifications		
Amount to be Dredged	768135	m3
Density Soil	1.95	ton/m3
Dredging Depth	12.8	m
Water Depth Sailing	12.8	m
Minimum Water Depth Sailing	7.0	m
Distance with min. Water Depth	1000.0	m
Water Density	1.025	ton/m3
Number of Blows	15	blows/foot
Fixed Visor Min Angle	40	deg
Fixed Visor Max Angle	50	deg
Sailing Distance One Way	5093	m
Discharge		
Length Discharge Pipe	875	m
Line Speed Discharging	4.39	m/s
Diameter Discharge Pipe	0.762	m
Discharge Mixture Density	1.296	ton/m3
Speed Sailing		
Speed Loading Average	0.91	knots
Speed Transit Loaded Max	9.50	knots
Speed Transit Empty	10.50	knots
Acceleration		
Acceleration Loaded	58	kn/h
Deceleration Loaded	-46	kn/h
Acceleration Empty	74	kn/h
Deceleration Empty	-85	kn/h
Fuel Specifics		
ULSD Heating Value	45640	kJ/kg
ULSD Price	541	$/m3
ULSD Density	0.846	ton/m3
Soil Specifics		
d10	0.1	mm

Table 20: Input for Rehoboth Beach

7.2 Chapter 4: Methods and their Viability to Reduce Emissions

This sub chapter shows the figures and tables of chapter 4.

7.2.1 Combined Drive Mechanical Power Arrangement

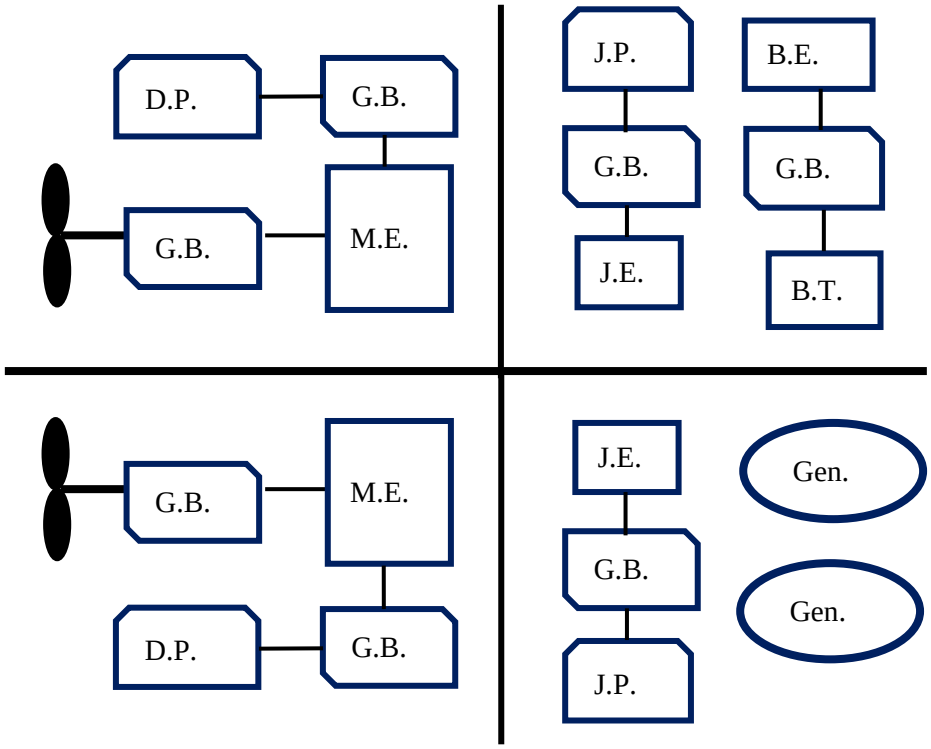

Figure 62: Mechanical Power Arrangement (Combined Drive)

Legend:

J.P.	Jet Pump	D.E.	Dredge Engine	Gen.	Generator
G.B.	Gearbox	J.E.	Jet Engine	B.T.	Bowthruster
M.E.	Main Engine	D.P.	Dredge Pump	B.E.	Bowthruster Engine

7.2.2 Hybrid Power Arrangement with Mechanically Driven Dredge Pumps

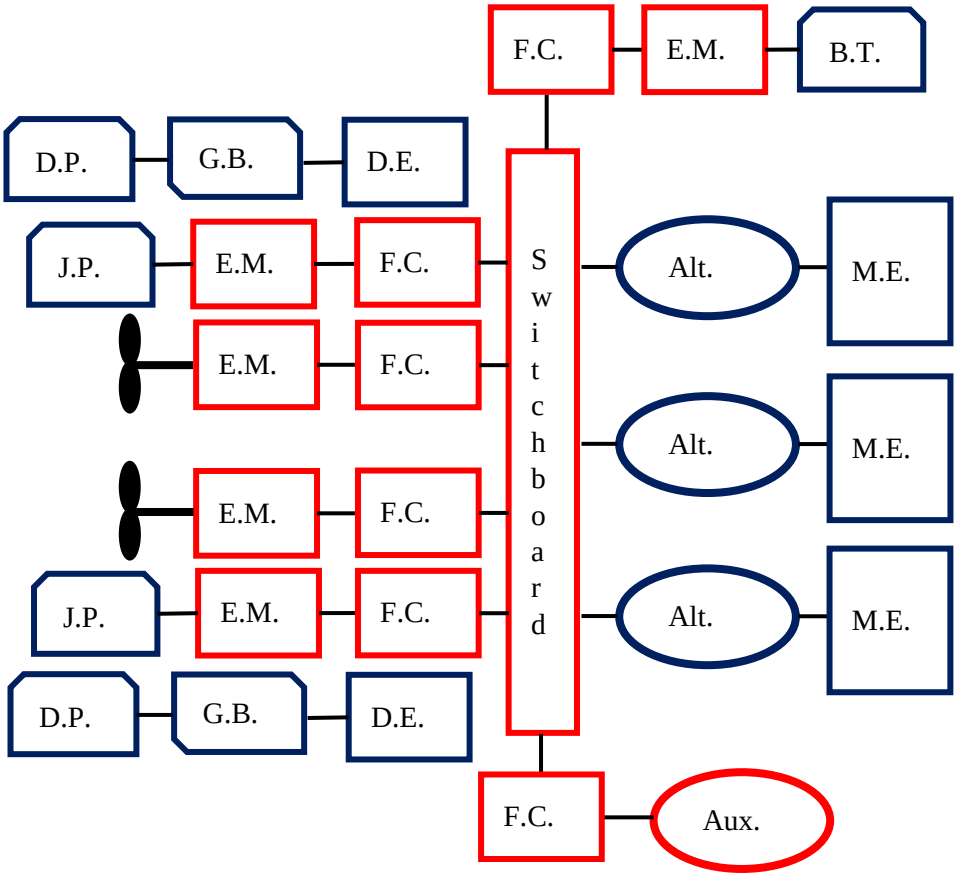

Figure 63: Hybrid Power Arrangement with Mechanically Driven Dredge Pumps

Legend:

J.P.	Jet Pump	D.E.	Dredge Engine	E.M.	Electrical Motor
G.B.	Gearbox	B.T.	Bowthruster	F.C.	Frequency Converter
M.E.	Main Engine	D.P.	Dredge Pump	Alt.	Alternator

7.2.3 Hybrid Power Arrangement with Mechanically Driven Propulsors

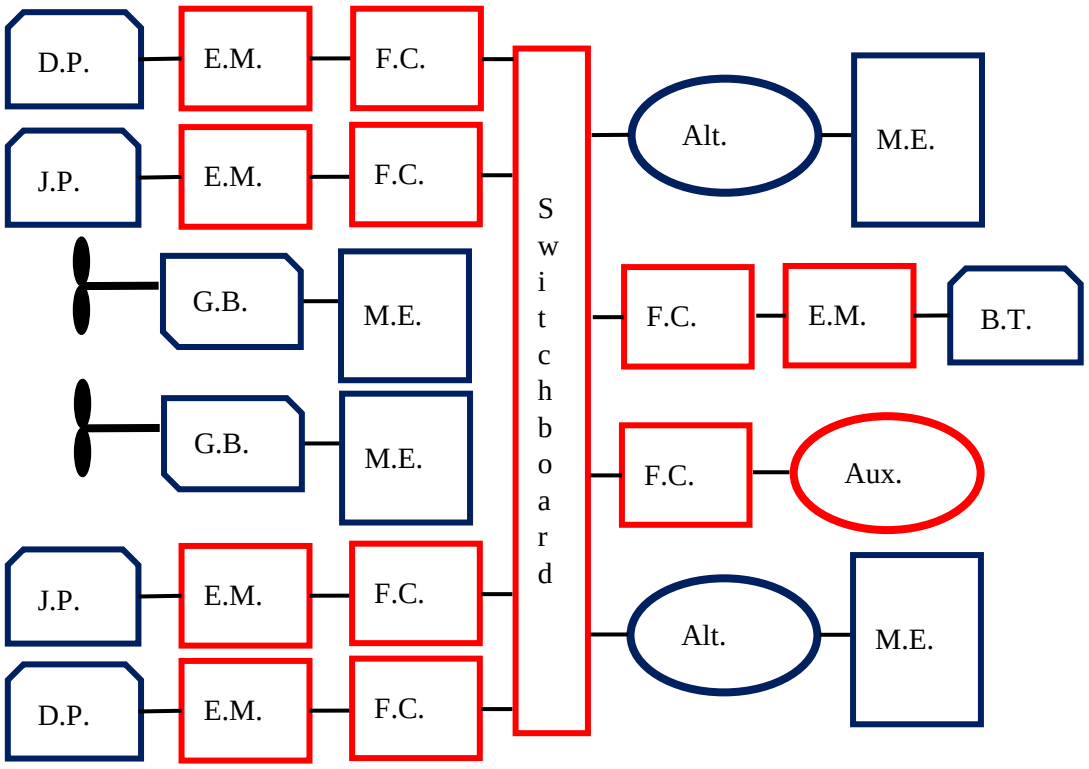

Figure 64: Hybrid Power Arrangement with Mechanically Driven Propulsors

Legend:

J.P.	Jet Pump	Aux.	Auxiliary Engine	E.M.	Electrical Motor
G.B.	Gearbox	B.T.	Bowthruster	F.C.	Frequency Converter
M.E.	Main Engine	D.P.	Dredge Pump	Alt.	Alternator

7.2.4 Electrical Power Arrangement

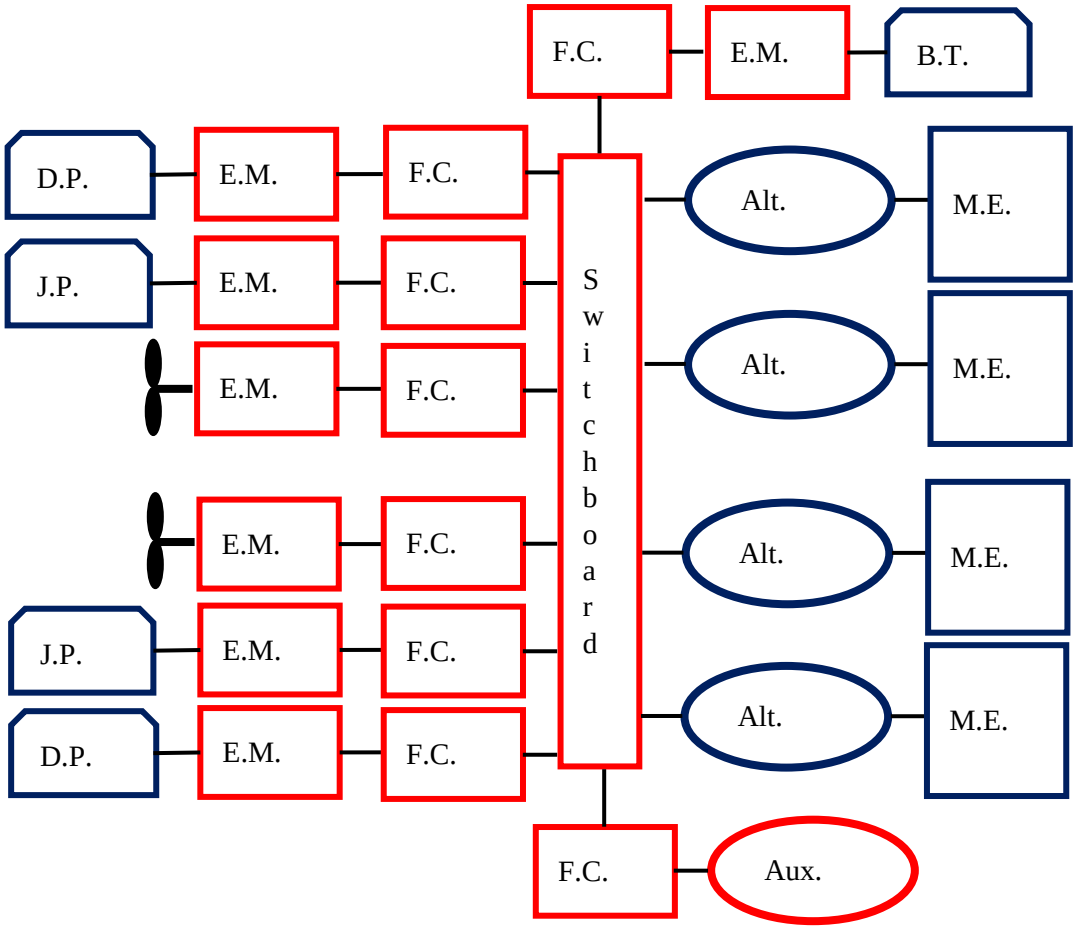

Figure 65: Electrical Power Arrangement

Legend:

J.P.	Jet Pump	Aux.	Auxiliary Engine	E.M.	Electrical Motor
B.T.	Bowthruster	F.C.	Frequency Converter	Alt.	Alternator
M.E.	Main Engine	D.P.	Dredge Pump		

7.2.5 Power Requirement per Trailing Speed

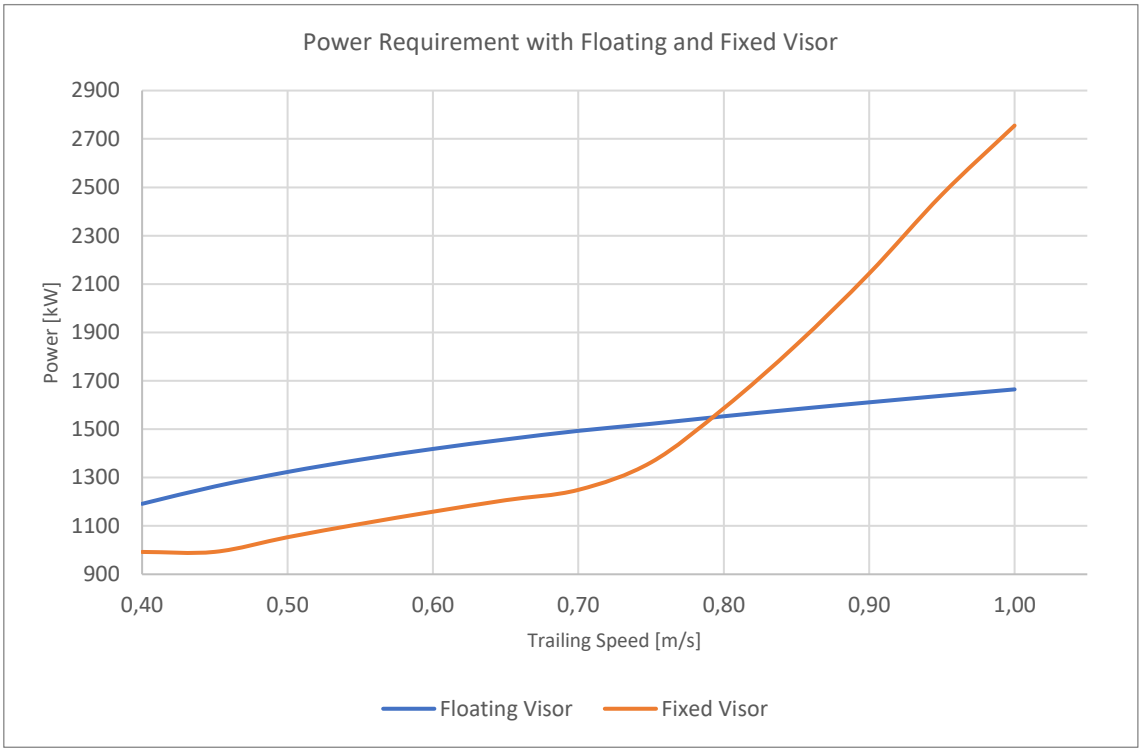

Figure 66: Power Requirement per Trailing Speed

7.2.6 Production versus Trailing Speed

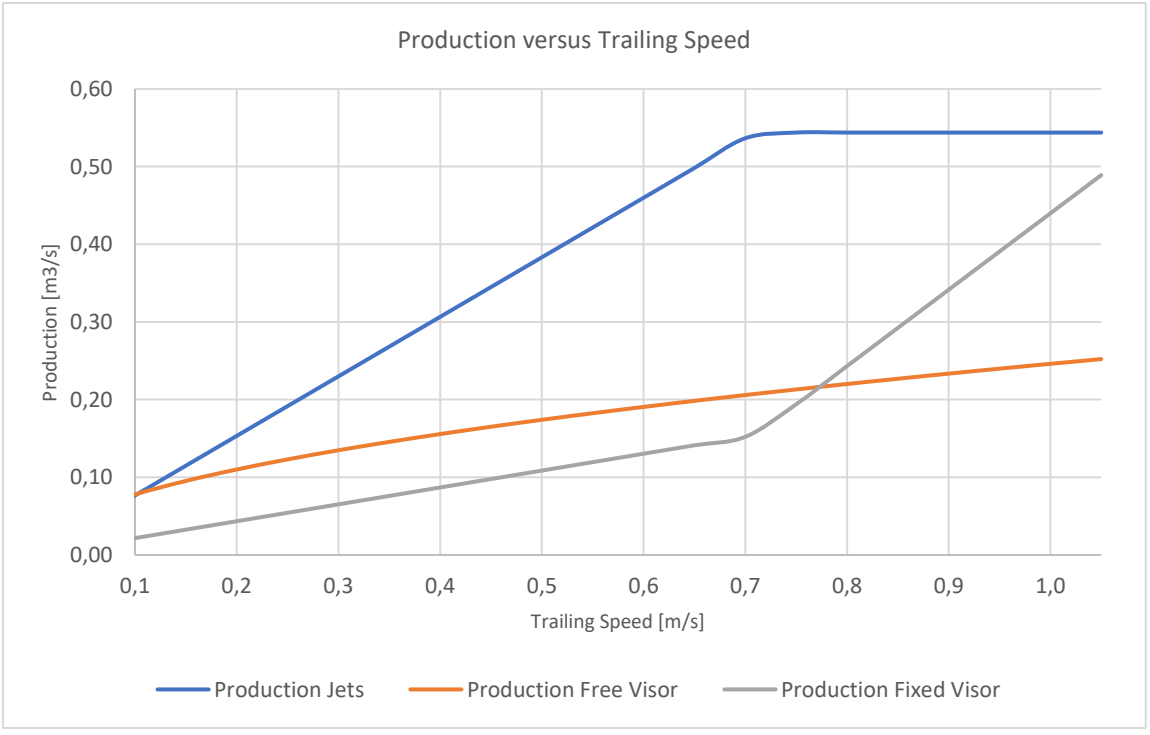

Figure 67: Production versus Trailing Speed

7.2.7 Production versus Trailing Speed

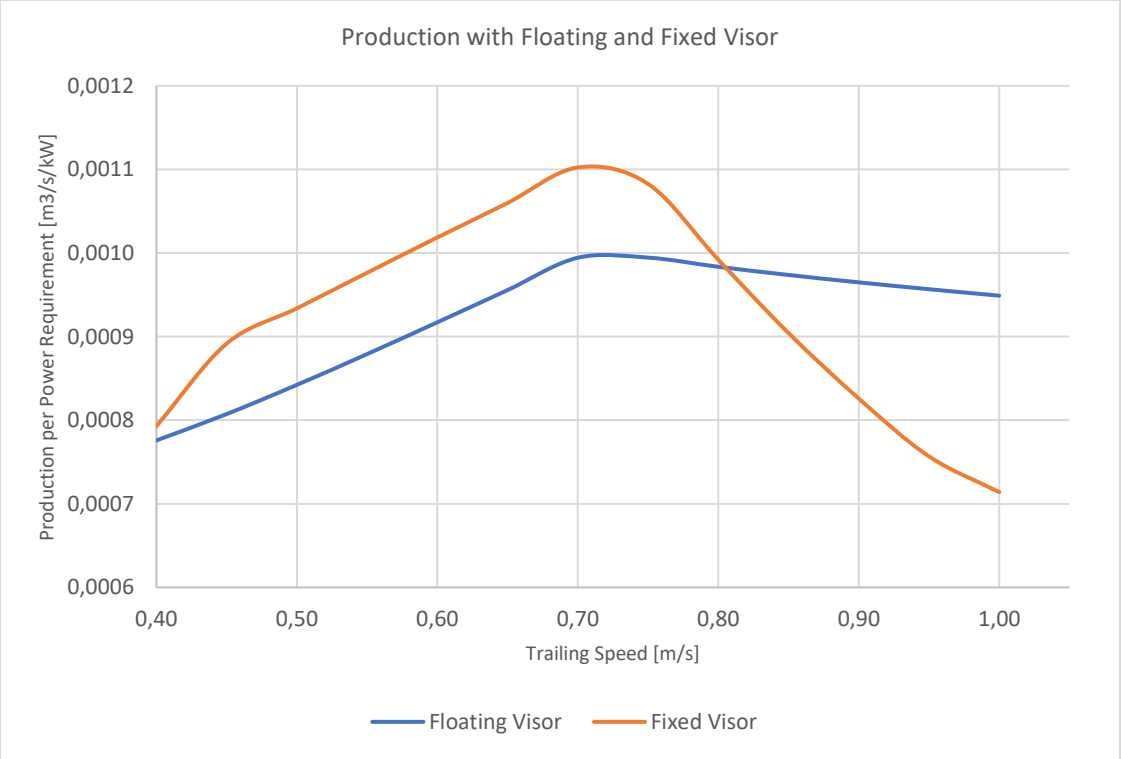

Figure 68: Production versus Trailing Speed

7.2.8 Production per Amount of Fuel versus Trailing Speed

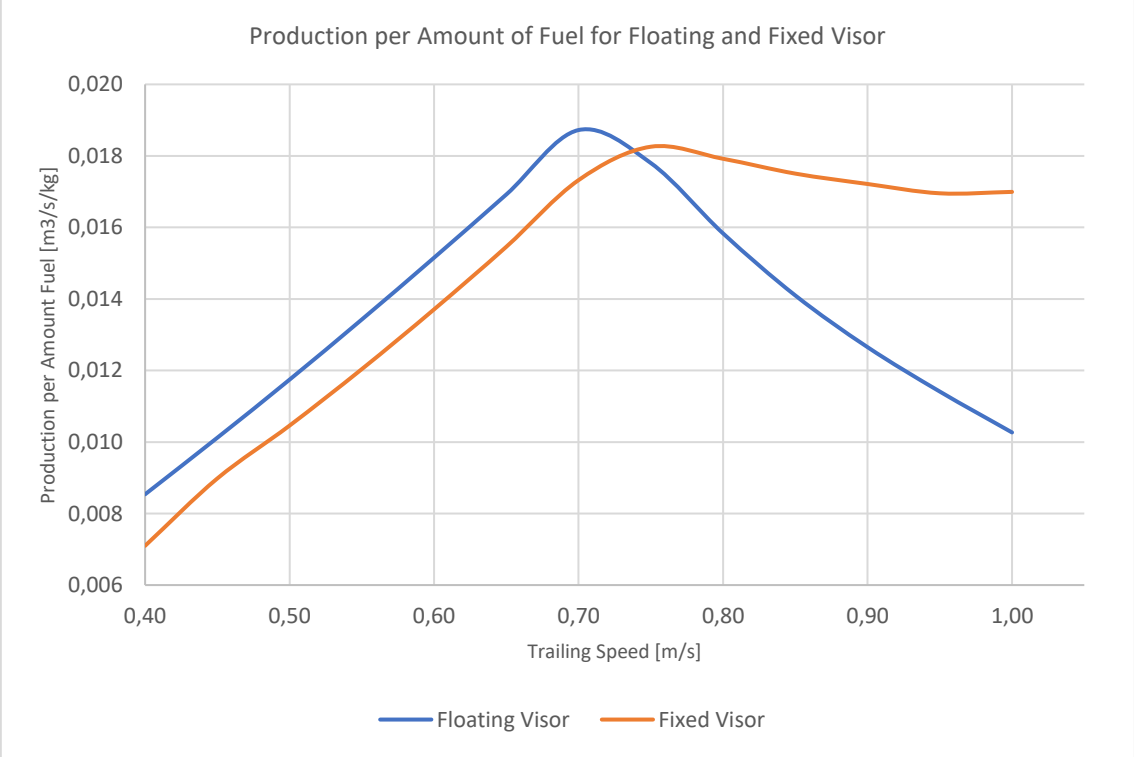

Figure 69: Production per Amount of Fuel versus Trailing Speed